UNIVERSITY OF LEEDS

# Characterising Mesoscale Convective Systems and Evaluating Precipitation Forecasts over West Africa

by

Michael Baidu

Submitted in accordance with the requirements for the degree of Doctor of Philosophy

The University of Leeds
School of Earth and Environment

September 2022

# Declaration of authorship

The candidate confirms that the work submitted is his own, except where work which has formed part of jointly authored publications has been included. The contribution of the candidate and the other authors to this work has been explicitly indicated below. The candidate confirms that appropriate credit has been given within the thesis where reference has been made to work of others.

DETAILS ON PUBLICATIONS

# Acknowledgements

I would like to thank my primary supervisor, Dr Juliane Schwendike, for her patience, encouragement and support in every step during this PhD. I would also like to thank my co-supervisor Prof John Marsham for always believing in me and inspiring me with great ideas, making me feel like a scientist. Thanks to Dr Caroline Bain, my Met Office supervisor, for the opportunities she gave me to visit the Met Office, arranging meetings with other Met Office scientists, inviting me home, and most importantly taking her time to explain many concepts to me. I greatly appreciate those moments.

A great thanks to GCRF African SWIFT, the UKRI and the University of Leeds for proving funding (Grant/Award Number: NE/P021077/1) for my PhD. Thank you all so much, without this funding all my dreams and achievements wouldn't have been possible. Thank you, especially for the funding extension and extra support during the difficult COVID period!

A special thanks to Prof Doug Parker, Prof Alan Blyth, Prof Benjamin Lamptey and many others of the African SWIFT team for organising the SWIFT Summer School, the opportunity to attend other SWIFT science meetings, contribute to works going on in workpackages 3,4,5 and 6 and many more opportunities I got through SWIFT! The community I had through SWIFT has created for me the relevant contacts I require for my career and to make significant contribution to African Meteorology. Thanks to Dr Linda Hirons, Dr Caroline Wainwright, Dr Joshua Talib, Dr Elijah Adefisan and all other SWIFT scientists for your encouragement and support in many ways. Thanks to you all as well as Prof Andy Dougill, Dr Amanda Maycock and many others for selecting me for the attendance of the Queen's Anniversary Prize awards ceremony, which is one of the greatest honours of my life! I am so grateful.

To the vibrant research group, Atmospheric Dynamics and Clouds group, thanks to you

all for your support and the opportunities to have like minded people to share ideas with and discuss my research challenges with. Special thanks to Dr Simon Peatman for always being there to help me with my python problems. Thanks for responding to my emails and texts even at weekends and odd hours. Thanks to Dr Beth Woodhams for always being so inspiring and helpful. Thanks to Dr Sam Clarke for taking your time to help me analyse some plots and taking your time to explain some concepts about MCSs to me. Thanks to Fran Morris, Amethyst Johnson, Paloma Castro, Rachel Sansom, James Warner (Met Office) and the endless list of supportive family and friends who have helped me enjoy my stay in Leeds.

Finally a big thanks to my parents, V. Rev Eric Ato Baidu, Mrs Mavis Baidu and all my siblings for your prayers and support that have made it possible for me to fulfil my PhD dreams and career goals. I am very grateful to everyone I couldn't mention for the opportunity to contribute to addressing the problem of Tropical Weather Forecasting. This had been my motivation from the beginning and I feel so privileged to have gotten the opportunity to make a significant contribution towards addressing the problem I have always been concerned about. Thanks so much, I love you all.

# Abstract

Mesoscale Convective Systems (MCSs) and their associated rainfall, winds and lightning pose threats to the lives of citizens and the economy of West African countries. These systems are poorly predicted as they are not well represented in Numerical Weather Prediction (NWP) models. To address this forecasting challenge, the (thermo-)dynamic environment associated with mature MCSs and its effect on the intensity of MCSs has been investigated. This analysis includes the effects of vertical wind shear, which plays a key role in the intensification of MCSs. The ability of current convection-permitting NWP models to represent rainfall and the effects of vertical wind shear on MCSs has also been evaluated by comparing the forecast skill of the Met Office 4.4 km Tropical Africa Model (TAM) to that of the Global model.

Matured MCSs were mostly found in regions of strong surface convergence and high orography. These storms were also found to be associated with environments of strong vertical wind shear. Long-lived moderate speed storms had larger sizes, colder brightness temperatures (BTs) and associated with a strong vertical wind shear as compared to short-lived slow moving storms. Long-lived moderate speed storms were also associated with the presence of the African Easterly Waves. Oceanic storms were mostly slow-moving but had higher rain-rates as compared with land storms.

A detailed investigation of the effects of vertical wind shear on MCSs has revealed that, a strong vertical wind shear results in colder BTs relative to their temperatures at the level of neutral buoyancies (LNBs). It is hypothesised that, vertical wind shear results in colder BTs by increasing updrafts and minimising entrainment. Oceanic storms could reach their LNBs compared to land storms, suggesting that, high entrainment rates over land, as well as entrainment dilution by drier air over land, prevents storms over land from reaching their LNBs. Over the Sahel, Southern West Africa (SWA), and the Coast, a strong vertical wind shear did not only result in colder BTs but also high rain-rates.

The effects of vertical wind shear on MCSs was found to be better represented in the TAM compared to the Global model. The skill of the TAM is highest over coastal areas and mountainous regions suggesting the model's ability to simulate land-sea breeze and orographic effects more accurately. The TAM outperforms the Global model in forecasting sub-daily rainfall over West Africa, as well as in simulating the closest location of convective rainfall as compared to observations, although this location is still too coarse for forecasters to make useful decisions. The skill of the TAM is also significantly affected by the long spin-up period of the model, making Day 2 forecasts better than that of Day 1. The TAM also outperforms the Global model for higher rainfall intensities, demonstrating the model's ability to simulate organised convective systems more accurately.

These findings are useful for forecasters, model developers and policy makers as a better representation of the (thermo-)dynamic environments of mature MCSs and the effect of vertical wind shear on rainfall, which is poorly represented in current convection-permitting climate models, will not only enhance better rainfall forecasts but also help to provide more accurate climate projections.

# Contents

# List of Figures

# Abbreviations

**AEJ** African Easterly Jet

**AEW** African Easterly Wave

**AMMA** African Monsoon Multidisciplinary Analysis

**AMO** Atlantic Multi-decadal Oscillation

**AWJ** African Westerly Jet

**BT** Brightness Temperature

**BTavg** Average Brightness Temperature

**BT_diff** Brightness Temperature difference (difference between brightness temperature and temperature the the level of neutral buoyancy)

**CAPE** Convective Available Potential Energy

**CIN** Convective Inhibition

**CLAUS** Cloud Archive User Service

**CP** Convection-permitting

**CP4-A** 4.4 km Convection-permitting model for Africa

**DJF** December, January, February

**ECMWF** European Centre for Medium-Range Weather Forecasts

**ENDGame** Even Newer Dynamics for General atmospheric modelling of the environment

**ENSO** El Niño–Southern Oscillation

**ERAI** European Centre for Medium-Range Weather Forecasts (ECMWF) Re-Analysis Interim

**FSS** Fractions Skill Score

**GA6.1** Global Atmosphere version 6.1

**GA7.0/7.1** Global Atmosphere version 7.0/7.1

**GPCP** Global Precipitation Climatology Project

**GPM** Global Precipitation Measurement

**HIW** High Impact Weather

**IMERG** Integrated Multi-satellitE Retrievals for GPM

**IOD** Indian Ocean Dipole

**IPCC** IPCC — Intergovernmental Panel on Climate Change

**ITCZ** Intertropical Convergence Zone

**ITD** Intertropical Discontinuity

**JJA** June, July, August

**JULES** Joint UK Land Environment Simulator

**LFC** Level of free convection

**LFSS** Localised Fractions Skill Score

**LL_moderate** Long-lived moderate speed storms

**LLMC** Layer Lifting Model of Convection

**LNB** Level of Neutral Buoyancy

**MAM** March, April, May

**MCS** Mesoscale Convective System

**MCV** Mesocale Convective Vortex

**MSE** Mean Square Error

**MetUM** Met Office Unified Model

**ML** Monsoon Layer

**NCEP** National Centers for Environmental Prediction

**NLLJ** Nocturnal Low-level Jet

**NWP** Numerical Weather Prediction

**OLR** Outgoing Longwave Radiation

**OSTIA** Operational Sea Surface Temperature and Ice Analysis

**PV** Potential Vorticity

**RAL1-T** Regional Atmosphere and Land version 1.0 Tropical

**RAL1-M** Regional Atmosphere and Land version 1.0 Mid-latitude

**RAL2-T** Regional Atmosphere and Land version 2.0 Tropical

**RAL2-M** Regional Atmosphere and Land version 2.0 Mid-latitude

**SHL** Saharan Heat Low

**SL_moderate** Short-lived moderate speed storms

**SL_slow** Short-lived slow moving storms

**SL_fast** Short-lived fast moving storms

**SON** September, October, November

**SST** Sea Surface Temperature

**SWA** Southern West Africa

**TAM** Tropical Africa Model

**TRMM** Tropical Rainfall Measuring Mission

**UTC** Coordinated Universal Time

**VCP** Voluntary Cooperation Programme

**WAM** West African Monsoon

**WAWJ** West African Westerly Jet

**WMO** World Meteorological Organisation

**WRF** Weather Research and Forecasting

# Chapter 1

# Introduction

High Impact Weather (HIW) systems over West Africa pose serious threats to farmers, fishermen, industries, lives, and properties of the general public. HIW systems are not well understood and poorly predicted. The representation of process interactions in these weather systems, especially Mesoscale Convective Systems (MCSs) are one of the greatest source of uncertainties in weather and climate models (Edwards et al. 2020; Fitzpatrick et al. 2020a; Senior et al. 2021). To save lives, properties, and improve the economy of West Africa, the understanding and prediction of HIW systems, is crucial. This study aims to investigate the dynamics and predictability of MCSs over West Africa.

Mesoscale convective systems and their associated winds are one of the most devastating HIW systems in West Africa. Rainfall in West Africa is contributed mainly by MCSs (Laurent et al. 1998; Nicholson 2013; Maranan et al. 2018). MCSs, particularly squall lines, contribute to about 90% of the rainfall in the West African Sahel (Laurent et al. 1998; Nicholson 2013; Maranan et al. 2018) and about 56% in Southern West Africa (SWA) (Maranan et al. 2018). MCSs range from tens to hundreds of kilometres across (Houze Jr 2018). Due to their horizontal scales, MCSs are not explicitly resolved in global climate models. Global models with convection parameterisation schemes generally struggle to capture the structure, initiation and evolution of convective systems across multiple grid-boxes in Africa (Fink et al. 2011; Lin et al. 2022). Parameterised models also struggle to accurately capture the size, intensity, direction of propagation of MCSs Crook et al. (2019) as well as the effects of vertical wind shear on convective systems in West Africa. Explicit convection on the other hand, has been shown to produce more realistic representation of the spatial variability in rainfall over West Africa (Kniffka et al. 2020). Regional models with explicit convection are therefore key for a

better understanding and prediction of MCSs and their associated impacts.

Studies with the Met Office Unified Model (MetUM) (e.g. Marsham et al. 2013; Woodhams et al. 2018; Keat et al. 2019; Hanley et al. 2021) have revealed that high-resolution models with permitted moist convection perform better in representing the diurnal cycle of convection than their parameterised counterparts. However, significant biases are still seen when compared with observations. For instance, there is a significant difference between the model and observations in the mean rainfall rates over the Sahel and SWA and a difference in the diurnal cycle of the mean rainfall rate (especially after 1500 UTC). Convection-permitting models produce too much high intensity rainfall with fewer less intense rain events (Kendon et al. 2012; Lean et al. 2008). These biases are partly due to uncertainty in the initial conditions of the models (Paxian et al. 2016; Walker et al. 2019). The sparse nature of observations in some parts of the region and inadequate upper air measurements to be assimilated into the models further complicates this problem. Data assimilation in convective regimes is also a challenge even if there are suitable observations. The representation of the diurnal cycle of the monsoon, our understanding of the role of vertical wind shear and cold pool outflows from moist convection also remain incomplete. Vogel et al. (2020) found that both the European Centre for Medium-Range Weather Forecasts (ECMWF) and Meteorological Service of Canada models poorly simulates convective organisation. The post processed forecasts struggled to outperform the climatology. Forecasters in West Africa do not trust the location and intensity of convective storms produced by Numerical Weather Prediction (NWP) models. West African forecasters rely on the synoptic-scale circulation, satellite animations, knowledge of land surface properties of different regions and other experiences to make their predictions (personal correspondence Ghana Meteorological Agency). A better understanding of the (thermo-)dynamic environments that generate MCSs in different parts of West Africa (such as the Sahel, SWA and the Coast introduced in Maranan et al. (2018)) is needed to better represent MCSs in NWP models and to make best use of NWP forecasts.

In the West African Sahel, an increase in the meridional temperature gradient between the dry and hot Sahara and the humid Gulf of Guinea results in an increase in the frequency of intense MCSs over the region and is expected to further increase under climate change (Taylor et al. 2017, 2018). Excess warming intensifies the Saharan heat low (SHL) (Lavaysse et al. 2009) and increases the meridional temperature gradient (Vizy and Cook 2017). The meridional temperature gradient results in a strong

African Easterly Jet (AEJ). The intense SHL also causes a stronger monsoon flow. The AEJ and the strong monsoon flow creates a strong 600 - 925 hPa wind shear. The strong vertical wind shear favours more intense MCSs (Alfaro and Khairoutdinov 2015; Alfaro 2017; Rotunno et al. 1988; Taylor et al. 2017). The effect of vertical wind shear on MCSs is however different for the different sub-regions in West Africa as different environmental conditions dominate the regions in the various seasons (Taylor et al. 2018; Klein et al. 2020). Understanding the effect of shear on the dynamics of storms in the different sub-regions of West Africa and for different seasons is therefore key to addressing the challenges associated with MCS prediction.

Tomasini et al. (2006) have developed an MCS climatology for West Africa by grouping the MCSs into four classes based on their speed and lifetime. This classification has been widely used in other studies of MCSs in the region. These include Lafore et al. (2017), who among others showed the preferred triggering and dissipation regions of each MCS class, Maranan et al. (2018) who described the rainfall types that are likely to be associated with each MCS class and Crook et al. (2019) who evaluated the the representation of each MCS type in convection-permitting and parameterised models. However, the environments of these MCS classes and the reasons for their characteristic lifetimes and speeds have not been thoroughly investigated.

The aim of the thesis is to understand the effect of the dominant environmental condition in the different parts of West Africa on the storm characteristics and to compare the different regions with one another. The thesis also aims at providing an understanding of the mechanism through which vertical wind shear results in intense storms by evaluating the (thermo-)dynamic environments of MCSs. And finally, to evaluate the representation of rainfall in the convection-permitting MetUM over West Africa.

This thesis addresses the following main research questions:

1. What is the climatology of the dynamic and thermodynamic conditions associated with different MCS types in West Africa?
2. What are the reasons for the characteristic lifetimes and speeds of these MCS types?

3. How does the vertical wind shear affect the intensity of MCSs in the sub-regions of West Africa?

4. How well does the 4.4-km MetUM forecast rainfall in West Africa?

Chapter 2 provides an overview of the West African Monsoon (WAM), convection in West Africa, MCSs, effects of vertical wind shear on MCSs, and the Tropical African Model (4.4 km MetUM). Chapter 3 gives a description of the study areas, the sources of the data, and the description of the methods used for the analysis. Chapter 4 discusses the environments, characteristic lifetime and speeds of MCSs in West and Central Africa with the aim of providing insight into the (thermo-)dynamic environments that result in MCSs of different intensities. Chapter 5 focuses on investigating the effects of vertical wind shear on MCSs with a special focus on the effect of vertical wind shear on the brightness temperatures of MCSs as compared to their temperatures at their levels of neutral buoyancies. Chapter 6 focuses on the evaluation of the performance of the Met Office convection-permitting Tropical Africa Model. The conclusions and recommendations from this work are finally presented in Chapter 7.

# Chapter 2

# Background

## 2.1 The West African Monsoon (WAM)

The WAM is the seasonal reversal of the prevailing near surface wind over West Africa due to a thermodynamic contrast between the Sahara and the Gulf of Guinea (Fink et al. 2017; Nicholson 2013). The north-easterly winds known as Hammattan, experienced in wintertime are replaced by the summertime southwesterly winds. The region exhibits a high north to south climatic variability due to varying rainfall amounts from the Gulf of Guinea to the Sahara (Vizy and Cook 2002; Le Barbé et al. 2002). This north-south climatic variability has led to the concept of the four weather zones introduced first by Hamilton et al. (1945).

The first zone, zone A is the region located north of 20°N. This region is usually located at the north of the intertropical discontinuity (ITD) and is characterised by a hot and dry northerly surface flow (Figure 2.1). The ITD is the front that separates the hot and dry northerly surface winds in the north of the region from the cool and moist southerly monsoon winds in the south. The zone usually has less than 750 mm annual rainfall and an extended dry season that lasts for about 10 months (Ferguson 1985; Kessler and Breman 1991; Casenave and Valentin 1992). The region has very high maximum temperatures and low dew points (<15 °C). The SHL is located in this zone (Fink et al. 2017). The southern (ITD) region is characterised by low-level convergence between the northeasterlies and the southwesterly monsoon. Over the ocean, this convergence zone coincides with the region of maximum rainfall but on land, the maximum rainfall region is located at about 10° south of the ITD (Nicholson 2009a, 2018).

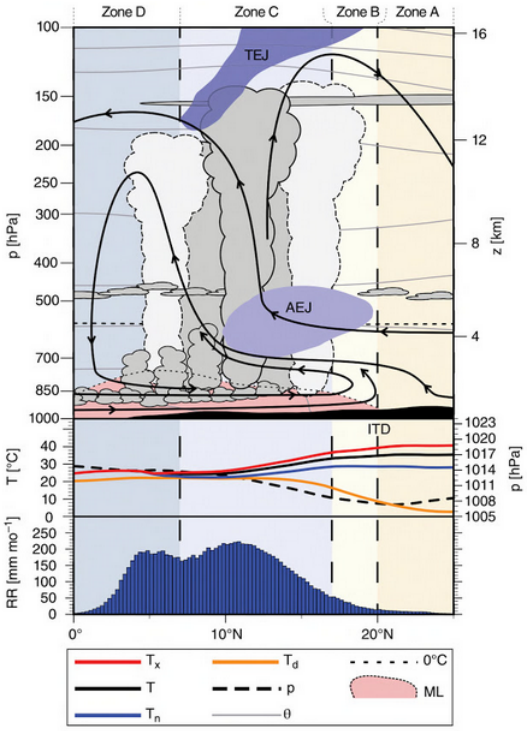


Figure 2.1: Schematic cross-section of West African atmosphere (10°W and 10°E) for July, illustrating the 4 weather zones of the WAM. The positions of the ITD, AEJ, TEJ, and the monsoon layer (ML) is shown. Also shown are the mean monthly rainfall totals ($RR$), isentropes ($\theta$), minimum and maximum temperatures ($T_n$ and $T_x$ respectively), dew point temperatures ($T_d$) and atmospheric pressures ($p$) (from (Fink et al. 2017)).

The region between about 17 to 20°N is known as zone B. This zone is characterized by a shallow moist monsoon layer with only short-lived thunderstorms. Maximum thundery activity is experienced in zone C (located between ∼7°N and 17°N). Mid-level easterlies associated with the AEJ that forms a waveguide on the AEWs are located in this zone. The tropical easterly jet (TEJ) is also located at upper-levels (about 200 hPa) in this zone. The AEJ region is the region with the deepest cumulonimbus clouds (Fink et al. 2017). The maximum rainfall is located between the AEJ and the TEJ (Nicholson 2008).

The region between the equator and ∼7 °N is zone D. This zone is dominated by shallow stratus or mid-level altostratus as well as a few deep convective clouds. Relatively fewer MCSs occur in this region as compared to zone C due to lower Convective Available Potential Energy (CAPE), Convective inhibition (CIN) and wind shear (Parker 2017). These systems also propagate slower than their counterparts in zone C. A larger

percentage of the annual rainfall in this region is contributed by the monsoon rainfall associated with a cyclonic vortex within a regime of intense westerlies (Maranan et al. 2018). The resulting rainfall is usually continuous and intermittent as the large scale cyclonic vortex is slow moving. Maranan et al. (2018) found that about 90% of the rainfall systems in SWA (located in zone D) are these weakly organised classes, which explains the rainfall amounts located in zone D in Figure 2.1. A bimodal rainfall distribution is experienced in zone D with a short dry season occurring usually in August (Stern et al. 1981; Baidu et al. 2017; Aryee et al. 2018; Maranan et al. 2018). The monsoon layer depth is deepest at the Guinea coast (∼4-6 °N) (Fink et al. 2017).

### 2.1.1 Atmospheric circulation features that influence the variability of the WAM

The main circulation features that define the West African monsoon are the TEJ, the AEJ and the equatorial westerlies associated with the southwest monsoon flow (Nicholson and Grist 2003). The interannual variability of the WAM is linked to changes in these circulation features (Nicholson 2013).

The climatological positions of the main atmospheric circulation features have been plotted in Figure 2.2 using ERA-Interim (ERAI) reanalysis data (1980 - 2010). The mean positions of the ITD, SHL, 1010 hPa mean sea level presure (MSLP), the AEJ and TEJ are shown for the months of January, April, July and October. The ITD and the SHL are identified using the $15^oC$ dew point contour and 850 hPa potential temperature contours at 28 - $38^oC$. The AEJ and TEJ are also identified using the 10 and 15 $ms^{-1}$ wind contours at 700 and 200 hPa respectively. The criteria used are described in Parker (2017). The AEJ is pronounced during May - October while the TEJ is seen in July and August. Figure 2.3 shows the same features using a vertical transect of the zonal wind and ($v$, $\omega$) plotted along $0^o$ longitude (the dashed green line in Figure 2.2). Shades of blue indicates easterlies (locations of the AEJs and TEJs), while shades of red indicates westerlies (location of the sub-tropical jet (STJ) and low level westerlies). MCSs dominates the Sahel (∼10 - $20^oN$) at the peak of the monsoon season (July) (Janiga and Thorncroft 2014; Taylor et al. 2022). The dominance of MCSs in the Sahel in this season is sustained by a strong vertical wind shear characterised by the strong AEJ and low-level westerlies. However the exact mechanisms through which the strong vertical wind shear sustains MCSs are not thoroughly understood. The

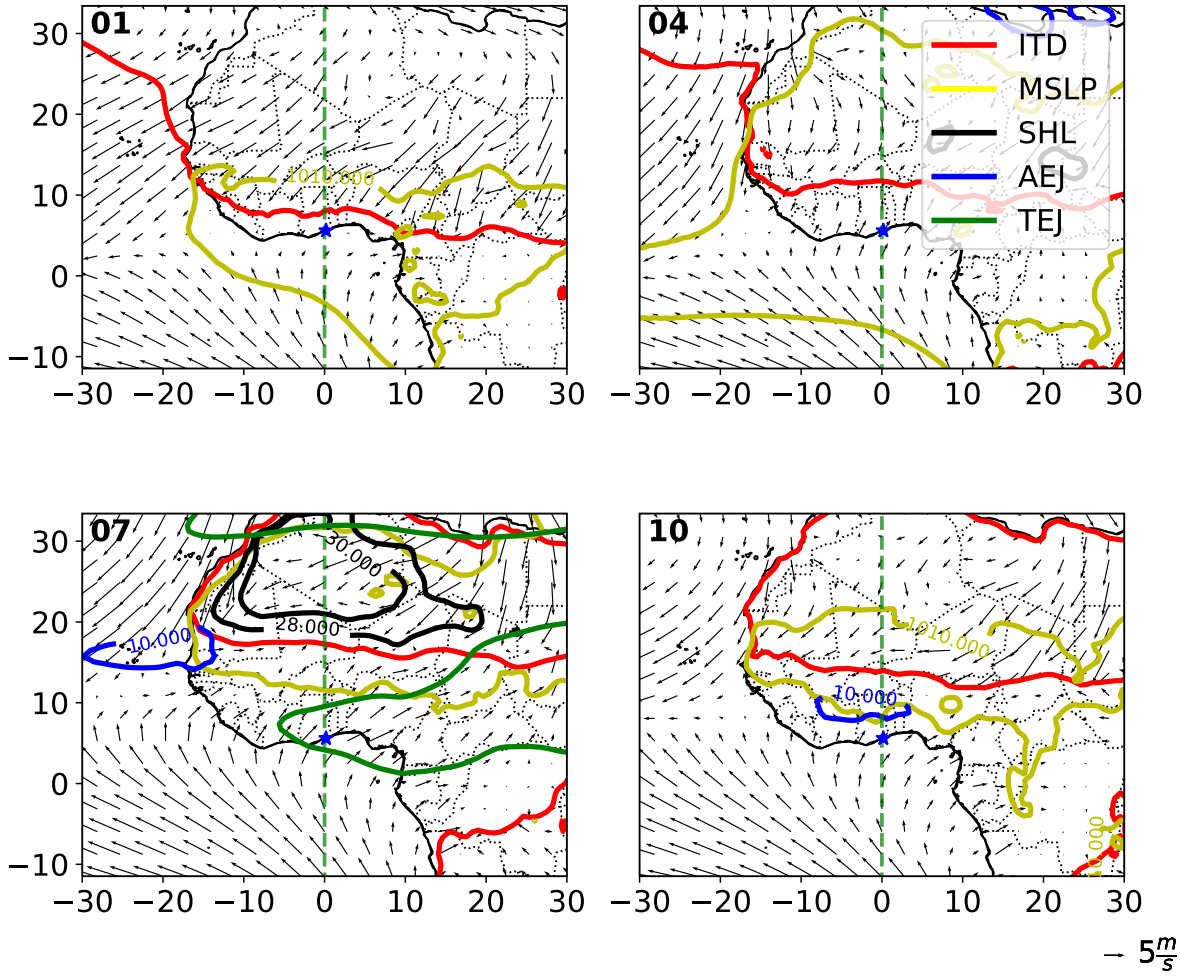


Figure 2.2: Climatology of the main features that describe the WAM using ERA-Interim data from 1980 - 2010. Overlaid are the 925-hPa wind vectors. AEJ - blue contour, TEJ - green contour, ITD - red contour, SHL - black contours and 1010 hPa MSLP in yellow contour. Dashed line: location of cross section in Figure 2.3. Numbers in top left corner refer to the months: 01 - January, 04 - April, 07 - July and 10 - October.

core of the TEJ is located on the eastern side of West Africa whereas that of the AEJ and the monsoon westerlies can be found over West Africa (Figure 2.4). In addition to these zonal flows are two meridional overturning circulations consisting of northerly flow at higher levels and southerly flow at low levels (Nicholson 2009a).

The AEJ is characterised by a maximum zonal wind speed of about $15\,m\,s^{-1}$ located in a region of strong meridional temperature gradient in the lower atmosphere (Parker 2017). It results from a reversed lower-tropospheric temperature gradient between the

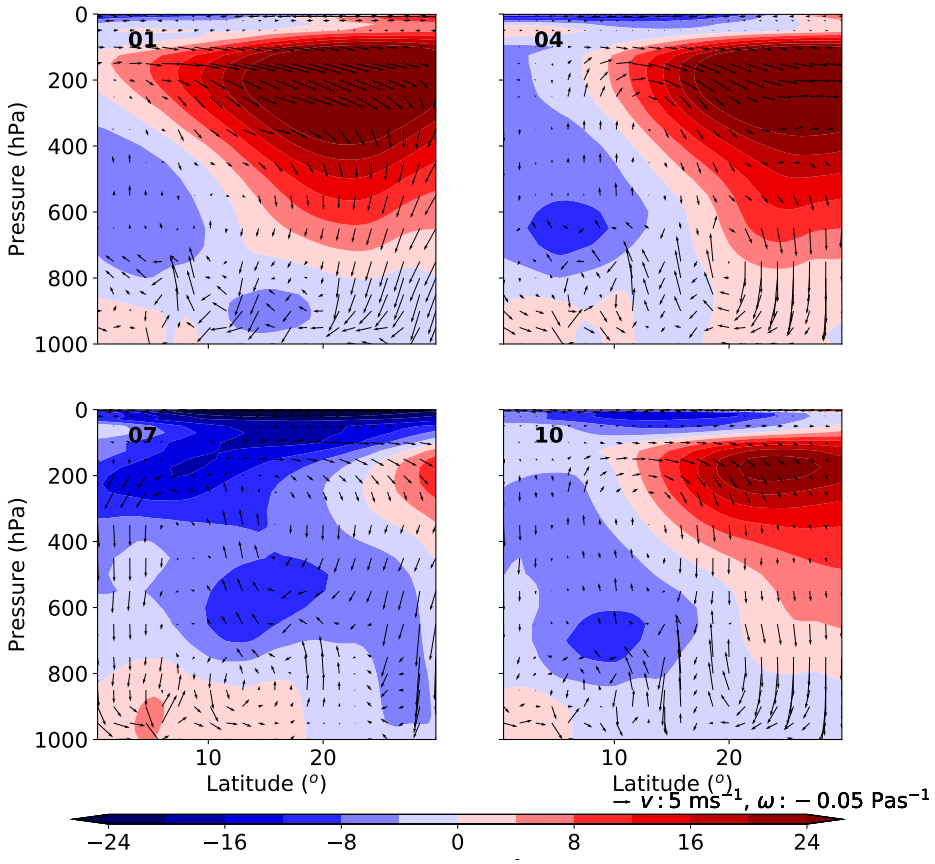


Figure 2.3: Vertical transect of the ERAI climatology (1980-2010) of the main features that describe the WAM (zonal wind -shaded, ($v$, $\omega$) -arrows). Numbers in top left corner refer to the months: 01 - January, 04 - April, 07 - July and 10 - October.

Sahara and the Gulf of Guinea due to extremely warm temperatures over the Sahara Desert in contrast with the cooler Gulf of Guinea (Cook 1999; Thorncroft and Blackburn 1999; Nolan et al. 2007; Nicholson and Grist 2001; Zhang et al. 2008). The AEJ is also associated with regions of strong horizontal shear pronounced between August and September and vertical shear pronounced from May to July (Maranan et al. 2018; Gu and Adler 2004). An anticyclonic circulation associated with the mid-upper troposphere over the Sahara sustains the AEJ (Chen 2005). The AEJ intensifies and moves more polewards prior to the onset of the rainy season over the Sahel (May - June) with the average speed of 12 $ms^{-1}$ (Nicholson and Grist 2003). The speed however decreases during the Sahelian phase of the monsoon. The development and intensifi-

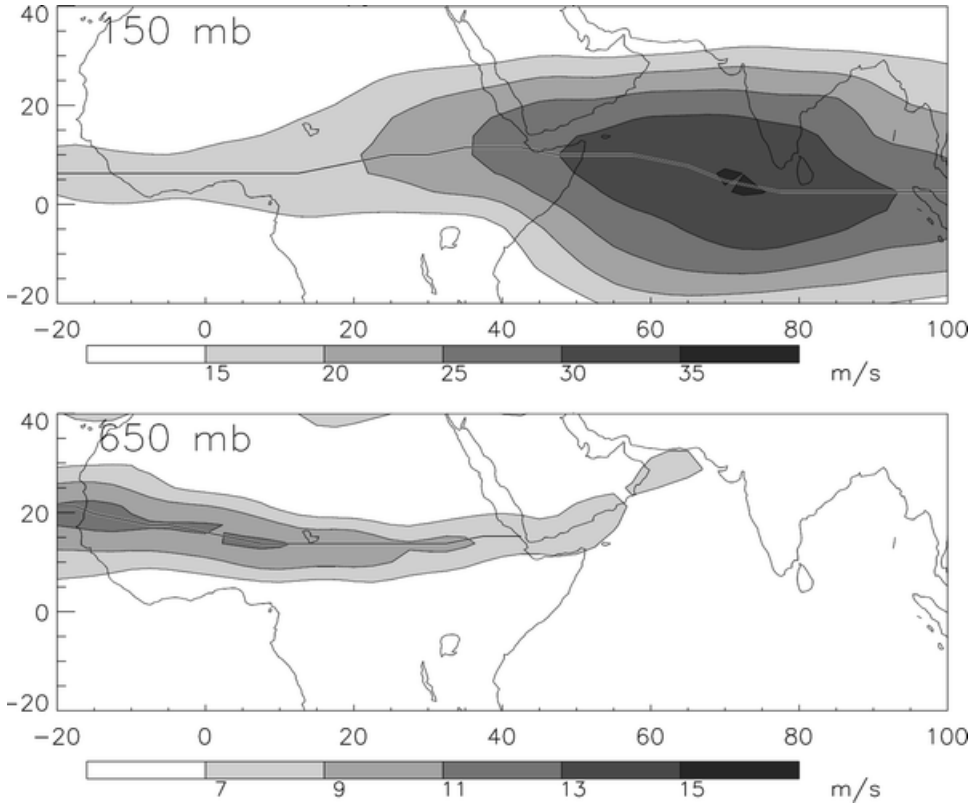


Figure 2.4: The mean easterly wind speed in August at 600 and 150 hPa, showing the AEJ (bottom) and TEJ (top) (from (Nicholson 2009a)).

cation of the AEJ is supported by the Saharan high (Chen 2005), moist processes and aerosols (Cornforth et al. 2009; Tompkins et al. 2005). Chen (2005) showed that, the AEJ which forms the southern rim of the Saharan high is maintained by the Coriolis acceleration associated the divergent winds from the Saharan high. Cornforth et al. (2009) also showed that moist processes increases the development rate of the AEJ, but reduces its speed and meridional extent. On the effect of aerosols on the AEJ, Tompkins et al. (2005) showed that, improving the aerosol climatology in the ECMWF forecasting system significantly improved the forecasts of the AEJ. The AEJ is also maintained by meridional circulations driven by the SHL and the Hadley cell (Thorncroft and Blackburn 1999; Cook 1999).

The AEJ varies zonally with two distinct cores: the eastern and western cores (Hall et al. 2006; Dezfuli and Nicholson 2011). The intensity of the two cores exhibits a significant interannual variability. The eastern core appears to be more prominent in

dry years whiles the western core seem more prominent in wet years (Nicholson 2013). The latitudes of the AEJ cores experiences both interannual and seasonal variability (Dezfuli and Nicholson 2011; Wang and Elsberry 2010). The region south of the AEJ core is characterised by a deep moist convection and a peak in mean rainfall amount while dry convection and less rainfall dominates the region north of the AEJ core. The northern side is however favourable for tropical squall lines (Parker et al. 2005b). Wang and Elsberry (2010) demonstrated that, the passage of an MCS modifies the structure of the AEJ.

Two distinct potential vorticity (PV) anomalies are associated with the AEJ. A positive PV anomaly dominates the region south of the AEJ whiles a negative PV anomaly dominates the region north of the AEJ (Thorncroft and Blackburn 1999). The PV anomaly is positive at the core of the AEJ and is associated with frequent generation of mesoscale convective vortices (MCVs). The presence of these PV gradients is essential for the development of AEWs (Parker 2017).

The AEWs are perturbations in the zonal wind field around 700 hPa with wavelength of about 3000 km that occurs at a 3 - 5 day time scale (Couvreux et al. 2010; Leroux et al. 2010). These perturbations result from barotropic and baroclinic instabilities on the AEJ (Thorncroft and Hoskins 1994; Wu et al. 2012). Two cyclonic vortices are associated with the AEWs located at 925 hPa on either side of the AEJ axis (Kiladis et al. 2006; Carlson 1969a,b). Leroux and Hall (2009) found that a strong AEJ and vertical shear are required for an AEW to be triggered. The strong vertical shear is found to be present when the core of the AEJ lies over strong surface westerlies (Grist 2002; Grist et al. 2002; Nicholson et al. 2008). The AEWs are the dominant synoptic-scale phenomenon in the WAM and usually occur in May - October (Parker 2017). Several studies (e.g. Cornforth et al. 2009; Hsieh and Cook 2005, 2008; Thorncroft et al. 2008; Mekonnen et al. 2006) suggest convection as the mechanism through which AEWs are triggered. However, work by Leroux et al. (2010) and Hall et al. (2006) has demonstrated that dry dynamics also play a role in the development of the waves. Thus, dynamic instabilities remain a pre-requisite for the wave development.

In wet years, the equatorial westerlies extends to the mid-troposphere and results in strong horizontal wind shear (Grist et al. 2002). There are two main tracks of the AEW which are associated with the axes of the AEJ and the TEJ (Nicholson 2008). The

northerly track located between ∼18° N and 20°S and the southerly track located south of ∼11°N. The northerly track is located at lower levels (∼850 hPa) whiles the southerly track is usually located at higher levels (∼600 hPa) and extends to the Ethiopian Highlands (Fink et al. 2017). AEWs in the southerly track are mostly associated with convection and produce more rainfall than those of the northerly track (Druyan et al. 2006; Pytharoulis and Thorncroft 1999). The northern track coincides with the ITD.

In moist conditions faster growth rates, phase speeds and stronger AEWs are observed than under dry conditions. A deep barotropic structure occurs in moist conditions (Grist 2002; Grist et al. 2002; Nicholson et al. 2008). Grist (2002) analysed the seasonal cycle of AEWs over the Sahel and found a peak development between July and September. Interestingly, this happens to be the period where horizontal shear and baroclinic instability peak. Cornforth et al. (2009) also showed that the low-level amplitude of the AEW becomes weak during the peak monsoon season due to the interaction between convection and the AEWs. The zonal wind however undergoes rapid intensification due to a rapid warming of the lower layers through the combined action of both dry and moist convection. The warming of the lower layers reverses the mid-tropospheric temperature gradient more efficiently resulting in the intensification of the zonal wind. The jet is further sustained by the diabatic heating and the heating associated with the surface fluxes. The average moist basic state jet however remained slightly weaker.

The TEJ is located around 200 hPa and is identified as one of the most intense circulation features in West Africa (Grist and Nicholson 2001). Northerly winds dominate the region south of the TEJ core while southerly winds are dominant north of the core. This creates a region of strong divergence at 200 hPa (Thorncroft et al. 2011). This pattern is very prominent during the Sahel wet years and plays a key role in determining the rainfall amounts in the region. Over the eastern Sahel, the TEJ has a mean speed of 18 $m\,s^{-1}$ during the boreal summer. The core of the TEJ shifts to the southern hemisphere during January - March (Nicholson and Grist 2003). Over West Africa, the TEJ exhibits a strong zonal variation but varies little meridionally (Grist and Nicholson 2001; Nicholson 2008; Nicholson and Grist 2001; Sathiyamoorthy 2005). A stronger TEJ is associated with wetter conditions over West Africa while a weaker TEJ is associated with drier conditions (Dezfuli and Nicholson 2011; Nicholson 2008, 2009b). The TEJ exhibits a very strong interannual variability especially over the Sahel. The mean speed of the TEJ during the wet years is about 30 $m\,s^{-1}$ but drops to about 10 $m\,s^{-1}$ or less during the dry years (Nicholson and Grist 2001; Sathiyamoorthy 2005). The TEJ has also been found to be associated with the El Niño Southern Oscillation (ENSO). A

strong El Niño results in a weaker TEJ (Chen and van Loon 1987). A stronger TEJ also results in cooler temperatures in the upper troposphere (Nicholson 2008). The dynamic instability of the TEJ has been related with both borotropic and barotropic-baroclinic instabilities resulting in the development of waves on the TEJ (Mishra 1993; Mishra and Tandon 1983; Nicholson et al. 2007). Using a model simulation and NCEP reanalysis data, Nicholson et al. (2007) found that the waves were planetary scale waves, had a period of 5-6 days and developed through interactions between the TEJ and the surface.

Three equatorial westerlies are associated with the southwest monsoon flow. These include: the African westerly jet (AWJ), the West African westerly jet (WAWJ) and Nocturnal low-level jet (NLLJ). The AWJ is dominant during the Sahelian wet years with the average speed of about 10 $m\,s^{-1}$ (Grist and Nicholson 2001). The WAWJ is also a low-level westerly jet over the equatorial Atlantic and pronounced between May and September. The jet usually lies in the zone where the trade winds converge (usually around 10° N) with the speed of about 13 $m\,s^{-1}$. The WAWJ is significant for the advection of moisture from the Atlantic unto the humid region of West Africa (Southern-West Africa) (Grodsky et al. 2003; Pu and Cook 2010).

A NLLJ also lies within about 200 - 400 m above the surface (Parker et al. 2005a; Abdou et al. 2010). According to Sultan et al. (2007) the NLLJ reaches it's maximum during the onset of the monsoon and minimum when the ITD begins to retreat. The boundary layer in West Africa exhibits a strong diurnal variability with turbulence during the day and a laminar flow during the night (Parker et al. 2005a). There is relatively low wind speed during the day. An inversion layer develops in the night which leads to the development of the NLLJ. The jet has a maximum wind speed of about 10 $\mathrm{ms}^{-1}$ (Lothon et al. 2008; Bain et al. 2010). The direction of the jet changes with the seasons. It is generally southwesterly during the monsoon season and northeasterly during the Harmattan. (Parker et al. 2005a; Lothon et al. 2008). The NLLJ helps the development of deep convection by supplying moisture during the monsoon onset (Sultan et al. 2007; Bickle 2021; Bickle et al. 2022).

As mentioned earlier, the SHL is another key feature of the WAM. The SHL is characterised by a thermal depression that exists below 700 hPa with high surface temperatures and low surface pressure (Lavaysse et al. 2009, 2010a). The SHL influences the variability of the WAM on intraseasonal, interannual and decadal timescales (Lavaysse

et al. 2010b; Biasutti et al. 2009). During the monsoon season, a low-level cyclonic circulation develops around the SHL. An intensification of the low-level cyclonic circulation results in an increased convection in the central Sahel. A reverse response happens in the western Sahel (Parker et al. 2005a). A direct relationship between the SHL and the monsoon circulation has been discerned. An interaction between the SHL and midlatitude depression has been found to result in a wide spread convective activity in the Sahel (Chauvin et al. 2010; Lavaysse et al. 2010a).

### 2.1.2 The role of Sea Surface Temperatures (SSTs) on the variability of the WAM

The relationship between SSTs and the WAM was first proposed by Lamb (1978a,b). Folland et al. (1986) followed by emphasising the role of inter-hemispheric SST gradients. Subsequent studies have reviewed that a variety of regional and global SST patterns influences the WAM at different timescales (interannual and interdecadal) (Lau et al. 2006; Rowell 2003; Ward 1998; Joly et al. 2007; Joly and Voldoire 2010). The influence is however strong for low frequency variations (Delworth et al. 2007; Ting et al. 2011; Zhang and Delworth 2006). Hoerling et al. (2006) suggested that the drying trend observed in West Africa during the latter part of the 20th century was due a positive SST anomaly in the South Atlantic. These findings were supported by Losada et al. (2010). Losada et al. (2010) also highlighted that the equatorial Atlantic SST is a major factor in modulating the northward migration of the WAM. A strong link to the extratropical South Atlantic has also been found by Sun et al. (2010) and Nicholson and Webster (2007). Polo et al. (2011) found that changes in weather regime frequencies in the North Atlantic could partly account for the interannual rainfall variability in West Africa.

The influence of the Pacific Ocean especially ENSO on West African rainfall has been studied by Ropelewski and Halpert (1987, 1989); Nicholson and Kim (1997); Rowell (2001); Ward (1998); Ndehedehe et al. (2017). Ropelewski and Halpert (1987) investigated the global and large-scale regional precipitation patterns associated with ENSO. They identified several regions that showed consistent ENSO-related precipitation which included parts of Africa. However, ENSO-precipitation relationships over the Sahel could not be separated from the influence of Atlantic SST relationships because of the long-term negative trend in precipitation found by Nicholson (1985). Nicholson and

Kim (1997) did a comprehensive study of the relationship between ENSO and Africa rainfall using the harmonic method used in Ropelewski and Halpert (1987) over the period 1991-1990. ENSO was found to modulate rainfall in 15 multi-region sectors in Africa with the strongest signals found in eastern equatorial and south-eastern Africa. Rowell (2001) investigated the impact of Pacific SST anomalies on fluctuations in Sahelian rainfall. They found that the El Niño phase increases the likelihood of Sahel drought. Ward (1998) showed a strong link between ENSO and inter-annual variability of the WAM. This relationship has been confirmed by several studies (Joly et al. 2007; Losada et al. 2012). However, Bader and Latif (2003) have suggested that the influence of the Pacific Ocean is stronger in the eastern than western Sahel. Ndehedehe et al. (2017) examined the impact of the ENSO, the Indian Ocean Dipole (IOD) and the Atlantic Multi-decadal Oscillation (AMO) on terrestrial water storage. ENSO was found to be associated with the terrestrial water storage over the Volta basin with an r value of -0.40. The association was however stronger in the coastal West African countries (regions below latitude 10°N).

A relationship between the WAM and the Indian Ocean has also been found (Raicich et al. 2003; Chung and Ramanathan 2006; Giannini et al. 2003; Lu and Delworth 2005). Bader and Latif (2003) proposed that the Indian Ocean was the driver of the drying trend in the Sahel in the latter half of the 20th century. They affirmed this by associating the extreme drought year of 1983 with Indian ocean SSTs as opposed to previous studies which related the drought to the Atlantic (Bader and Latif 2011). The anomalies of the Indian and Pacific Oceans can also affect the latitudinal displacement of the ITD (Mohino et al. 2011).

Rowell (2003) was among the first to report on the link between the WAM and the Mediterranean. His study revealed an influence comparable to that of the Pacific over West Africa. Polo et al. (2008) suggested a direct relationship between rainfall over the Sahel and the Mediterranean. The eastern Mediterranean basin has a stronger influence as compared to the western Mediterranean (Fontaine et al. 2011). Other studies have suggested an association of the Mediterranean with an enhancement in the south-westerly monsoon flow, moisture flux, Saharan heat low, and increased convergence (Fontaine et al. 2010, 2011; Gaetani et al. 2010).

The competing physical mechanisms influencing high and low frequency variability

of the WAM as discussed above makes it difficult to isolate the contribution of any particular ocean.

### 2.1.3 The onset of the WAM

The onset of the WAM, defined by the northward jump in rainfall, is usually preceded by a poleward shift in the position of the ITD (Fitzpatrick et al. 2016). The oscillation of the ITD influences the onset and cessation of the monsoon (Amekudzi et al. 2015). However there is lack of spatial coherence in the onset dates due to breaks in the monsoon (Marteau et al. 2009; Dalu et al. 2009). The mean onset period over the Sahel is the last dekad of June (Fitzpatrick et al. 2015; Sultan and Janicot 2000) whereas that of the Southern West Africa is the second and third dekads of March (Amekudzi et al. 2015). The retreat of the ITD is however abrupt and result in a more uniform distribution of the cessation dates throughout the region (Nicholson 2018).

Flaounas et al. (2012a) demonstrated that, lowering albedo over the desert regions through the intensification of the SHL induces a northward shift of the ITD. An enhanced SHL combined with the presence of an oceanic cold tongue led to a reduction in rainfall over the Sahel through a low-level mositure flux divergence. They also showed that the presence of mountains over North Africa increases rainfall amount over West Africa although this didn't have a corresponding effect on the timing of monsoon onset. They however, found that, the onset of the WAM was dominantly controlled by large scale dynamics such as the dynamics of the Indian monsoon. Flaounas et al. (2012b) showed that the onset of the Indian monsoon is vital for the predictability of the WAM onset at the intraseasonal timescale. From Flaounas et al. (2012b), the convention associated with the Indian monsoon can excite a Rossby wave (Yang et al. 2017) that reaches North Africa within 7 - 15 days. The passage of the Rossby wave is associated with the intrusion of dry air from the subtropical westerly jet over West Africa and a subsequent suppression of convection. Low-level moisture transport is also reinforced at the same time. Once the wave passes, the dry air intrusion is suddenly weakened, releasing convection over the Sahel. Hence the onset of the WAM occurs about 20 days after the onset of the Indian monsoon.

## 2.2 Atmospheric moist convection

Atmospheric moist convection is the vertical transport of heat, momentum, mass, water and vorticity in the atmosphere due to buoyant air parcels. Atmospheric moist convection is often associated with clouds, thunderstorms and mesoscale cloud systems. It involves the phase changes of water and its associated release or absorption of latent heat. Atmospheric moist convection forms an essential part of the global atmospheric circulation through the large-scale circulations such as the Walker Circulation, Hadley Circulation, ENSO circulation and the MJO. Atmospheric moist convection plays a significant role in cloud-radiation feedback and global climate change (Lin et al. 2014; Bony et al. 2015). It controls the sensitivity of climate models and explains half the variance among the IPCC models (Sanderson et al. 2010; Sherwood et al. 2014; Zhao 2014).

Convection is initiated by several factors such as high sensible heat flux, steep lapse rate and high humidity (Couvreux et al. 2012). Convection results from an unstable vertical distribution of thermodynamic energy. Heated surfaces by solar radiation leaves excess moist energy in the atmosphere which is eventually loss by radiative processes in the free atmosphere (Lafore et al. 2017). Global circulations such as the Hadley and Walker circulations have not been sufficient in accounting for atmospheric energy and momentum budgets and this imbalance has largely been explained by convection (Riehl and Malkus 1958). Convective systems usually initiate in the windward side of mountains, consistent with thermal forcing from elevated heat sources (Hagen et al. 2011; Flaounas et al. 2012a; Berthou et al. 2019). The organisation and propagation of convective systems is associated with low to mid-tropospheric shear (Rotunno et al. 1988; Laing et al. 2008; Weisman and Rotunno 2004; Alfaro and Khairoutdinov 2015; Alfaro 2017; Bickle et al. 2021).

Forecasting convection over West Africa is one of the greatest forecasting challenges. Convection is a sub-grid scale process and therefore not explicitly resolved by Global NWP models. Even convection-permitting NWP models struggle to represent convection. A better understanding of convective processes is required to better parameterise convection and to evaluate their representation in high resolution models.

### 2.2.1 Development of convection

The process of convection can be described by the parcel theory which assumes an adiabatic ascent and neglects the pressure gradient force (Manzato and Morgan Jr 2003). The process can be illustrated using Figure 2.5. A parcel warmer than it's environment will be positively buoyant. The parcel therefore rises following the dry adiabat line as seen on the skew-T while conserving its mixing ratio. The parcel however expands and cools as it rises till the point where the temperature of the parcel becomes equal to it's dew point temperature. This level is known as the lifting condensation level $Z_{lcl}$. The parcel becomes saturated at this point and begins to follow the saturated adiabatic lapse rate. Condensation begins at this point, warming the parcel by the release of latent heat. The parcel becomes more buoyant at this stage and rises beyond the level of free convection ($Z_{lfc}$) where it becomes warmer than the environmental temperature. The buoyant parcel continues to rise at this stage until it reaches the equilibrium level ($Z_{Ptop}$) where its temperature becomes equal to the environmental temperature and becomes neutrally buoyant. The upward acceleration of the buoyant parcel as it rises from the $Z_{lfc}$ to the $Z_{Ptop}$ is provided by the convective available potential energy (CAPE). Which according to Lafore et al. (2017) is given by:

$$CAPE = \int_{Z_{lfc}}^{Z_{Ptop}} g\frac{(T_v - T_{vo})}{T_{vo}}dz \tag{2.1}$$

Where $T_v$ is the virtual temperature of the parcel and $T_{vo}$ is the virtual temperature of the environment. $g$ is the acceleration due to gravity. The virtual temperature is the temperature at which a dry air would have the same pressure and density as the moist air parcel (McIlveen 1991). The CAPE is converted to kinetic energy providing the maximum vertical velocity for convective updrafts ($w_{max}$) given as:

$$w_{max} = \frac{1}{2}\sqrt{CAPE} \tag{2.2}$$

In reality, the $w_{max}$ is minimised through entrainment of environmental air (non adiabatic ascent) by a few tens of metres per second for MCSs in West Africa (Lafore et al. 2017). Takahashi and Luo (2012) showed that, the height of storms in reality (the level of maximum mass outflow in Figure 2.6) occurs at about 3 km lower than their theoretical levels of neutral buoyancies (LNBs) estimated by the adiabatic ascent. The height of real life storms is therefore dependent on the amount and type of environmental air entrained. Studies on the LNB following Takahashi and Luo (2012) over different

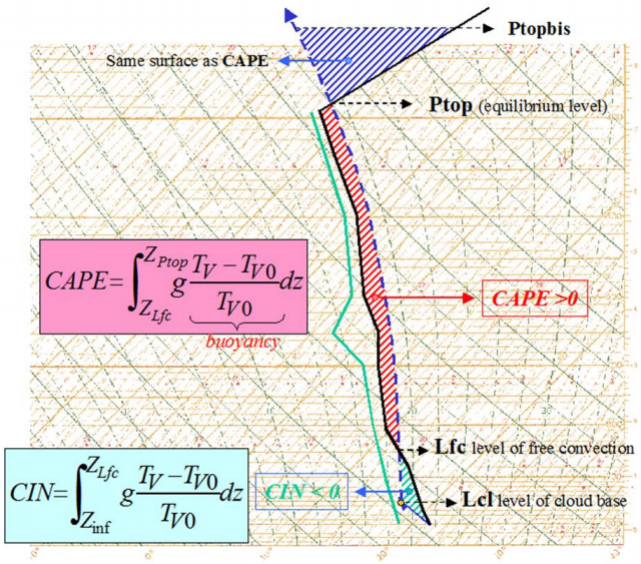


Figure 2.5: A Skew-T illustrating the parcel theory from Lafore et al. (2017). The solid green line is the environmental dew point temperature, the solid black line is the environmental air temperature and the dashed blue line is the the path of a saturated air parcel.

regions (such as the Warm pool, Amazon, Africa and other tropical regions) and using different observations and methods, have confirmed the findings of Takahashi and Luo (2012) (Takahashi and Luo 2012; Takahashi et al. 2017; Wang et al. 2020; Mullendore et al. 2013). The difference between LNB and the level of maximum mass outflow has since been used as a proxy for entrainment (Takahashi et al. 2017; Wang et al. 2020).

Above the ($Z_{Ptop}$), the parcel continues to move momentarily before finally coming to halt creating an overshooting top. There is usually an energy barrier to overcome in order to lift an air parcel from the surface to the ($Z_{lfc}$). This is known as the convective inhibition (CIN). The CIN is basically the integral of buoyancy from the surface ($Z_{inf}$) to the ($Z_{lfc}$):

$$CIN = \int_{Z_{inf}}^{Z_{lfc}} g \frac{(T_v - T_{vo})}{T_{vo}} dz \tag{2.3}$$

Sufficient CAPE generally exist over West Africa during the monsoon period but the exact location of convection normally depends on where the CIN is overcome (Lafore et al. 2017). CIN increases from south to north in West Africa with maximum values of $\sim$200 J kg$^{-1}$ in the Sahel (Lafore et al. 2017). The high CIN over the Sahel means that, external factors are required to trigger convection, which include orographic forcing,

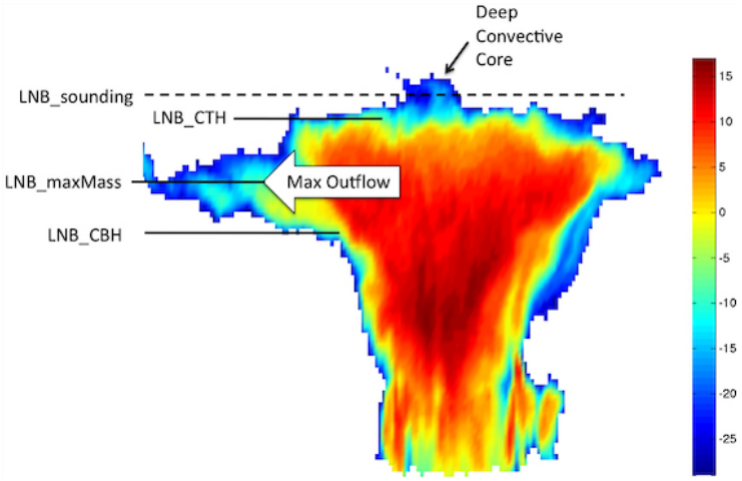


Figure 2.6: CloudSat radar reflectivity profile of tropical deep convective cloud of 24 February, 2007 (unit: dBZ) (Takahashi and Luo 2012). The LNB_CTH is the LNB defined by the anvil cloud top height. The LNB_maxMass is the LNB defined by the maximum mass outflow form the storm. The LNB_CBH is the LNB defined by the anvil cloud base height.

coastal circulations, surface-atmospheric coupling, synoptic forcing and convergence lines, gravity waves and large scale convergence.

For most applications, instead of temperature ($T$), potential temperature ($\theta$) is useful in describing the state of the system. Potential temperature is defined as the temperature a dry parcel will have when it is brought adiabatically to the surface:

$$\theta = T(\frac{P_o}{P})^{\frac{R}{C_p}} \tag{2.4}$$

where R is the gas constant for dry air (287.15 J kg$^{-1}$K$^{-1}$), $C_p$ is the heat capacity at constant pressure (1005 J kg$^{-1}$K$^{-1}$), and $P_o$ is the reference pressure at 1000 hPa. Vertical perturbations within the atmosphere is driven by buoyancy perturbations ($-g\frac{\rho'}{\rho}$). Applying the ideal gas law ($p = \rho RT$) and substituting equation 2.4, we obtain:

$$b = g\frac{\rho'}{\rho} \approx -g\frac{\theta'}{\theta} \tag{2.5}$$

In the case of a moist parcel, equivalent potential temperature ($\theta_e$) or liquid water

potential temperature ($\theta_l$) may be used. These are defined respectively as follows:

$$\theta_e \approx \theta exp(\frac{q_v L_v}{c_{p,d} T}) \tag{2.6}$$

$$\theta_l \approx \theta exp(\frac{-q_v L_v}{c_{p,d} T}) \tag{2.7}$$

where $L_v$ is the latent heat of vapourisation while $q_l$ and $q_v$ are the mixing ratios of liquid water and vapour respectively. $\theta_l$ (also known as the evapouration temperature) reduces to $\theta$ in the absence of a condensate. Similarly, $\theta_e$ is the condensation temperature.

### 2.2.2 Organisation of convection

Convective organisation refers to the clustering together of convective cells in space usually surrounded by relatively drier regions (Moncrieff and Waliser 2015). A convective cell refers to an updraft region that extends vertically through the troposphere. There are three types of organised convective storms. These include a single-cell storm, a multicell storm and a supercell storm.

A single cell storm consists of a growing cumulus which can develop into a cumulonimbus cloud with updraughts that results in an anvil cloud at upper levels and downdraughts that dominates it's mid-levels with associated precipitation (Weisman and Klemp 1986). Single-cell storms are usually short-lived storms found in environments of weak vertical wind shear (Richardson et al. 2007; Lafore et al. 2017). These single cell storms are commonly found in regions south of the AEJ core (Lafore et al. 2017).

A multicell storm involves a group of single cell storms that propagates together as one system. Multicell storms are usually characterised by environments of moderate to strong vertical wind shear (Weisman and Klemp 1982; Markowski 2007; Richardson et al. 2007). Downdraughts from a mature single cell usually initiates a new cell which also grows to sustain the system (Birch et al. 2014; Rotunno et al. 1988). This self sustaining mechanism contributes to form a long-lived system and is usually associated with a severe weather (Houze Jr et al. 1990). The propagation of a multi-cell storm is believed to be a combination of the mean environmental wind speed of the convective

layer and the speed of the rate of triggering of the new cells which may depend on the speed of the cold pool outflow from the storm and environmental wind shear (Newton and Rodebush Newton 1959; Corfidi et al. 1996; LeMone et al. 1998; Lafore et al. 2017).

A supercell storm involves a single quasi-steady rotating updraught formed in environments of strong vertical wind shear that rotates at lower levels. Supercells are not common in West Africa but may occur in mountainous regions or on the flank of squall-lines where rotation of vertical wind shear may occur (Lafore et al. 2017).

### 2.2.3 Mesoscale Convective Systems

An MCS is a large area of deep cloud with a spatial scale $>$ 2,000 km$^2$ which encompasses a number of convective systems (Houze Jr 2004; Yang et al. 2017). Studies of long-lived MCSs in convection permitting climate simulations by Yang et al. (2017) over the central United States showed life times of longest lived storms between 10-24 hours. However MCSs over West Africa may live longer as they can get coupled with the AEWs (Maranan et al. 2018). Many studies have provided a comprehensive detail of MCSs (e.g. Fritsch and Forbes 2001; Houze Jr 2004). A typical MCS usually has a large anvil stratiform cloud top with ice usually identified using a threshold of about 235 K (Fiolleau and Roca 2013). A well developed MCS produces both convective and stratiform rains (Cheng and Houze Jr 1979; Chong and Hauser 1989; Rutledge and Houze Jr 1987), resulting in extended period of precipitation and sometimes leads to flooding (e.g. Rasmussen et al. 2015). Although an MCS is associated with an intense convection, the stratiform precipitation accounts for 73 % of the rain area and contributes to about 40 % of tropical rainfall (Schumacher and Houze Jr 2003). An MCS activity usually initiates in the afternoon and can last for about 4 - 6 hours. However, over the ocean, MCS activities initiate in early mornings and last for about 5 - 7 hours (Huang et al. 2018; Ricciardulli and Sardeshmukh 2002). Over West Africa, MCSs contributes to about 90 % of the rainfall in the Sahel but about 56 % in the coastal zone (Mathon et al. 2002b; Maranan et al. 2018).

As shown in Figure 2.7, the convective cells of an MCS are embedded within the stratiform cloud. The individual convective cells are usually deep convective cells which may be arranged in a line (commonly known as a squall line). Regions of strong updrafts and downdrafts are contained in the convective cells. The stratiform cloud around

the convective cells extend between 100-200 km and are located mainly from the mid troposphere to the tropopause. It contains detrained ice particles from the convective systems (Houze Jr 1989, 2004, 2018). A mesoscale updraft exist in the upper troposphere within the stratiform region with a corresponding mesoscale subsidence in the lower troposphere (Houze Jr 1989; Lafore et al. 2017). Heavy showers of rain are associated with the downdraft regions of the convective cells while the deep stratiform clouds are associated with lighter precipitation (Houze Jr 2018).

**Squall lines**

Squall lines are the most dominant type of MCS in West Africa. The environmental conditions required for the initiation of West African Squall lines includes the presence of low-level moisture supply, mid-level dry air and vertical wind shear (Rowell and Milford 1993). West African Squall lines consist of a convective region which is characterised by a curved line of powerful cumulonimbus with a length scale of several hundreds to a thousand kilometres. Infrared satellite images indicates that the overshooting tops from the convective region extends into the lower stratosphere (Lafore et al. 2017). A low pressure develops at the mid levels due to the latent heat released by the convective cells which supports the formation of intense precipitation that feeds the convective downdrafts (Figure 2.8) (Gray et al. 1998; Lafore et al. 2017; Schumacher and Rasmussen 2020). The presence of this mid-level low pressure creates a horizontal pressure gradient within the system that supports the formation of a rear inflow which brings drier air into the storm (Houze Jr 2004). The rear inflow also strengthens the AEJ behind the squall line. Diabatic cooling resulting form the drier air intrusion forces the mesoscale subsidence and a subsequent cold pool outflow which supports the initiation of new cells in the presence of a strong vertical wind shear (Rotunno et al. 1988).

The cold pool spread out as density currents upon reaching the surface (Simpson 1969; Charba 1974). The spreading out of the cold pools displaces warmer environmental air. As the environmental air is less dense, it is lifted and results in the formation of new cells (Goff 1976; Warner et al. 1980). Cold pools are associated with gusty winds that influence latent and sensible heat fluxes and hence alter the thermodynamic profiles of the boundary layer (Tompkins 2001; Langhans and Romps 2015). Provod et al. (2016) showed that cold pools from West African squall lines results in pressure increases of 0 to 8 hPa, temperature decreases of 2° to 14° and wind gust of 3 to 2 m $s^{-1}$.

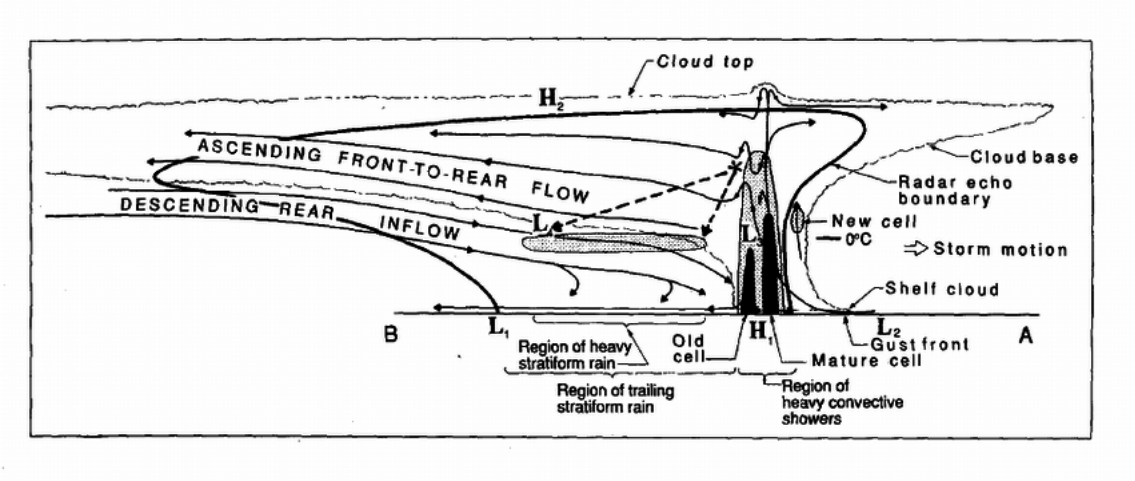


Figure 2.7: Conceptual model of a squall line MCS adapted from Houze Jr (1989).

Studies have shown that cold pools play a role in the maintenance of long lived squall lines, storm organisation and the cell development (Rotunno et al. 1988; Weisman and Rotunno 2004; Khairoutdinov and Randall 2006; Jeevanjee and Romps 2013). Drager and Van den Heever (2017) investigated the characteristics of cold pool composites and found that, in environments where the ground had been soaked by rain from a previous storm, cold pool dissipation is delayed due to the low surface temperatures in these regions.

### 2.2.4 Effect of vertical wind shear on MCS in West Africa

Studies have shown that the intensity of an MCS is driven mainly by low-level humidity, drier mid-levels and a stronger low-level shear (Richardson 1999; Weisman and Rotunno 2004; Parker et al. 2016; Taylor et al. 2017, 2018; Klein et al. 2020). Among these, shear and low level humidity have been identified in recent studies as the dominant factors in determining MCS frequency, rainfall and outgoing longwave radiation. (Taylor et al. 2017, 2018; Klein et al. 2020; Fitzpatrick et al. 2020a). The contribution of each factor and the exact mechanism through which these factors may influence storm intensity have not been completely understood. Earlier studies have proposed the mechanism through which shear might impact storm intensity. Rotunno et al. (1988) described the role played by vertical wind shear on the lifetime and self organisation of storms. According to Rotunno et al. (1988), an intense MCS results when the horizontal vorticity generated by the cold pools from an MCS is balanced by the

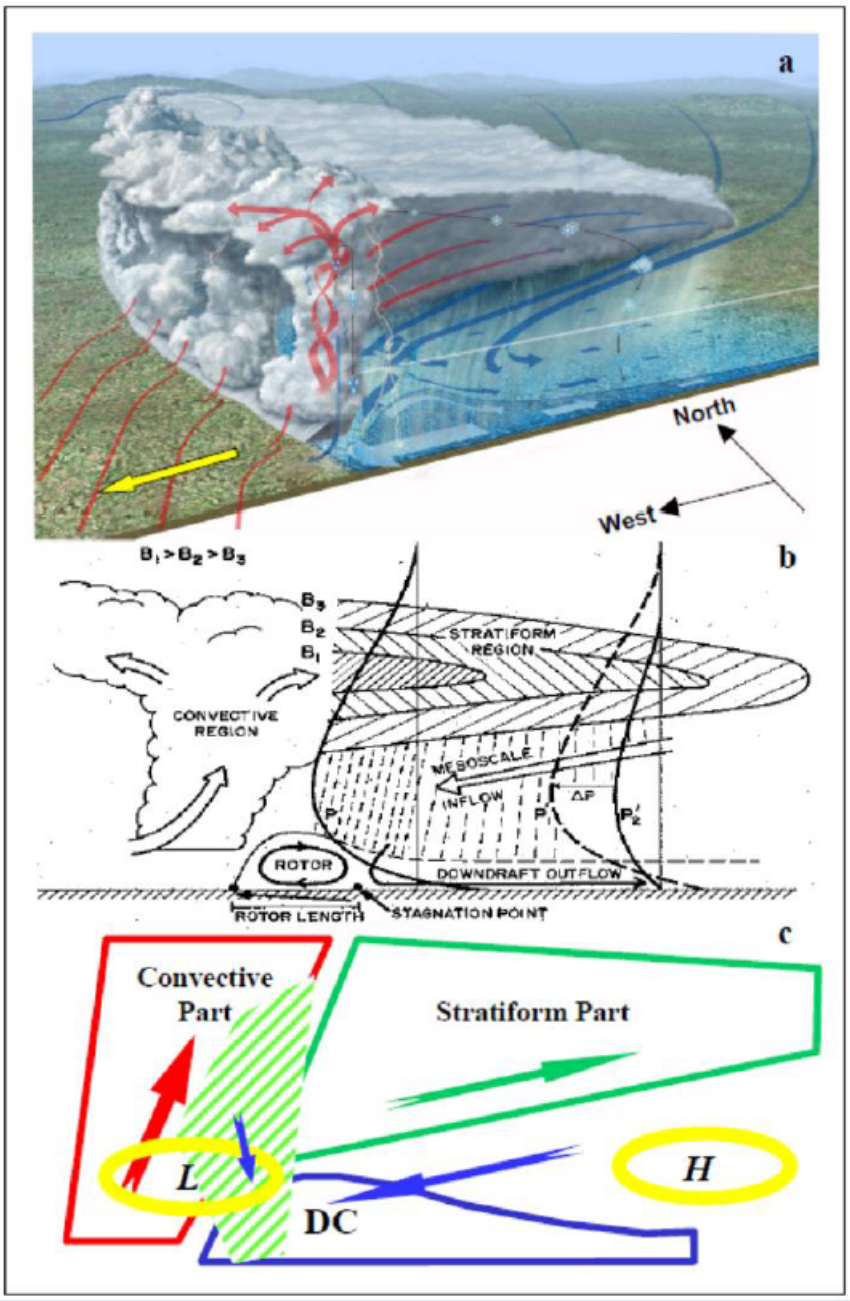


Figure 2.8: Conceptual model of a West African squall line MCS as shown in Lafore et al. (2017). a) a fast-moving squall line in 3D, showing the airflow circulation, the cold pool outflow forming the density current (DC)(blue shading) and hydrometeor trajectories. b) A conceptual model of squall line in 2D (from Lafore and Moncrieff (1989)). c) a box representation of b).

vorticity generated by the environmental low-level wind shear. Bryan et al. (2006) assessed the relevance of the Rotunno et al. (1988) theory to squall line characteristics using output from four numerical models. The results confirmed that the structure of a squall line is governed by the intensity of the cold pool and low-level vertical wind shear.

Alfaro and Khairoutdinov (2015) investigated the role of environmental thermodynamics on storm structure and intensity by focusing on the vertical distribution of CAPE and level of free convection (LFC). They highlighted the relevance of latent heating in determining storm intensity and explained that low-level wind shear intensified storms by increasing the inflow of latent unstable air which results in the increase in latent heating within storms. Alfaro (2017) developed the Layer Lifting Model of Convection (LLMC) which places importance on the thermodynamic role of wind shear on moist convection (Figure 2.9) by introducing a thermodynamic role to the Rotunno et al. (1988) theory. The LLMC describes how low-level shear modulates the inflow of convectively unstable air and water vapour. He found that stronger low-level shear leads to a larger inflow of large convectively unstable air into storms hence increasing their intensity through an increased latent heating within the storm.

Bickle et al. (2021) performed idealised simulations of Sahelian squall lines with the aim of isolating the thermodynamic effects from the dynamic (shear) effects. They found that, the LLMC works well for variations in vertical wind shear, but it was hard to capture effects of thermodynamic changes from this simple framework alone (Bickle et al. 2021, 2022). A study with a high resolution convection-permitting climate model for Africa (CP4-A) showed no correlation between present day vertical wind shear and precipitation rates although it showed a relationship between vertical wind shear and outgoing longwave radiation (a proxy for cloud top temperatures) (Fitzpatrick et al. 2020a; Senior et al. 2021). This result means that vertical wind shear could result in a higher cloud top but not necessarily higher rain-rates. The study by Fitzpatrick et al. (2020a) further revealed that future extreme rain-rates over the West African Sahel scaled predominantly with low-level moisture. However studies conducted using observations over West Africa not only showed a correlation between vertical wind shear and rainfall but also emphasised the effect on vertical wind shear on the frequency and intensity of storms (Taylor et al. 2017, 2018; Klein et al. 2020; Senior et al. 2021).

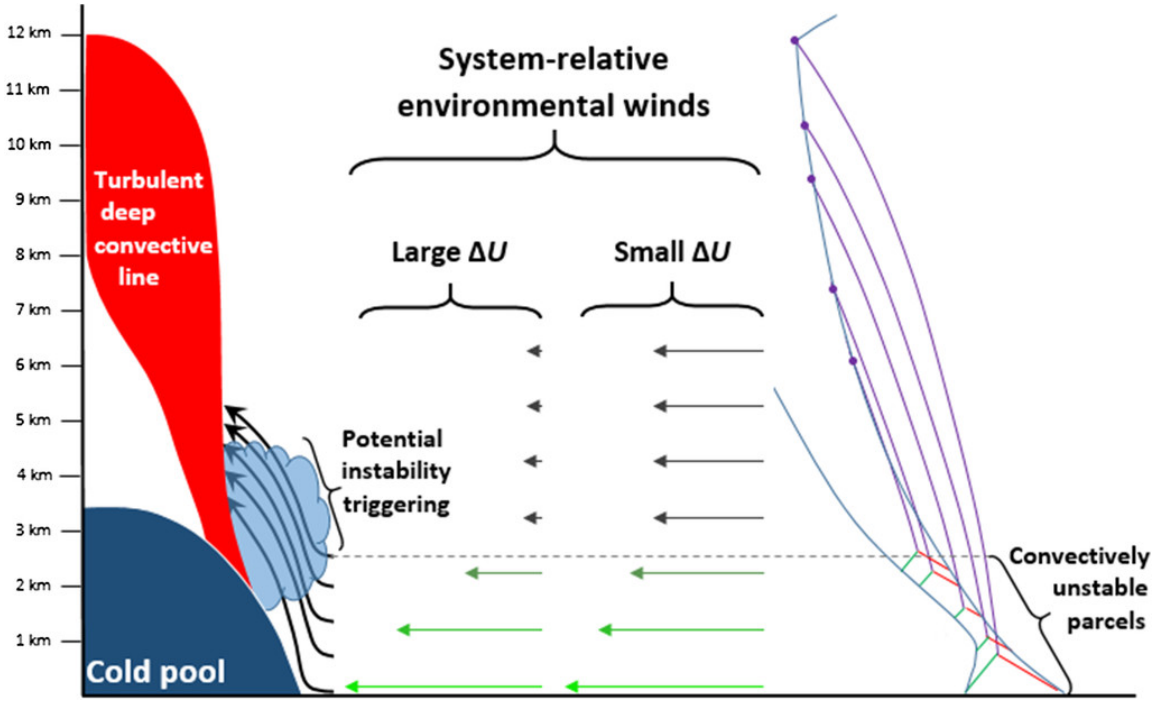


Figure 2.9: A schematic illustrating Alfaro (2017) LLMC. The model illustrates how the cold pool from an MCS lifts convectively unstable air (left) in the presence of vertical wind shear. The skew $T-lnp$ plot on the right illustrates the pseudoadiabatic ascent of parcels from different levels. In the middle, the system relative inflow of environmental air for large vertical wind shear versus low vertical wind shear is illustrated. Large vertical wind shear leads to a larger inflow of convectively unstable air into storms .

Taylor et al. (2017) used 35-year brightness temperature data from satellites to study trends in Sahelian storms. They found an increase in the frequency of extreme MCSs in recent years which correlated with an increase in low-level shear without a corresponding increase in trends in low-level relative humidity. They concluded that the increase in extreme storms in recent years was due to the increase in low-level shear. Similar work over the Congo basin showed a remarkable increase in intense MCS frequency in early spring due to an increased meridional temperature gradient and low-level wind shear (Taylor et al. 2018). Klein et al. (2020) repeated this study over SWA by combining 34 years cloud top temperatures with rainfall and reanalysis data. It was found that both low-level shear and humidity were important for MCS intensification. They went ahead to compare the sensitivity of MCS intensity and peak rainfall to pre-storm low-level moisture and wind shear. Low-level wind shear played a dominant role in SWA March-May storms but switched to low-level moisture from June - November (as the band of intense convection shifts northwards after June). However, the regions with the band of strongest convection remained dominated by the role of vertical wind shear. These regions were dominated by the presence of the AEJ which migrates northwards (towards the Sahel) at the start of June explaining why the dominance of vertical wind shear is weakened after June in SWA.

A recent work by Mulholland et al. (2021) using an idealised model suggested that vertical wind shear increases the updraft strength of squall lines by minimising entrainment-driven dilution. Simulations with strong vertical wind shear resulted in wider updrafts, less entrainment driven dilution and larger buoyancy than simulations with lower vertical wind shear. This seem to support an earlier speculation by (Peters et al. 2019) from their work on the role of vertical wind shear on the updraft strength of supercells. Peters et al. (2019) hypothesised that, vertical wind shear increases the low-level inflow into supercells and results in wider and faster updrafts. They found that, entrainment dilution of the updraft cores weakens the updraft intensity of the supercells. They also demonstrated that, strongly sheared environments makes supercell updrafts wider than updrafts in environments of weaker shear. A follow up on Peters et al. (2019) has also confirmed that, larger vertical winds shear results in larger updraft sizes Peters et al. (2021).

The number and severity of extreme weather events over the Sahel is projected to increase under global warming (Fitzpatrick et al. 2020b) due the intensification of the meridional temperature gradient between the Sahara and the Gulf of Guinea. The in-

tensification of the meridional temperature gradient is expected to result in the increase in low-level shear over the region. It is important that climate models are able to simulate this effect for a more accurate future projection. However the inability of CP4-A to represent the shear - rainfall relationship stated above (Fitzpatrick et al. 2020a; Senior et al. 2021) have cast doubts on our minds about these projections. Does CP4-A represent these processes accurately? Observations are therefore needed to provide a better understanding of atmospheric processes in order to constrain climate models.

## 2.3 Convection-Permitting models

Convection-permitting (CP) models have improved tropical rainfall forecasting by providing a more realistic representation of the diurnal cycle of convection as compared to parametrised models (Marsham et al. 2013; Clark et al. 2016; Woodhams et al. 2018). The diurnal cycle of convection in CP models is more realistic because the sub-grid scale processes relevant for an accurate simulation of convective initiation and lifecycle are explicitly modelled. The relevant sub-grid scale processes include surface characteristics such as orography, vegetation and soil moisture which vary significantly on scales less than 1 km (Taylor et al. 2011). Rapidly evolving boundary layer features, atmospheric stability and associated cloud developments also occur within these scales and may be resolved in CP models (Weckwerth and Parsons 2006; Morcrette et al. 2007). As a result, the organisation and propagation of convection as well as the representation of process interaction is better captured in convection permitting models (Weisman et al. 2008; White et al. 2018; Fitzpatrick et al. 2020a). Global models (resolutions of the order of 10 km or more) parameterize convection and as a result produce too much widespread light rain and struggle to capture rainfall of high intensity (Stephens et al. 2010; Cafaro et al. 2021). Global models also struggle to correctly represent the coupling between AEW dynamics and convection (Bain et al. 2014). CP models on the other hand produce more realistic precipitation fields (Marsham et al. 2013). Stein et al. (2015) evaluated storm structures in a 1.5 km by 100 m MetUM and found that the physical representation of convective storms compares better with radar observations and retrievals such as updraft strength, size and rainfall intensity. Over West Africa, CP models provides a better representation of not only the diurnal cycles but also the lifetimes and direction of storm propagation (Crook et al. 2019). Convection-permitting models are therefore being explored for climate projections (Fitzpatrick et al. 2020a; Senior et al. 2021).

Convection-permitting models still struggle to represent sub-grid scale processes and their interactions, because tropical storms are still not fully resolved even in CP models of grid lengths of the order 1 km (Petch et al. 2002; Bryan et al. 2003). Studies with the high resolution convective-permitting climate model for Africa (CP4-A) shows that CP4-A struggles to represent the relationship between vertical wind shear and precipitation rates of individual storms (Fitzpatrick et al. 2020a; Senior et al. 2021). The rainfall produced by CP4-A models are also mostly more intense compared to observations (Lean et al. 2008; Kendon et al. 2012; Marsham et al. 2013). The sources of error in CP models may include, larger horizontal grid spacing than most convective updrafts, longer spin up times in high resolution simulations and errors in initial conditions and boundary conditions of the driving model (Lean et al. 2008; Guichard et al. 2010; Birch et al. 2013; Luo and Chen 2015; Clark et al. 2016). The accuracy of model initial conditions are of much concern in most parts of the tropics because data is sparcely distributed in most of these regions. There is inadequate upper air observations in most parts of the tropics. Errors in initial conditions therefore grow and influence larger scales.

**The Met Office convection-permitting modelling for Africa**

Convection-permitting versions of the MetUM are run over the United Kingdom and some tropical regions (Tang et al. 2013) including Southern Africa, Eastern Africa and West Africa. A 4-km tropical Africa Model is run over Africa with its output data made available since September 2020. The data covers the latitudes 11°S to 22°N degrees and longitudes 19°W to 53°E. The output is freely accessible to the African operational meteorological centres in real time as part of the Met Office's contribution to the World Meteorological Organisation (WMO) Voluntary Cooperation Programme (VCP) (Hanley et al. 2021). Little work has been done on the evaluation of these products to date and there is no evaluation or understanding of forecast skill over West Africa.

Some validation have been done on different versions of the Met Office CP models over East Africa and the domain in Southern Africa. Chamberlain et al. (2014) evaluated the performance of the East Africa model and found a higher skill in predicting the timing of the storms as compared to the global model. Woodhams et al. (2018) assessed the added value of the CP model for forecasting extreme rainfall over tropical East Africa. The CP model showed greater skill than the global model. An increased hit rate of up to 20% was obtained over Lake Victoria. Hanley et al. (2021) evaluated the prediction of convective storms over Lake Victoria by comparing the Met Office CP

model configurations. They compared a Met Office CP model tuned for the tropical regions to that based on the UK model configuration. They found that, the tropical configuration compared better with satellite-derived rain-rates although the two configurations generally produced too much rain and too many small storms. When evaluated for different seasons, a delayed onset was observed over Lake Victoria in the tropical configuration. They hinted that, the precipitation field continues to spin up during the first 12 - 24 hr of the simulations and affects the accuracy of the outputs within this period. It is therefore suggested that using an ensemble approach could lead to a more skilful forecast (Woodhams et al. 2018). Cafaro et al. (2021) examined the CP ensemble forecasts produced by the UK Met Office over tropical East Africa using 24 cases from April-May 2019. The CP ensemble was generally more skilful in forecasting heavy rainfall than the CP deterministic forecast. CP ensembles remained skilful at scales greater than 100 km and were significantly better than the Global ensemble. The skill however decreases with lead time and varies diurnally. Keat et al. (2019) evaluated the the initiation of convective storms over South Africa during the summer months using the MetUM simulations at 1.5 km horizontal grid length. The maximum number of storm initiations occurred earlier in the model (at least 2 hours) as compared to the observations although the diurnal cycle was well captured. Contrary to previous CP studies in other regions, the modelled storms were generally less intense compared to the observations. However, the simulated storms exhibit similar intensity as the observed during the month of February where tropical influences dominate.

## 2.4 Summary

Since AMMA 2006 many studies have been performed over West Africa focusing on understanding the WAM and it's associated MCSs. However most of these studies have focused on the Sahel and in the JJA season. Relatively fewer studies have focused on SWA, the coast and other sub-regions of West Africa. Given the significant spatial variability of the climate of the regions and the uniqueness of the storms that dominate each sub-region in different seasons, a detailed investigation of the (thermo-)dynamic environment of MCSs in the various sub-regions and for all seasons is very important not just for forecasters but also for model developers.

The intensity of an MCS is affected among others by low level humidity, mid-level dry-

ness, availability of CAPE and vertical wind shear. Among these, studies such as Klein et al. (2020) have shown that vertical wind shear plays a dominant role in the intensification of an MCS. Studies by Rotunno et al. (1988), Alfaro (2017), Mulholland et al. (2021) and several others have used idealised models to propose the role of vertical wind shear in MCSs intensification. However, the exact mechanism through which vertical wind shear affects MCS intensity hasn't been thoroughly understood. It is therefore important to investigate the role of vertical wind shear in the intensification of an MCS.

MCSs are however poorly represented in NWP models as most models parameterise convection. With the availability of high resolution models comes the need to evaluate the representation of explicit convection in the models. An earlier version of the Met Office 4.4 km Tropical Africa model has been evaluated over East Africa (Woodhams et al. 2018). However, no detailed evaluation has been performed over West Africa since the model got operationalised in 2019. The Met Office Tropical Africa model is to be evaluated over West Africa in this study. This is to include the representation of precipitation and the the effects of vertical wind shear in the models.

# Chapter 3

# Method and datasets

## 3.1 Study area and MCS dataset

To understand the unique (thermo-) dynamic environments associated with MCSs in different parts of West Africa, the study area is demarcated into 6 sub-regions: Sahel, SWA, Coast, the North Atlantic (N. Atlantic), the Gulf and the Congo area where most MCSs are initiated (Figure 3.1). The demarcation of the region is useful to understand the dynamics of the different types of storm that dominates each sub-region as the climate of the region varies spatially from south to north (Nicholson 2018).

A 10-year MCSs dataset (1998-2007) from the data made available by Huang et al. (2018) was used for the development of the climatological characteristics of MCS features over West Africa. The MCSs were tracked from Cloud Archive User Service (CLAUS) brightness temperatures using a tracking algorithm that combines Kalman filter with the area overlapping method enabling small and fast moving MCSs to be tracked more effectively. The CLAUS brightness temperature data used is at 3 hourly intervals and at a 30 km resolution. In tracking the MCSs, an area threshold of 5000 $km^2$ and a brightness temperature threshold of 233 K were used. The brightness temperature threshold of 233 K was consistent with Goyens et al. (2012) who suggested the adoption of a 233 K as the best indicator for tropical convection after an assessment of other thresholds. A long-term (1985-2008) tropical MCS dataset has been generated using this algorithm and made available at https://doi.pangaea.de/10.1594/PANGAEA.877914. The various parameters defined in the data include a storm ID, lifetime, latitudes and longitudes of the geometric centre of the tracked storm, latitudes and longitudes of the weighted centre of the tracked storm, the storm size, eccentricity, the average brightness temperature, the minimum brightness temperature, the time of the occurrence of

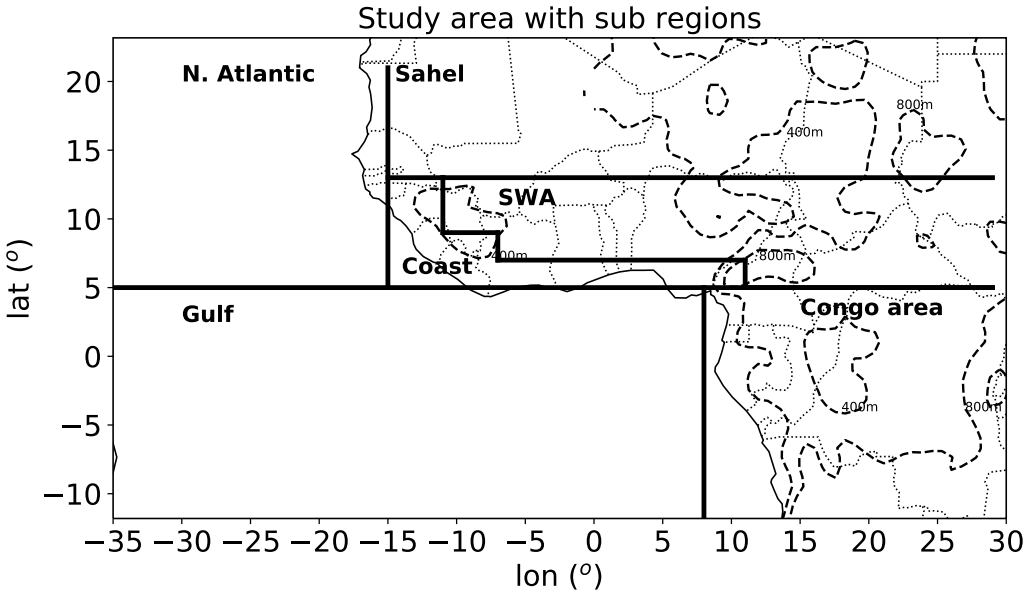


Figure 3.1: The study area and the various sub-regions: Gulf, N. Atlantic, Congo area, Sahel, SWA and Coast. Contours of orography (elevations greater than 400 m above sea level) are overlaid.

the storm, the storm speed and direction. Statistics performed on the tracked MCS dataset confirmed the robustness of the dataset and effectiveness of the tracking algorithm. The frequency of MCS occurrence corresponded with TRMM and GPCP rainfall distribution (Huang et al. 2018). The Huang et al. (2018) data being 3-hourly however means that, short lived storms (including storms with 4-5 h duration) can easily be missed. Such storms are more frequent over the Congo area and southern West Africa but might not be frequent over the Sahel where storms are mostly long-lived. However, given that, the number density of the storms used in this study is dominated by short-lived storms, the composites of short-lived storms used is still expected to be representative of the characteristics of short-lived storms.

A distribution of the MCSs by speed and lifetime (as proposed in Tomasini et al. (2006)) for the year 2007 is shown in Figure 3.2a. For the purpose of addressing the second research question, a re-classification of the storms by a selection of extremes of the lifetimes and speeds were made (Figure 3.2b). This resulted in:

1. Short-lived slow moving (SL_slow) - lifetimes <20 hr; speeds <10 km $h^{-1}$
2. Long-lived moderate speed (LL_moderate) - lifetimes >40 hr; speeds >25 km $h^{-1}$ and <50 km $h^{-1}$
3. Short-lived moderate speed (SL_moderate) - lifetimes <10 hr; speeds >25 km $h^{-1}$ and <50 km $h^{-1}$
4. Short-lived fast moving (SL_fast) storms - lifetimes <20 hr; speeds >60 km $h^{-1}$

Composites of above mentioned storm categories were analysed to assess the unique (thermo-) dynamics environments associated with these storm types for each of the sub-regions of West Africa (Figure 3.1). As many studies have already been done on storm initiations (e.g. Lafore et al. 2017), mature storms were selected for this study. Mature storms were defined as the point in the lifetime of an MCS where its brightness temperature was coldest. The features analysed include, the MCS lifetime, propagation speed, brightness temperature, diurnal cycle and inter-seasonal variability.

**TRMM 3B42 precipitation and ERA-Interim datasets**

The TRMM 3B42 version 7 precipitation product is used as the main satellite observational data in this study. The TRMM 3B42 estimates precipitation at $0.25^\circ \times 0.25^\circ$ spatial resolution and at a 3 hourly interval. This products combines inputs from mi-

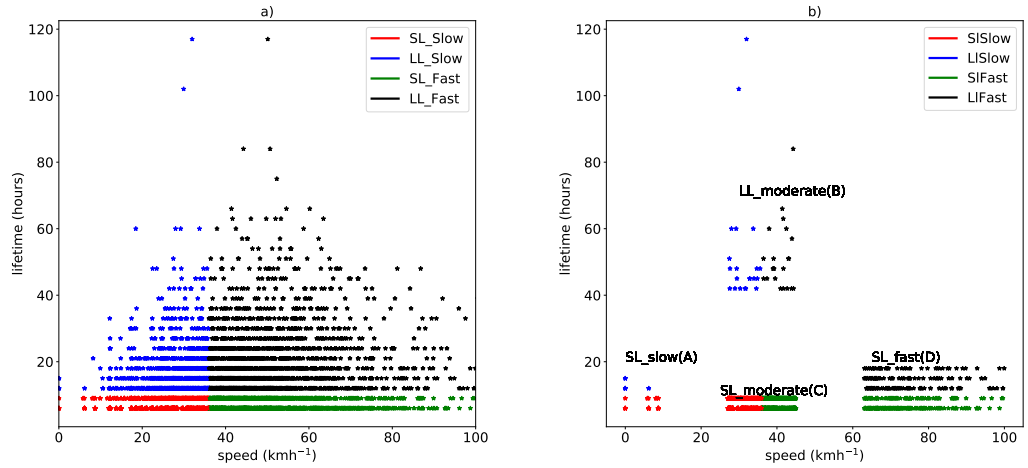


Figure 3.2: Distribution of MCSs for the year 2007 based on lifetime and speed as proposed in Tomasini et al. (2006): (a) whole distribution, (b) re-classification.

crowave and infrared sensors on board a variety of low Earth orbit satellites (Huffman et al. 2007; Chen et al. 2013). The data is available from 1998 - 2014. It is worth noting that the 3-hourly rain-rates estimated from TRMM do not exactly occur at the said hour. For instance, rain-rate at 06 UTC is the instantaneous rain-rate for the 04:30-07:30 UTC period. Studies with TRMM 3B42 have shown an improved representation of rainfall distribution (Michot et al. 2018; Zulkafli et al. 2014) as compared to the previous versions. However, an evaluation by Chen et al. (2013) suggests that, TRMM 3B42 may overestimate rainfall over the oceans and under estimate over lands although it is still generally more accurate over the oceans than over land (Chen et al. 2013; Ebert et al. 2007; Kubota et al. 2009).

Dinku et al. (2010) found that TRMM 3B42 underestimates rainfall over the Ethiopian highlands and other regions of complex terrain. Studies over West Africa have also shown a good agreement with gauge data (Nicholson et al. 2003; Dembélé and Zwart 2016). Dembélé and Zwart (2016) found a high correlation between TRMM 3B42 and gauge rainfall events in Burkina Faso but low correlation for rainfall amounts.

ERA-Interim reanalysis data is used for the investigation of the (thermo-) dynamic environments of the MCSs studied. It consist of a large range of 3-hourly surface parameters and 6-hourly upper air parameters available from 1989 - 2018 (Dee et al. 2011). The spatial resolution of the datasets is 0.7° × 0.7°. A detailed description of

the ERA-Interim product archive is provided by Berrisford et al. (2009).
In this study we use ERA-Interim upper air data and TRMM 3B42 version 7 for the period 1998-2007. The thermodynamic environments of each MCS were selected from ERA-Interim at the time of occurrence of the mature storm. As the temporal resolution of ERA-Interim was 6 hourly, only storms occurring at times coinciding with the ERA-Interim times were selected for the final analysis. Vertical wind shear was calculated by computing the vector difference between the wind at 925 hPa and 600 hPa which corresponds to the low-level south westerlies and the mid-level AEJ respectively.

It is recognised that there are likely some systematic biases in the ERA-Interim data set over Africa. Rainfall biases are more readily discussed in the literature (e.g. Gleixner et al. 2020) but information on wind biases, especially upper winds, have little information on reliability, probably due to a lack of upper level soundings over West Africa to compare to. It is with this in mind that we caveat our studies, understanding that there is uncertainty in the magnitude of the wind shear, and large scale comparisons or relative differences are used where possible.

## 3.2 Met Office Tropical Africa Model evaluation

### 3.2.1 The Met Office Tropical Africa Model

The TAM is run at 06Z and 18Z daily, out to 54 hours. It uses a 0.04 degree grid ($\sim$ 4.4 km), spanning 1850 $\times$ 900 grid-points. It covers the domain: 20°W to 54°E and 13°S to 23°N. It has 80 vertical levels with a model lid at 38.5 km. Timestep used is 120 seconds. It uses the Arakawa C horizontal grid, with Charney-Phillips vertical staggering. The JULES land surface scheme is used. SST's are prescribed using the OSTIA analysis, and soil moisture is initialised from the global model. The lateral boundary conditions from the Global model is used to force the model every 3 hourly. The edges are smoothed to remove discontinuities. The model does not have data assimilation but uses a 'cold start' approach to initialisation where the analysis is a downscaled version of the T+6h global model. This has the disadvantage that there are few convective structures in the analysis but the advantage is that there is data assimilation in the global model.

The TAM has been ran in a non-operational real time mode from March 2019 and became operational in March 2020 as a replacement to the East Africa CP model (Woodhams et al. 2018; Hanley et al. 2021). It has however been been upgraded from

the first Met Office Unified Model-JULES Regional Atmosphere and Land version 1.0 Tropical (RAL1-T) configuration (Bush et al. 2020) to RAL2-T since December 2020. Convection is treated explicitly in this configuration with one-way nesting inside the Global model (Hanley et al. 2021). In this study, TAM data for the period December 2019 - November 2020 was used.

### 3.2.2 The Met Office Global Model

The Global model (and the TAM) uses the Even Newer Dynamics for General atmospheric modelling of the environment (ENDGame) as it's dynamical core (Wood et al. 2014). The horizontal resolution of the Global model is 17 $\times$ 25 km over Africa. It is initialised every 0000, 0600, 1200 and 1800 UTC. For an easy comparison with the TAM only the 0000 and the 1200 UTC initialisations were used. The mass-flux scheme by Gregory and Rowntree (1990) was used for the parametrisation of convection in the Global model.

The Met Office Unified Model solves non-hydrostatic, deep-atmosphere dynamics using a semi-implicit, semi-Lagrangian scheme which allows stable integrations over long timesteps (Wood et al. 2014). The Global model has used the Global Atmosphere version 6.1 (GA6.1) configuration (Walters et al. 2017) but has recently moved to GA7.0/7.1 (Walters et al. 2019).

### 3.2.3 GPM IMERG products

The Integrated Multi-satellitE Retrievals for GPM (IMERG) Final Precipitation version 6 (V06) level 3 product was used to validate the models as in situ observations are sparse over the region (Hou et al. 2014; Huffman et al. 2015, 2017; Prakash et al. 2018). It has a 0.1 $\times$ 0.1° and 30 minutes spatial and temporal resolutions respectively. However only the times that marched the model outputs were used in this work. The data resulted from the inter-calibration, merging and interpolation of a network of satellite precipitation estimates from the GPM and TRMM eras and monthly gauge analysis (Huffman et al. 2015).

GPM outperforms it's predecessor, the TRMM 3B42 V7 product, in different parts of the world (Sharifi et al. 2016; Tang et al. 2016; Kim et al. 2017; Xu et al. 2017)

however other studies have revealed that GPM under-performs in dry climates and high altitudes (Tang et al. 2016). Particularly, there are uncertainties with orographic convection (Kim et al. 2017; Xu et al. 2017; Sungmin and Kirstetter 2018). This is a cause for concern in the mountainous regions of the Congo areas as well as the dry Sahel regions in the current study. Some studies have also highlighted the underestimation of high intensity rainfall events (Foelsche et al. 2017; Wang et al. 2017) which is also worth noting.

### 3.2.4 Verification method

The main challenge of tropical forecasting is the difficulty of NWP models to forecast the exact location and intensity of convection. Global models which parametrise convection result in widespread, weaker rainfall. So they miss the extreme rain-rates and put weak rainfall where there is no rain causing so much false alarms. To assess the TAM's ability to address this problem, the Fractions Skill Score (FSS) is used instead of the point-to-point verification method: this is because the traditional verification methods are unsuitable for verifying storm location. The small grids of the TAM means that the model gets penalised when rainfall is displaced and then for creating a false alarm (know as the 'double penalty problem').

The FSS addresses this problem by comparing the fraction of precipitation forecasted to the observed over several grid boxes known as the neighbourhood size (Roberts and Lean 2008).

This is done by:

1. Creating fractions matrix for different neighbourhood sizes ($n$).
2. Drawing an $n \times n$ box around each grid point.
3. Counting the the fraction of grid points with rain.
4. Computing the mean square error (MSE) between the model $M$ and observed $O$.
5. Finally calculating the FSS using the equation:

$$FSS = 1 - \frac{MSE_{(n)}}{MSE_{(n)ref}} \tag{3.1}$$

where $MSE_{(n)}$ and $MSE_{(n)ref}$ are given respectively as:

$$MSE_{(n)} = \frac{1}{N_x N_y} \sum_{i=1}^{N_x} \sum_{j=1}^{N_y} [O_{(n)i,j} - M_{(n)i,j}]^2 \tag{3.2}$$

$$MSE_{(n)ref} = \frac{1}{N_x N_y} \sum_{i=1}^{N_x} \sum_{j=1}^{N_y} [O^2_{(n)i,j} + M^2_{(n)i,j}] \tag{3.3}$$

It is important to note when computing the FSS fractions that, a threshold for precipitation need to be set above which a grid box will be considered as having rain or no rain. This can either be absolute or a percentile. Woodhams et al. (2018) and other similar works show that both the TAM and the Global models are too wet. Moreover, CP models have excessive rain rates – therefore percentile thresholds is chosen to define events in the FSS analysis instead of absolute rainfall intensities. Also using percentile threshold helps to reduce the problem of observation uncertainty.

To do a detailed evaluation of the TAM, the following tasks are performed:

1. Compute FSS for all the sub-regions of study and for all seasons using both daily and sub-daily rainfall accumulations.

2. Determine the nearest neighbourhood size for which the models have skill for the various sub-regions in order to ascertain the models' ability to simulate the location of convection.

3. Compute the Localised Fractions Skill Score (LFSS) as defined in Woodhams et al. (2018) for all season over the whole domain in order to determine the spatial variation in the skill of the models).

4. Compute and compare the skills of the global model and the TAM for varying rainfall intensities in order to evaluate the performance of the models in capturing high intensity rainfall events.

5. Compute the FSS for different times of the day for all regions and all seasons.

The above listed tasks were performed for both the TAM and the Global models, using the GPM rainfall data as observation. By performing these tasks, the models' ability to forecast rainfall of different intensities, including the timing, location, and the repre-

sentation of the diurnal cycle of convection was ascertained. The areas in West Africa with higher skill and their implication to forecasters as well as model developers were also identified and discussed, providing a better understanding of processes that are better represented in the models.

It is acknowledged that there are limitations of the datasets and methods used in the thesis. These limitations result from many underlying issues, most notably the sparse observation sampling network which makes it difficult to constrain both model and observation data sets over Africa. However, the methods and datasets used are well documented and curated and this means that the findings in this thesis will be more closely linked to wider literature.

# Chapter 4

# The environment, characteristic lifetime and speed of Mesoscale Convective Systems in West Africa

## 4.1 Introduction

Improving our understanding of the (thermo-)dynamic environment associated with MCSs is crucial as forecasting MCSs remains a major challenge in this region. This chapter focuses on improving our understanding of the environments associated with MCSs in the sub-regions of West Africa and investigates the reasons behind the characteristic lifetime and speed of these storms. Such knowledge will not only benefit forecasters but also aid to improve the representation of MCSs in NWP models and improve climate projections as the intense warming of the Sahel under climate change is expected to increase the frequency of MCSs with colder cloud tops and high rain-rates through a strong meridional temperature gradient (Taylor et al. 2017). Two main research questions are addressed in this chapter: (i) What is the typical environment associated with intense MCSs in the various sub-regions of West Africa? and (ii) What determines the lifetime and speed of an MCS in West Africa?

Maranan et al. (2018) investigated the convective environment associated with seven different types of rain bearing systems in SWA using three-dimensional reflectivity data

from TRMM-Precipitation Radar. The seven categories of rain bearing systems were Isolated Shallow Echo (ISE), Moderate Convection (MOD), Strong Convection (STR), Deep Convective Core (DCC), Wide Convective Core (WCC), Deep and Wide Convective Cores (DWC) and Broad Stratiform Regions (BSR). They found that highly organised MCSs (mainly the WCC, DWC and the BSR as they were linked to matured MCSs) normally occurred in strongly sheared environments in the presence of mid-level northerlies ahead of a cyclonic vortex. MCSs in SWA propagated slowly compared to those in the Sahel and occur mostly during the first coastal rainy season. Weakly organised MCSs (mainly the MOD, STR and DCC) contributed to about 90% of the rainfall systems in SWA. Less organised convection occurred during and after the passage of a cyclonic vortex. These less organised storms occurred within a regime of deep westerly anomalies, low wind shear and low to moderate CAPE (known as the monsoon or vortex rainfall). Organised convection in SWA typically lasted for more than 9 hours whereas less intense rainfall types were short-lived. Maranan et al. (2018) also found that the most intense storms were associated with mid-level wave disturbances and highlighted the need for further investigation on this.

Over the Sahel however, Taylor et al. (2017) identified changes in surface temperature gradients and associated changes in wind shear to be important for MCS intensification in recent decades. Following the work of Taylor et al. (2017) over the Sahel, Klein et al. (2020) identified a relationship between trends in intense MCSs and their associated atmospheric drivers in SWA. These drivers are vertical wind shear which resulted from increased meridional temperature gradients, specific humidity and drier mid-levels. The peak of the monsoon season has been characterised by a strong instability in SWA. However, Klein et al. (2020) also identified a less unstable but moist period in SWA after June. They speculated that MCSs during this period are more likely to be influenced by total column water vapour. They compared the sensitivity of MCS intensity and peak rainfall to low-level moisture and wind shear conditions preceding events and concluded that wind shear plays a dominant role in the intensification of MCSs. These studies and other previous works have shown that the environment for most intense MCSs in SWA and the Sahel but no single study has shown how the storm environment vary across all sub-regions in West Africa.

To investigate the environments associated with long-lived storms, Yang et al. (2017) simulated a realistic structure and frequency distribution of the lifetime and precipitation of MCSs over central United States using the convection-permitting Weather

Research and Forecasting (WRF) simulations. It was found that, MCSs systematically form over the central Great Plains ahead of a trough in the westerlies in combination with an enhanced low-level moist jet from the Gulf of Mexico. Long-lived MCSs occur closer to an approaching trough than shorter-lived MCSs. They also showed that long-lived storms exhibit the strongest feedback to the environment through diabatic heating (in the trailing regions of the MCS). The feedback strengthens the synoptic scale trough associated with the MCS by producing an anomaly circulation which is characterised by a divergent perturbation at higher levels over the MCS and a mid-level cyclonic circulation perturbation near the trough line in association with the trailing portion of the MCS. By comparing short-, medium- and long-lived MCSs, Yang et al. (2017) found that it was only the medium-lived MCSs that were associated with stronger upper-level vertical wind shear. They suggested that there might be an optimal environmental shear beyond which shear effects might not be realised. Coniglio et al. (2010) identified the nocturnal low level jet, frontal zone, moisture profile and wind shear as the key elements that distinguishes the longevity of MCSs in central United States. It is necessary to investigate the environments of long-lived MCS in West Africa and how these environments compare with studies in other regions.

The relationship between MCSs and their large-scale environment must be captured well by weather and climate models to be able to make accurate weather forecasts and future projections. Investigating the environmental conditions associated with long-lived storms is the first step in the quest to assess and improve model performance. All the above mentioned studies have made an attempt to describe the convective environments associated with intense MCSs but none of them has made a detailed comparison across the various sub-regions of West Africa. In this chapter, the characteristics of the various storm types that affect each sub-region and their associated (thermo-)dynamic environments is studied. The reasons for their characteristic lifetime and speed is also investigated. Section 4.2 describes the climatology of the (thermo-)dynamic environments associated with MCS in the study regions and section 4.3 identifies the reasons for the characteristic lifetimes and speeds of the MCSs. The results are summarised and concluded in section 4.4.

## 4.2 Climatology of the (thermo-)dynamic conditions associated with MCSs

### 4.2.1 Climatology of the number of MCSs and associated near surface winds

To understand the (thermo-) dynamic environments associated with the MCSs in the different regions in West Africa, the climatology of the number of MCSs and it's relationship with orography and the 925 hPa winds is first assessed with the aim of providing clarity on the relationship between near surface convergence, orography and number of MCSs that affect each region. A higher number of MCSs occurs in SWA, the Coast, the Gulf and the Congo area compared to the Sahel. This is because the former regions experience two storm seasons consistent with the oscillation of the Intertropical Convergence Zone (ITCZ) while the later experiences only one season (Baidu et al. 2017; Aryee et al. 2018; Maranan et al. 2018). Most of the MCSs are found in regions with a strong surface (925 hPa) convergence and elevated orography (Figure 4.1). Another prominent feature associated with MCSs is the effect of coastal convergence (Alestalo and Savijärvi 1985) on the number density of MCSs which seen mostly at the coast of Liberia, the Congo area and the eastern coast of Nigeria.

The number of MCSs that affects the different regions of West Africa varies with season. The relationship with orography and near surface convergence in each region is better understood when investigated for each season. The number of MCSs that affect West Africa in each season is shown in Figure 4.2. The number of MCSs appears to be associated with the north-south oscillation of the ITCZ. The number of MCSs is higher over the Gulf of Guinea in December - February (DJF), reaches the coast and SWA in March - May (MAM), the Sahel in June - August (JJA), and then retreats back in September - November (SON). The convergence associated with the ITCZ intensifies and results in more MCSs as it approaches the coastlines of Liberia, the Congo area and east coast of Nigeria, confirming the effects of the coastal convergence mentioned earlier (Alestalo and Savijärvi 1985). These regions are also regions with high orography. As the near-surface (925 hPa) winds approach the orographic features they are forced to lift leading to the initiations and strengthening of more MCSs (Houze Jr 2012; Marwitz 1983; Wei-Jen Chang 1982).

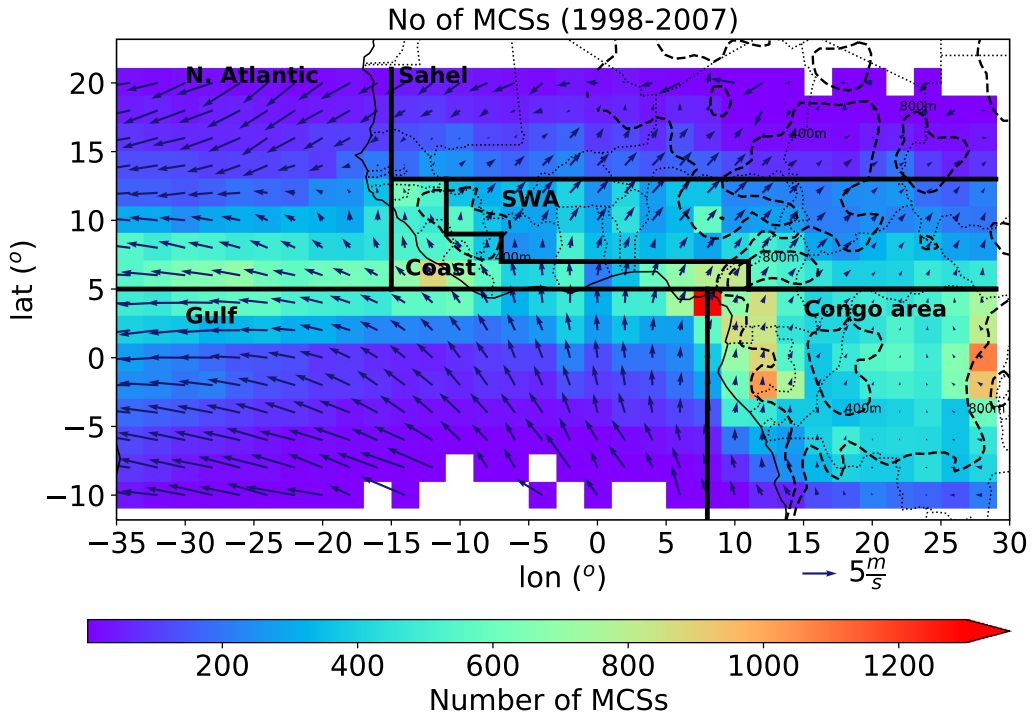


Figure 4.1: Number of MCSs in West Africa (1998-2007). The 925-hPa winds and contours of orography (elevations greater than 400 m above sea level) are overlaid. Also shown is the demarcation of the study region into the various sub-regions: Gulf, North Atlantic, Congo area, Sahel, SWA and Coast.

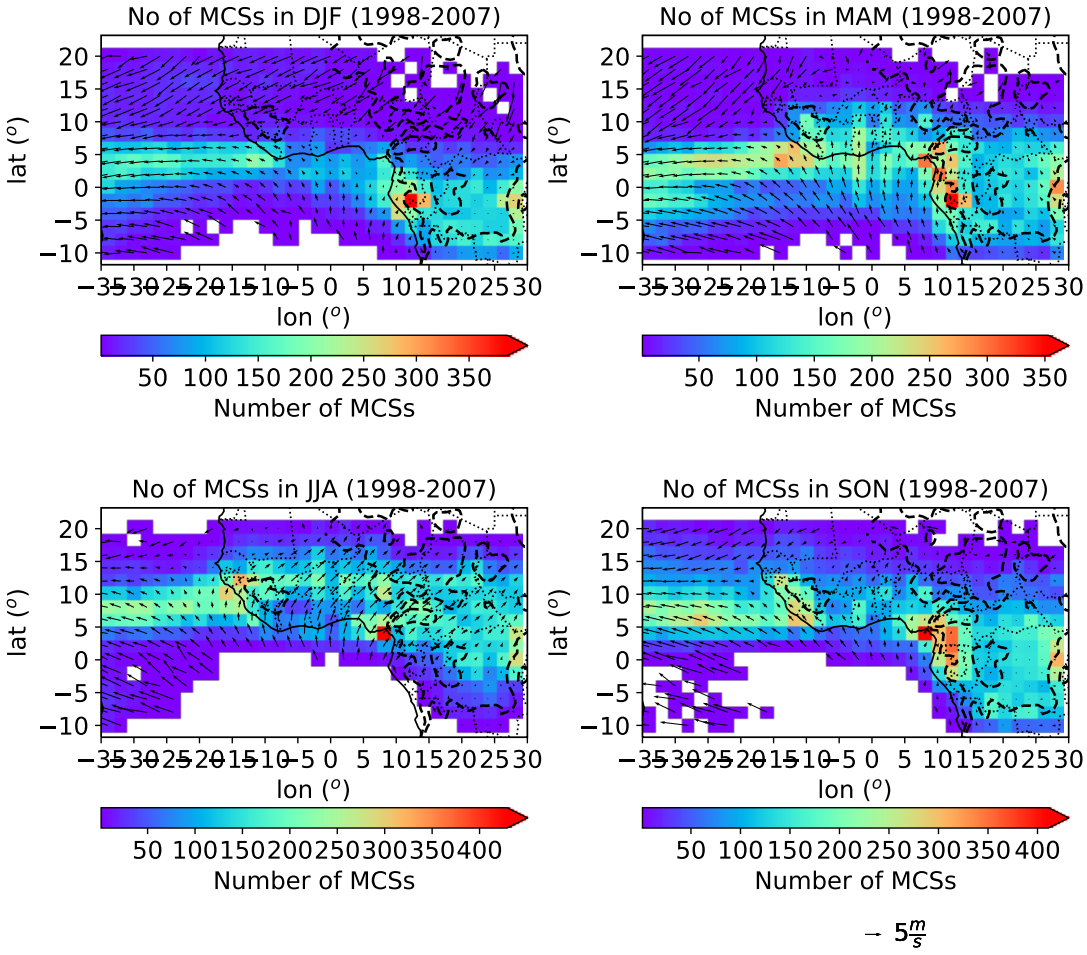


Figure 4.2: Same as figure 4.1 but for different seasons.

### 4.2.2 Characterising the thermodynamic environments of storms in various sub-regions

The climatology of the thermodynamic environments of storm composites in the different sub-regions of West Africa is examined for parcels lifted at different pressure levels beginning from the surface (925 hPa) to the upper levels (Figure 4.3). Generally storms over the oceans are associated with lower CAPE and a lower level of neutral buoyancy (LNB) as compared to MCSs over land. Storms over SWA and the Congo area are associated with the highest values of CAPE. The Coast and the Sahel follows respectively. Storms in the Sahel are associated with the highest Convective Inhibition (CIN) followed by SWA. The mean winds associated with the storms at all pressure levels are also shown in Figure 4.3. Storms over the land are dominated by strong easterlies from mid to upper levels. Storms over the ocean have weak or no easterlies at upper levels. The mean rain rates and storm speeds are given on the top left of each plot. Storms over the oceans and the coast have the highest rain rates but are slow moving. The Sahel has the lowest rain rate but the fastest storms.

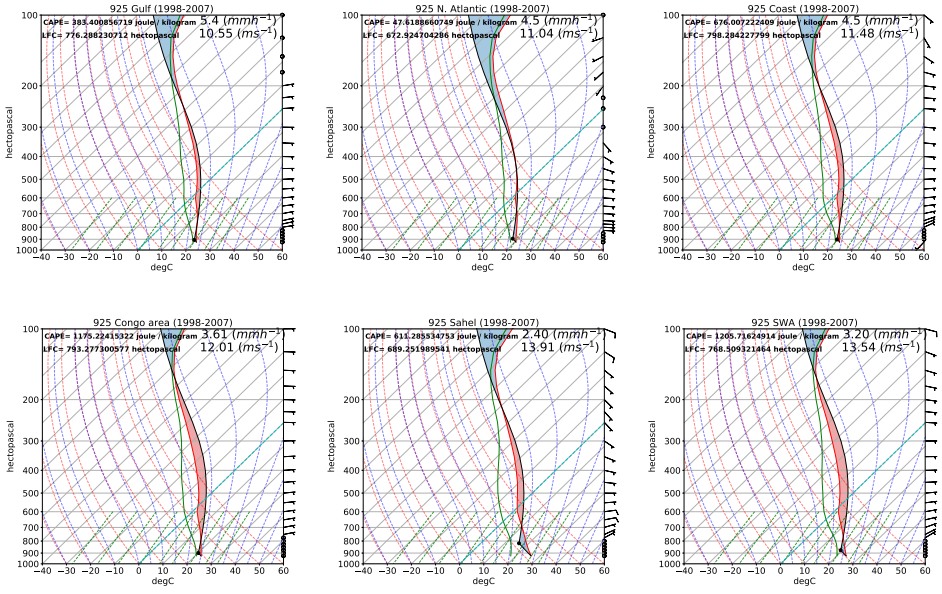


Figure 4.3: Tephigram of storm composites in the different sub-regions. The mean speed of the MCSs and their associated rain-rates are printed on the top right of each plot.

Figure 4.4 summarises the profile of the environments of storm composites when parcels

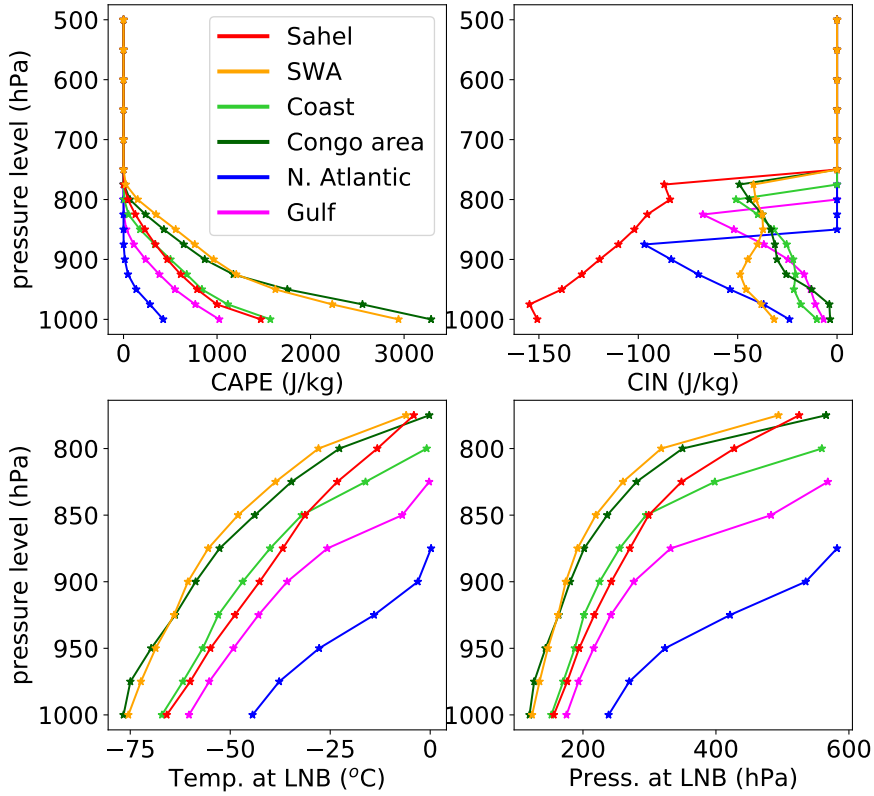


Figure 4.4: CAPE, CIN, temperature and pressure at the LNB of parcels lifted from different levels.

in the environments are lifted from different levels. The amount of CAPE available decreases sharply for oceanic storms when parcels are lifted from higher levels. Storms over SWA and the Congo area continue to have significant CAPE until about 800 hPa. Storms over the Sahel are associated with the highest CIN but this decreases as parcels are lifted from higher levels. Compared to the Sahel, storms in the remaining regions are associated with lower CIN values but the amount of CIN in these regions generally increases as the parcels are lifted from higher levels. In relation to the available amount of CAPE, storms in the Congo area and SWA have the coldest temperature at the LNB while the North Atlantic and the Gulf have the warmest temperature at the LNB.

### 4.2.3 Characterising pre to post convective environments

Before analysing the detailed dynamical environments of each sub-region in the various seasons, we investigate the pre to post storm environmental conditions to determine the features that lead to intense MCSs and when in time they occur. The relationship between divergence, vertical velocity and rain rate two days before and after the matured storm composites is investigated and the results presented in Figure 4.5. A strong surface convergence is associated with oceanic and coastal storms resulting in strong vertical velocities on the day of the storm and a corresponding upper-level divergence. This results in high rain-rates on the day of the storms as the strong surface convergence leads to a strong influx of moisture into the storms. Land storms are also associated with strong surface convergence, corresponding vertical velocities and upper level divergence, however, the convergence associated with land storms maximises at around 800 hPa for the Congo area and SWA but about 700 hPa for the Sahel. The surface convergence associated with the land MCSs is seen to occur at about 6 hours before the arrival of the storm. This convergence is elevated with time and maximizes around 800 hPa resulting in strong vertical velocities, a weak upper level convergence indicating the presence of the storm and an upper level divergence. The figure also shows the potential of new cells being triggered by an old storm. The surface convergence elevates with time, result in strong vertical velocities moving upwards with time resulting in high rain rate convective systems with associated upper level divergence. Low-level outflow (cold pools) from the storms and its associated surface divergence is also seen (with the possibility of triggering another convergence).

The relative vorticities associated with the matured storms 2 days before and after the arrival of the storms are shown in Figure 4.6. High relative vorticity values are observed between 800-600 hPa on the storm arrival day for all the regions except the Sahel and the Congo area. Over the Sahel relative vorticity is generally high between about 975-800 hPa but decreases about 12 hours towards the arrival of the storm and maximizes when the storm arrives. Elevated convection associated with Sahelian storms might be shallower than that associated with SWA storms as inferred from the level of relative vorticity maxima in the two regions. In the Congo area, relative vorticity remains generally high between 800-150 hPa. Generally, relative vorticity is maximized after about 6 hours after the arrival of the storm.

As will be shown later in Figure 4.14, the region of maximum relative vorticity at mid-

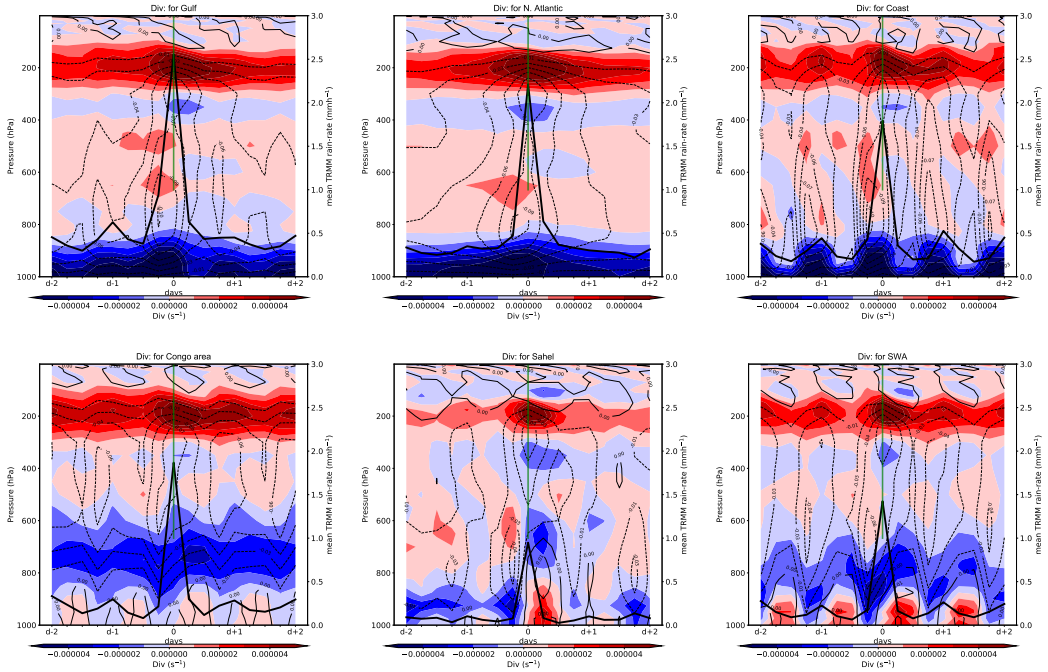


Figure 4.5: Divergence ($s^{-1}$), vertical velocity (Pa $s^{-1}$) and TRMM 3B42 rain rate (mm $h^{-1}$) 2 days before and after storm.

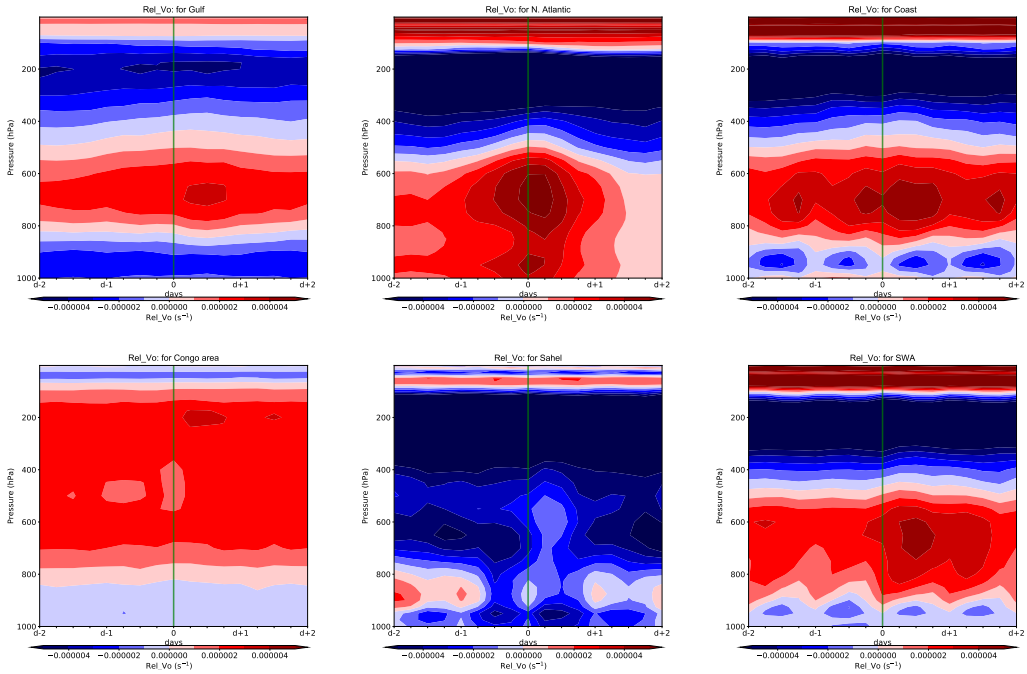


Figure 4.6: Relative Vorticity ($s^{-1}$) 2 days before and after storm.

levels (mostly between 600 - 800 hPa) coincides with the trough axis of the African Easterly Wave (AEW) (Tomassini et al. 2017). The North Atlantic, SWA, the Coast and the Sahel are the regions that are mostly influenced by the AEW. The influence of the AEW on MCSs is investigated and discussed in detail in section 4.3.2.

### 4.2.4 Spatial environments of MCSs in the various sub-regions

We now proceed to investigate the environments of the storm composites for the different regions in different seasons. The divergence at 925 hPa, relative vorticity at 600 hPa and the wind speed at 600 hPa (to help detect the AEJ core) are plotted in Figure 4.7. The results for the main seasons of each region are shown for the conditions 6 hours before the arrival of the storm as Figure 4.5 showed that maximum convergence and associated vertical velocities occurs at this time. The main seasons for each of the sub-regions was defined as the season with the the largest number of MCSs as shown in section 4.2.1. The main seasons for the Gulf and Congo area are MAM and SON, respectively, while JJA (the peak monsoon season) is the main season for the remaining regions.

The results generally show that a strong surface convergence is associated with high relative vorticities and wind speed at mid-levels for almost all the regions. Over the oceans and the coast, a strong convergence is associated with the storm locations whereas a relatively weaker convergence is associated with the location of land storms with the ITD region located north of the storm location.

Sahelian JJA storms are the storms with the strongest sheared environment (bottom-middle of Figure 4.7). The strong sheared environment is characterised by a strong AEJ with a core speed greater than 10.5 $\mathrm{m\,s^{-1}}$ located on the western side of the mean storm location and strong southerly 925-hPa winds (possibly driven by a strong St. Helena high pressure system). There are also north-easterly 925-hPa winds which together with the southerly winds results in the near surface convergence required for storm enhancement. The typical Sahelian storm in JJA is also located just southward of the ITD (the region of strongest surface convergence). A mid-level (600 hPa) relative vorticity maxima is located just southward of the mean storm location. This is the typical environment that results in the number of storms that occurs in the Sahel during the peak of the monsoon season (JJA).

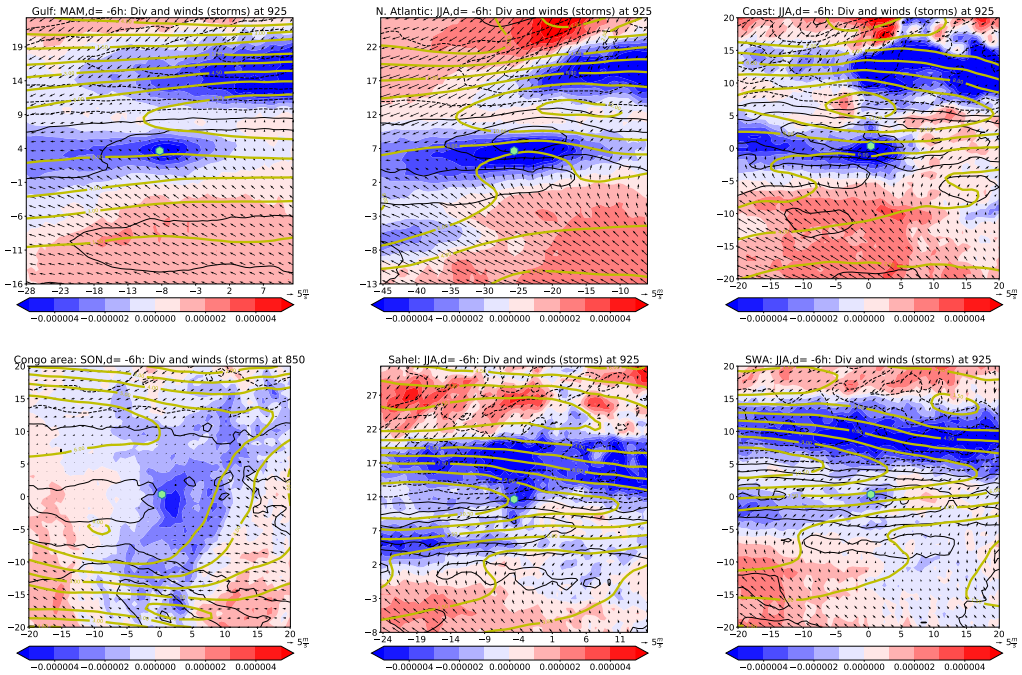


Figure 4.7: Divergence ($s^{-1}$) at 925 hPa (shaded), Relative Vorticity ($s^{-1}$) (black contours) and wind speed ($ms^{-1}$) at 600 hPa (yellow contours) associated with storm composites for the main season of each region.

The typical JJA SWA storm is located slightly southward of the AEJ within a zone of about 7.5 $\mathrm{m\,s^{-1}}$ AEJ speed (bottom-right of Figure 4.7). Located within a convergence zone created by strong south-westerlies and slightly weaker north-easterlies resulting in a significant vertical wind shear zone. The SWA JJA storm is located right at the core of the mid-level relative vorticity maxima and further south of the ITD (compared to the Sahel) resulting in more intense storms in this season.

North Atlantic storms happen to be the storms with the second highest shear environment after the Sahelian storms in JJA (top-middle of Figure 4.7). The typical North Atlantic JJA storm lies slightly southward of the AEJ core within a wind speed zone of about 8 $\mathrm{m\,s^{-1}}$. The North Atlantic storm is located within a strong convergence region characterised by strong 925 hPa southerlies and northerlies. The North Atanltic storms are located close to the centre of the relative vorticity maxima indicating a strong association with the AEW as will be shown later in section 4.3.2.

Coast JJA storms are located within a strong convergence zone and close to the center of the mid-level relative vorticity maxima. It is located at about 5 latitutes southwards of the AEJ core but lies within an AEJ wind speed of about 8 $\mathrm{m\,s^{-1}}$ and further south of the ITD.

The Gulf of Guinea MAM storm lies in a strong convergence region located at the south-western side of the AEJ core. It is usually associated with an AEJ speed of about 7 $\mathrm{m\ s^{-1}}$ and east of the mid level relative vorticity maxima. It is also located further south of the ITD latitude.

The Congo area SON storm has a unique environmental feature. It is located west of a convergence zone resulting form strong winds form the east (possibly the Indian ocean) but east of the mid level relative vorticity maxima. Lying further south of the AEJ core, the Congo area SON storm is located within the weakest shear region.

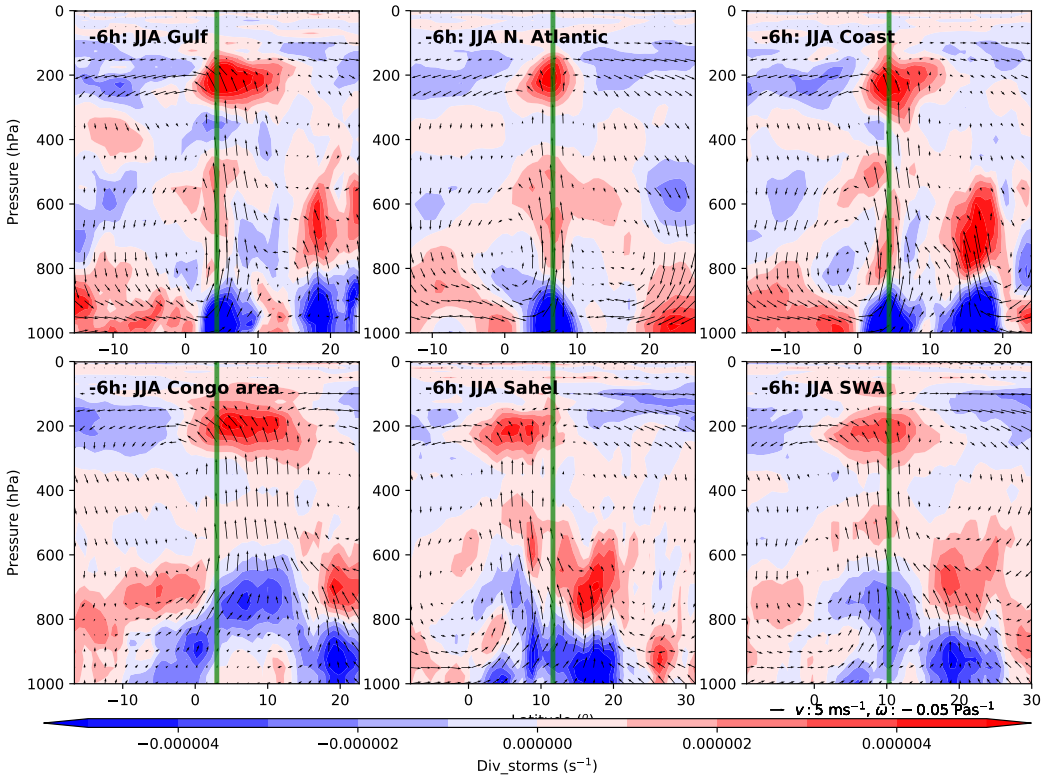


Figure 4.8: North-south vertical transect along the longitude of the storm composites showing divergence ($s^{-1}$, shaded) and the combination of meridional wind ($m\,s^{-1}$) and vertical velocity (Pa $s^{-1}$) (shown as arrows).

### 4.2.5 Vertical transect along the longitude of the storm

A vertical transect along the longitude of the storm composites in each region is shown in Figure 4.8. The low level convergence associated with the storm composites generally has it's associated divergence at upper levels (200 hPa). The low level convergence associated with land MCSs maximizes around 800 hPa.

Over the oceans and the coast, a low level convergence occurs at the surface and results in strong vertical velocities which induces an upper level divergence at the location of the storm. The low level convergence associated with the storms over the Gulf induces a mid-level dipole of divergence to the left and convergence to the right of the mean storm location. Winds from the southern side of the ocean and the land area converges

to sustain intense MCSs over the Gulf. There is an intense surface convergence zone at the northern side of the mean storm location with indicates the mean location of the ITD. Over the North Atlantic, a stronger surface convergence zone is associated with the mean storm location which induces intense vertical velocities and a mid-level divergence before an intense upper level divergence around 200 hPa. The storms over the Coast exhibits quite a similar environment to that of the oceans except for a few outstanding differences. There is a strong divergence over the ocean which feeds into the low level convergence at the Coast from the southern side. The northern side is supported by a weak inflow at the surface from the ITD region but stronger inflow from the mid levels due to mid level divergence induced by the convergence at the ITD region. Similar to the mean situation over the Gulf, a mid-level divergence is found to the left of the mean storm location with seem to induce a weak convergence to its right.

Over the Congo, SWA and the Sahel, the convergence associated with the storms seem to intensify at mid-levels; generally between 850-650 hPa. The Surface convergence associated with Congo storms is particularly interesting. A strong surface convergence occurs to the south and the north of the mean storm location which seem to elevate towards the storm centre and intensifies at the mid-levels around 750 hPa. This results in a large region of strong vertical velocities inducing a strong upper level divergence. The surface convergence at the northern side of the mean storm location over the Congo is likely a result of the presence of the ITD. Over the Sahel, the latitude of the mean storm location is very close to the location of the ITD (to its north). A strong surface convergence at its south which continues towards the mid-levels induces strong vertical velocities and an upper level divergence which dominates the southern side of the mean storm location. As seen in the other land regions, the convergence associate with the ITD induces a strong region of divergence at the mid-levels. Over SWA, the mean storm location is also sandwiched between two regions of low level convergence; to the south and the ITD region in its north. The surface convergence at the storm location intensifies at the mid-levels ($\sim$750 hPa) and induces strong vertical velocities and a corresponding upper level divergence. There is a small region of divergence above the level of the near surface convergence zone for the SWA and Sahelian storms. The elevation of the near surface convergence to mid levels seen with land storms is quite interesting and requires further investigation.

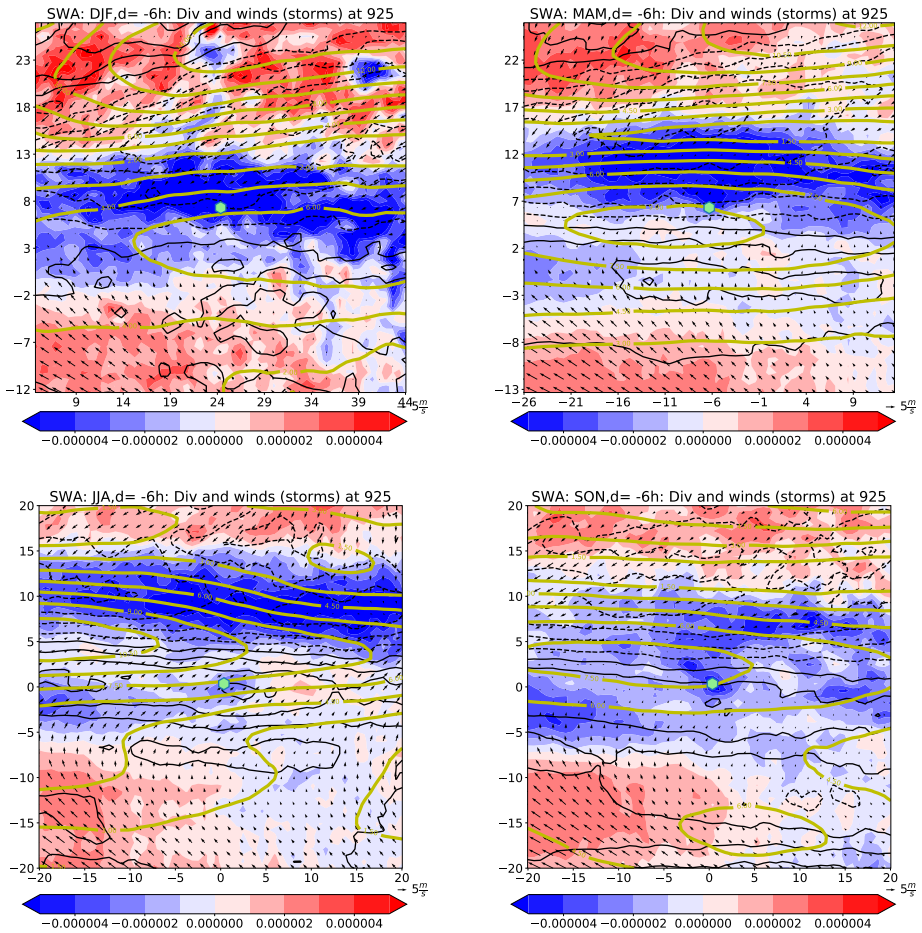


Figure 4.9: Same as Figure 4.7 but for all seasons in SWA.

### 4.2.6 Seasonal cycle in environmental conditions by region

The detailed seasonal cycle in environmental conditions associated with the MCSs in SWA, the Sahel and the Congo area is presented in this section. The evolution of the synoptic scale conditions associated with SWA storms in the various seasons is contrasted with that of the Sahel. The Congo area being the region where most West African storms are initiated is also investigated.

Figure 4.9 shows the results for SWA storms. Generally, the ITD region (the strong convergence zone) coincides with a region of negative 600 hPa relative vorticity and a strong 600 hPa wind speeds (the AEJ core) lying slightly south of the ITD region.

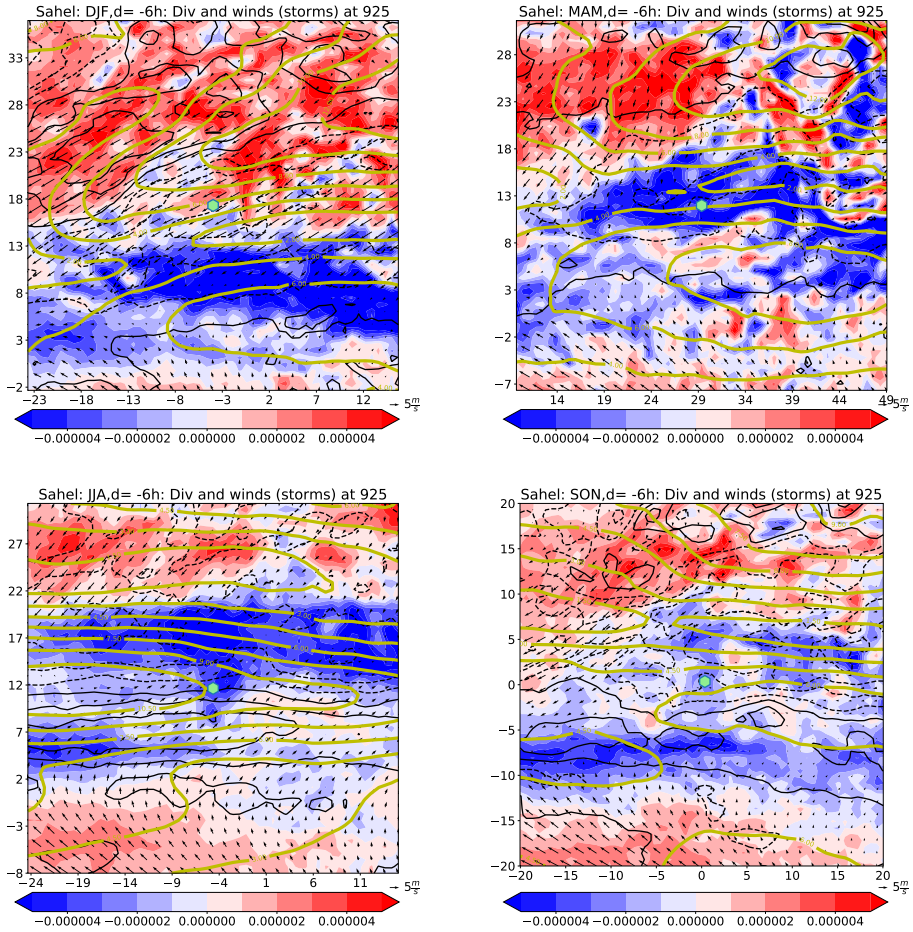


Figure 4.10: Same as in Figure 4.7 but for all seasons in Sahel.

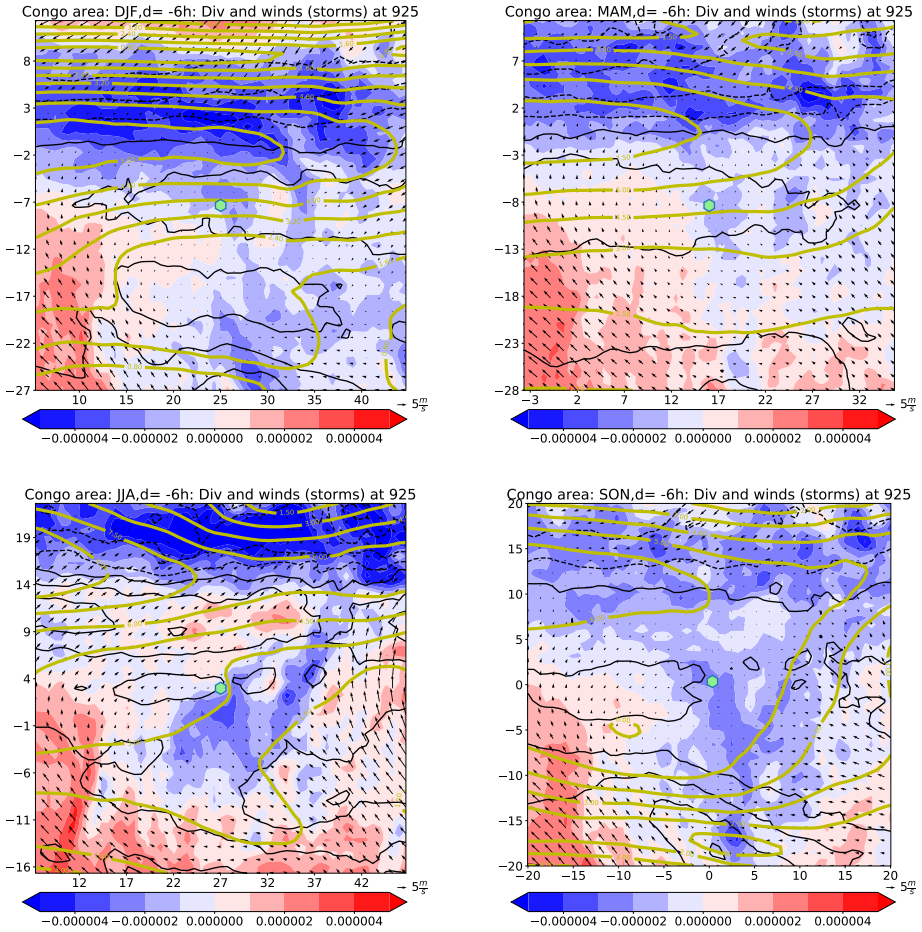


Figure 4.11: Same as in Figure 4.7 but for all seasons in Congo area.

DJF is the season with the least number of storms in SWA. The typical storm that occurs in the region during this period is normally associated with some convergence at 925 hPa 6 hours before the storm arrival. The convergence associated with the storm coincides with the strongest convergence zone (the ITD region). Weak 600 hPa winds and a positive relative vorticity lies slightly below the latitude of the storm.

The ITD begins its northward migration in MAM. SWA squall lines begin to occur in this season. Storms that occur in this season are normally located slightly below the ITD region (the band of strong convergence) and associated with stronger 600 hPa winds and positive relative vorticity lying slightly below the storm location.

The typical SWA storm that occurs in JJA is associated with a surface convergence located south of the ITD region. This is collocated with a region of very strong relative vorticity and south east of the AEJ core.

The ITD begins to retreat southwards in SON. The typical MCS that occurs in SWA during this season is located in a surface convergence zone located slightly south of the ITD region. This is collocated with a region of strong relative vorticity and east of the AEJ core.

Over the Sahel (Figure 4.10), very few MCSs occur in DJF. The typical MCS that occurs in the Sahel in DJF is located at a latitude above the ITD region. This is usually a region of weak 600 hPa wind speeds and a negative relative vorticity. However, in MAM, Sahelian storms are normally located in the ITD region which is a region of negative 600 hPa relative vorticities and slightly north of the AEJ core. However in JJA where the ITD is in its northernmost position, the Sahelian storm is located south of the ITD region, just north of the positive relative vorticity region and east of the AEJ core. As the ITD begins its migration southwards in SON, MCSs that occur in this region occur north of the ITD region, north-west of the AEJ core and north of the positive relative vorticity region.

The Congo area is also given a special focus because of it's unique features like orography that leads to the initiation and strengthening of most MCSs in West Africa (Figure 4.11). In DJF, storms in the Congo area are collocated with a convergence region south

of the deep convergence band (ITD region). This is south of the 600 hPa wind speed core and a region of maximum relative vorticity. In MAM, the deep convection band moves further north, the typical storm in this season is associated with a convergence zone south of the 600 hPa wind speed core and a maximum relative vorticity region. A strong convergence is associated with the Congo storms in JJA. This convergence zone is further south of the AEJ core. Relative voriticiy at 600 hPa is also maximum at this point. In SON, the convergence around the storm location gets stronger, the AEJ core retreats southwards. The storm is also located east of the strongest relative vorticity region. SON has the highest number of MCSs in the Congo. Followed by MAM. Number of MCSs in the Congo seem to follow the characteristics associated with the evolution of the ITD: AEJ, shear, moisture convergence etc. The coastal areas of the Congo trigger and sustain more storms possibly because of moisture convergence from the ocean which seem to converge around (the windward side of) the mountainous areas of this region. The jet core is greater than 5.6 $\mathrm{m\,s^{-1}}$ in DJF but greater than 7.5 $\mathrm{m\,s^{-1}}$ in MAM explaining why there are more MCSs in MAM than DJF. The jet core is greater than 9 $\mathrm{m\,s^{-1}}$ in JJA but lies further away from the region (north western side) during this season. The Jet core is greater than 6 $\mathrm{m\,s^{-1}}$ in SON but is associated with the greatest number of storms because it lies right over the Congo region creating a strong shear required for more intense storms. This seem to support the speculation by Taylor et al. (2018) that, increasing baroclinicity over West Africa may be contributing to long-term MCS intensification within the Guinea Coast region at latitudes where the AEJ provides a strong shear.

## 4.3 The characteristic lifetimes and speeds of the MCSs

The aim of this section is to understand the reason for the characteristic lifetimes and speeds of MCSs that affect West Africa. This is investigated using the classification introduced in section 3.1. The climatology of the number of storms in each category is first analysed before the reasons for these categories are investigated.

### 4.3.1 Number density, location and average sizes of different MCS categories

Figure 4.12 shows the number density of MCSs in the various categories introduced in section 3.1. SL_slow MCSs occur mostly over the oceans, SWA and parts of the Congo

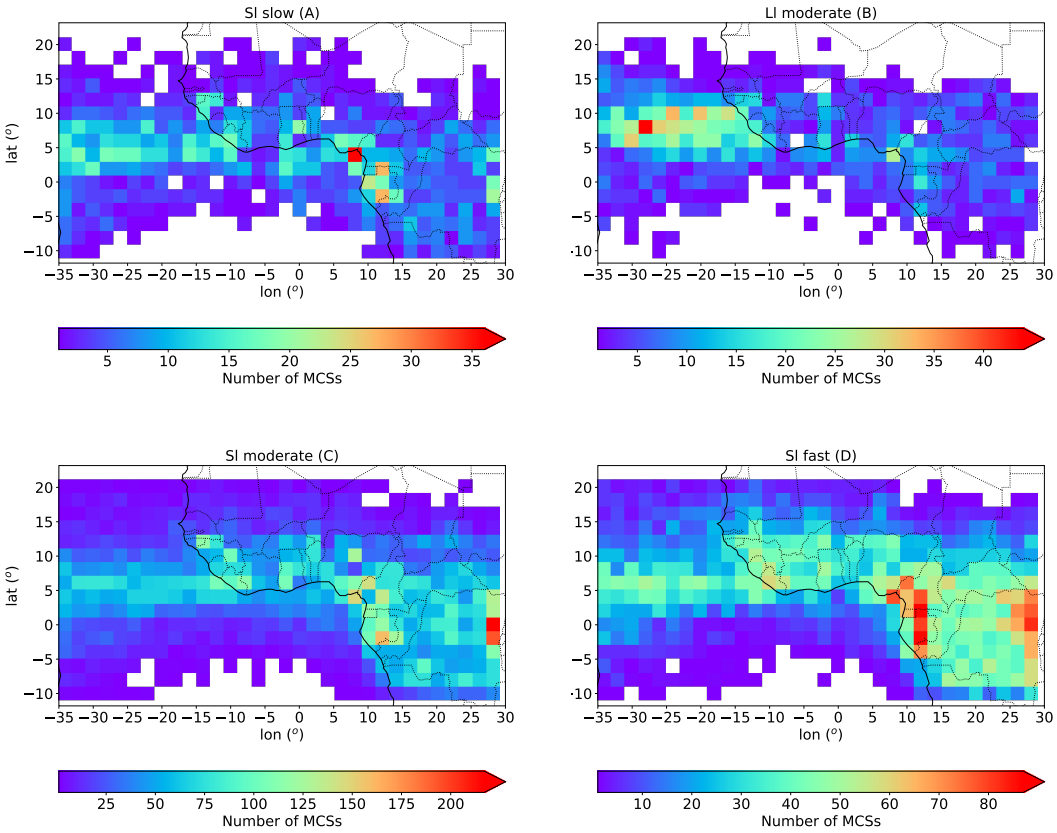


Figure 4.12: Number density of the four storm classes.

area where most storm initiations occur. LL_moderate storms dominates the North Atlantic and parts of the Congo areas. SL_moderate storms occur in all regions except the Sahel and southern parts of the Gulf of Guinea. SL_fast storms occur in all regions especially the Congo area, SWA and N. Atlantic.

The average sizes of the MCSs of each class was first computed over the 6 sub-regions and the results are shown in Figure 4.13. Generally, long-lived MCSs have larger sizes compared to short-lived ones. Long-lived moderate speed MCSs have the largest sizes. These MCSs are mostly associated with squall lines (Lafore et al. 2017). The next storm category with large sizes is short-lived fast moving MCSs. MCSs over land are generally larger than their oceanic counterparts.

Investigating the regional variation in storm sizes revealed Sahelian long-lived storms as the largest. Long-lived storms over the Congo also had large sizes following Sahelian

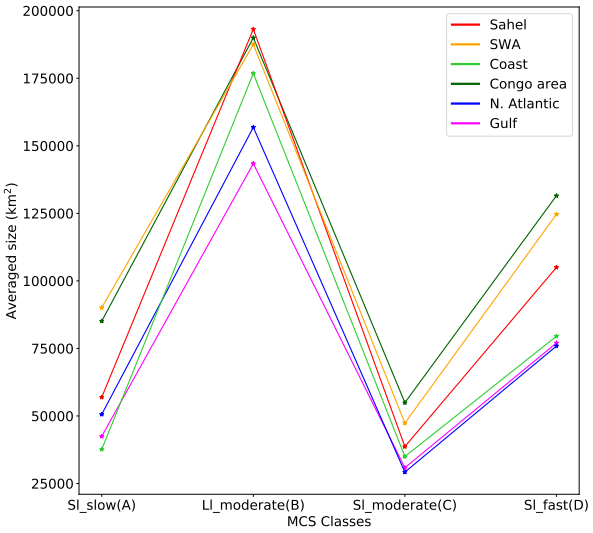


Figure 4.13: Average sizes of the various MCS classes.

long-lived storms. SWA long-lived storms were also found to be larger than long-lived storms found along the coast. Long-lived storms over the Gulf have the smallest sizes. For short-lived storms, SWA and the Congo have the largest storm sizes. The average size of a SWA/Congo short-lived slow moving storm size is about 80,000 km$^2$ while the average size of their corresponding short-lived fast moving counterparts is about 125,000 km$^2$. Sahelian short-lived storms follow with the average sizes of about 60,000, 30,000 and 110,000 km$^2$ for slow moving, moderate and fast moving respectively. The Coast, North Atlantic and the Gulf generally had the smallest of short-lived storm sizes of about 40,000, 27,000 and 74,000 km$^2$ for slow moving, moderate and fast moving respectively. The size of Sahelian long-lived storms (squall lines) is the largest possibly due to the presence of high CAPE and CIN over the region.

### 4.3.2 Impact of the AEW on the lifetime and speed of MCSs

To investigate the reason for the lifetime and speed of the MCSs, we first hypothesise that, long-lived storms are associated with the AEW. To confirm this the meridional winds associated with the different storm categories are plotted for the period 2 days before the arrival of the storms to 2 days after the arrival of the storms. The result for the regions that are directly influenced by the AEW is shown in Figure 19. These regions are North Atlantic, the Sahel and SWA. It can be seen that, LL_moderate storms are associated with the passage of a wave at mid-levels (800 - 500 hPa). For instance

over the North Atlantic, strong northerlies are observed at these levels between 2 days before the storm arrival and the day the storm arrives which shifts to southerlies after the arrival of the storm. The mean location of the North Atlantic storms can be inferred from the plot to be slightly ahead of the wave trough axis. Over the North Atlantic, Sahel and SWA the storm arrives <6h, ∼12h and ∼24h before the wave trough axis. The remaining storm categories do not show a distinct presence of the wave.

SWA and Sahel short-lived storms are associated almost consistent northerlies at mid-levels (800 - 600 hPa) while North Atlantic short-lived storms are mostly dominated by southerlies from mid to upper levels.

### 4.3.3 Controls of MCSs speed and lifetime

The controls of MCS speed and lifetime are investigated using average sizes, BTavg, rain-rates and wind shear for West African land storms (Figure 4.15). Short-lived slow moving storms are smaller in size compared to long-lived fast moving storms (Figure 4.15a). Similarly, short lived slow moving storms have mostly warmer BTs as compared to their long-lived fast moving counterparts (Figure 4.15b). Short-lived storms have generally warmer BTs and do not vary with speed. Long-lived storms on the other hand vary with speed. This relationship seem to show a good association with vertical wind shear and the associated rain-rate (Figure 4.15c and Figure 4.15d). Long-lived moderate speed storms are associated with the strongest vertical wind shear. These storms are also mainly associated with the highest rain-rates (Figure 4.15c). It therefore appears that, a strong shear results in long-lived colder storms, with high rain-rates and large sizes. The effect of vertical wind shear on MCSs is investigated in detail in Chapter 5.

## 4.4 Summary and Conclusions

The (thermo-) dynamic environments of MCSs in the different sub-regions of West Africa and the reasons for their characteristic lifetimes and speeds have been studied using an MCS dataset by Huang et al. (2018), and put into different categories based on the distribution of their lifetimes and speeds. The associated environments and rain-rates of the MCSs were taken from ERA-Interim reanalysis data and TRMM 3B42 precipitation dataset respectively.

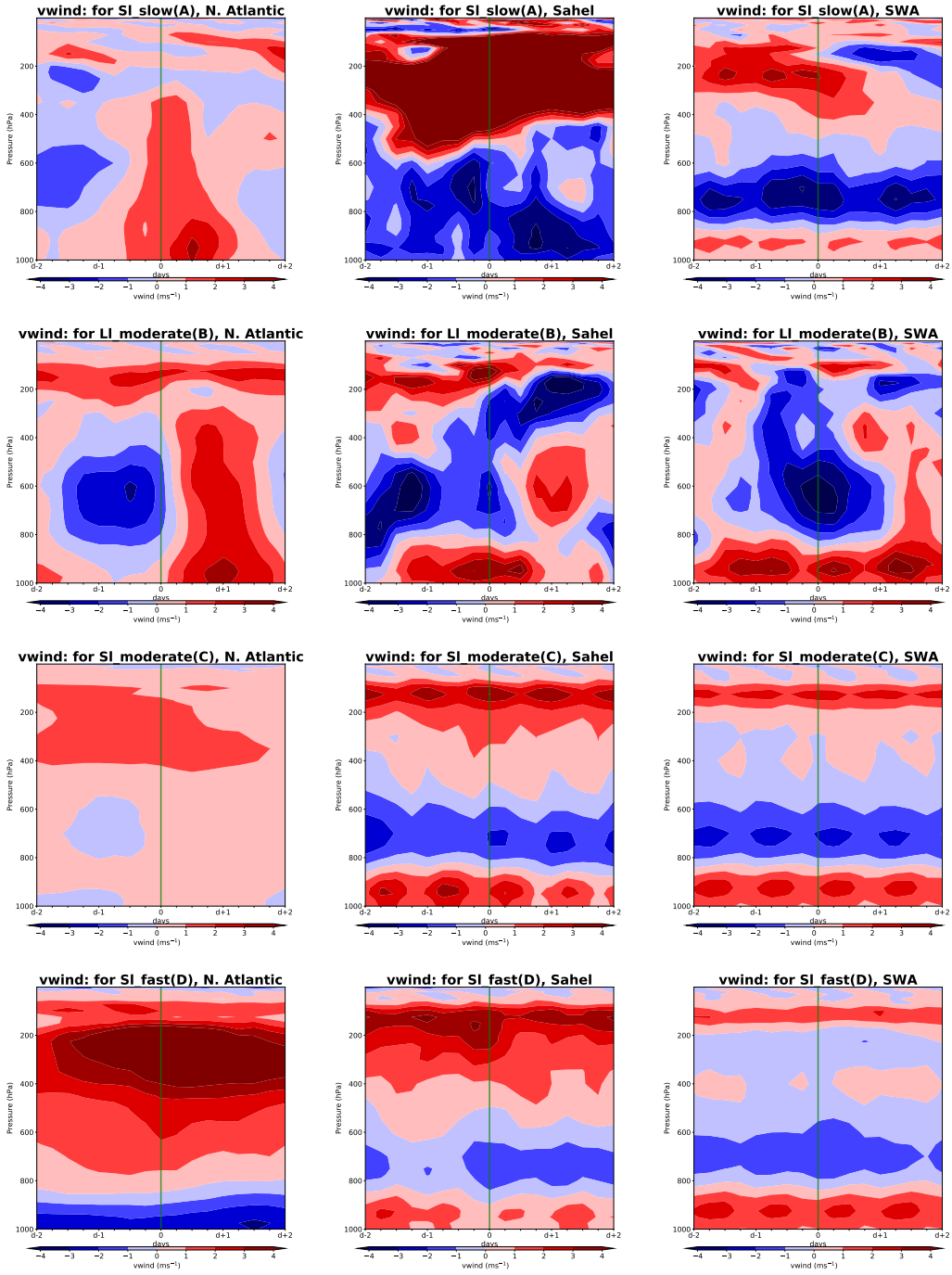


Figure 4.14: Meridional winds associated with the various MCS classes from 2 days before to 2 days after the arrival of an MCS. The SL_slow, LL_moderate, SL_moderate and SL_fast storms are shown in rows 1 to 4 respectively

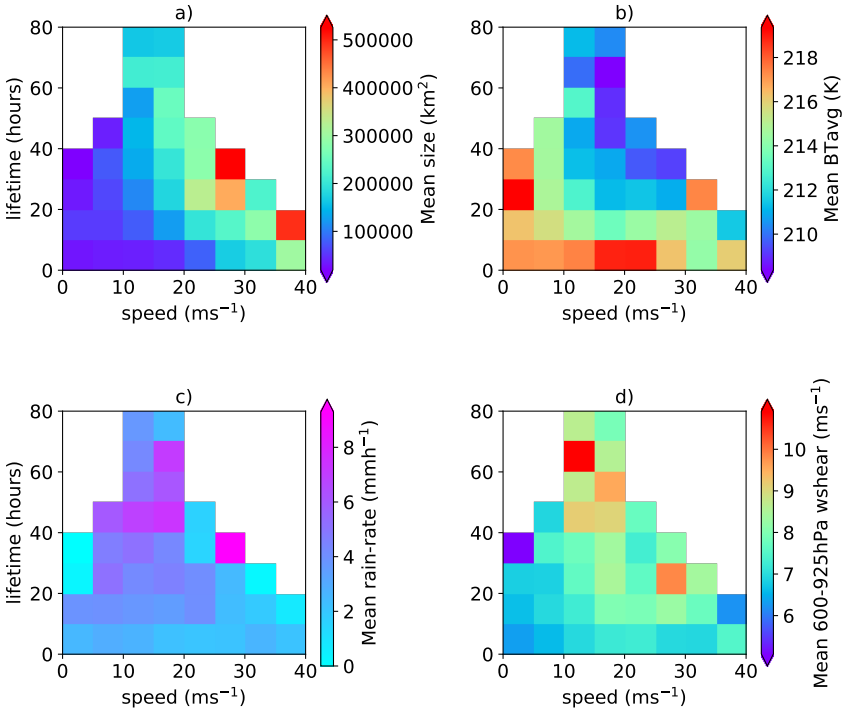


Figure 4.15: MCS lifetime against speed for (a) mean MCS size, (b) mean brightness temperatures (BTavg), (c) mean rain rate and (d) mean wind shear for the period 1998-2007.

The fastest moving MCSs were found in the Sahel with an average speed of 13.91 $\mathrm{m\,s^{-1}}$. SWA followed with an average speed of 13.54 $\mathrm{m\,s^{-1}}$. The Congo was next with a speed of 12.01 $\mathrm{m\,s^{-1}}$. The Coast, the North Atlantic and the Gulf of Guinea then followed with average speeds of 11.48, 11.04 and 10.55 $\mathrm{m\,s^{-1}}$ respectively. In general, land storms propagate faster than oceanic storms which we attribute to the stronger AEJ and high vertical wind shear values associated with land storms compared to oceanic storms. The main factors that determine MCS speed in the region are not fully understood but we hypothesise that, storm speed is determined by the steering level winds (mainly the AEJ) but also modified by wind shear (which could be inferred from the high speeds associated with the highly sheared Sahelian storms).

Generally, the oceanic storms have high rain rates compared to land storms. The highest mean rain-rate of 5.4 mm $\mathrm{h^{-1}}$ was associated with storms over the Gulf, followed by storms in the North Atlantic and the Coast with a mean rain rate of 4.5 mm $\mathrm{h^{-1}}$ each. Storms in the Congo area and SWA followed with mean rain rates of 3.6 mm $\mathrm{h^{-1}}$ and 3.2 mm $\mathrm{h^{-1}}$ respectively. The Sahel had the least mean rain-rate of 2.4 mm $\mathrm{h^{-1}}$. The rain-rate associated with a storm seem to depend on it's moisture availability rather than CAPE. Storms over the oceans are associated with lower CAPE and lower LNB compared to storms over land although storms over the oceans have higher rain-rates. Over land, the Congo and SWA regions have the highest CAPE values followed by the Sahel and the Coast. The highest CIN is seen to be associated with storms over the Sahel. Storms over the oceans and coast have the highest rain-rates but are slow moving while storms over the land have low rain-rates but fast moving. The Sahel has the lowest rain-rates but fastest storms.

Most MCSs occur around regions of strong surface convergence and high orography. Sahelian storms mostly occur in JJA. These storms are associated with the strongest sheared environments characterised by the presence of a strong AEJ core, high 925 hPa winds, a mid-level relative vorticity maxima, and a surface convergence just south of the ITD. The North Atlantic JJA storms were the next with the mean storm located just south of a strong AEJ core with a strong surface convergence. The North Atlantic storms were located at the centre of the mid-level relative vorticity maxima indicating a strong association with the AEW. The SWA JJA storms were located in a similar environment as the Sahel but south of the ITD and south-east of the AEJ core than the

storms in the Sahel. Congo area storms are associated with the weakest shear as they lie further south of the AEJ core. The convergence associated with land MCSs occur from the surface ∼6 h before the arrival of the storms. The convergence elevates with height and it is maximised around ∼800 hPa. Strong vertical velocities accompany these convergence regions which together with strong relative vorticities at mid-levels enhances the storms 6 hours later. It is worth noting that 6 hours is the highest temporal resolution available in the ERA-Interim dataset. The high rain rates and strong surface convergence associated with oceanic storms than land storms suggests that, high rain rates results from a strong surface convergence and corresponding strong vertical velocities in a moist environment, leading to a strong influx of moisture into the storms.

The study of the lifetimes and speeds of the storms also showed that: Short-lived slow moving storms are smaller, shallower (warmer BTavgs) and associated with weaker vertical wind shear compared to their long-lived and fast moving counterparts. Long-lived moderate speed storms are larger, deeper and associated with a stronger shear compared to their short-lived counterparts. The long-lived storms were also found to be associated with AEWs. Short-lived moderate speed storms have smaller to medium sizes, warm BTavgs, low rain-rates and vertical wind shear. Short-lived fast moving storms have large sizes relative to their slow moving counterparts, but still warm BTavgs, low rain-rates and shear. Most Congo storms are fast moving but short-lived as they are not associated with the AEW. This region is also a region with low vertical wind shear. The longevity of an MCS seem to depend on shear and an association with the AEW. Storms live longer when they are associated with higher wind shear and the AEW. Larger MCSs (greater than 100000 $km^{-2}$) mostly propagate faster. Most smaller MCSs are short-lived and slow moving. The effect of shear on MCSs is investigated in detail in the next chapter.

# Chapter 5

# Observed effects of Vertical Wind Shear on Intensities of Mesoscale Convective Systems over West and Central Africa

Most part of this chapter has been published in Baidu et al. (2022) in Atmospheric Science Letters (DOI: 10.1002/asl.1094).

## 5.1 Introduction

The (thermo-) dynamic environments associated with matured MCSs have been studied in chapter 4. It has been identified that, MCSs with colder BTs are long-lived, have high rain rates, and are associated with a strong vertical wind shear. In this chapter, we investigate in detail the effect of vertical wind shear on the intensities of an MCS as suggested from Figure 4.15 in the previous chapter.

Studies have shown that vertical wind shear plays a key role in the intensification of MCSs (Richardson 1999; Weisman and Rotunno 2004; Taylor et al. 2017, 2018; Klein et al. 2020). However, the exact mechanism through which vertical wind shear affects an MCS has not been thoroughly understood. Rotunno et al. (1988) describe the role played by vertical wind shear on the lifetime and self organisation of storms. According to Rotunno et al. (1988), an intense MCS results when the horizontal vorticity gen-

erated by the cold pools from an MCS is balanced by the vorticity generated by the environmental low-level vertical wind shear. Many studies (e.g. Bryan et al. 2006) now use and test this theory. Alfaro and Khairoutdinov (2015) and Alfaro (2017) provide an alternative explanation for the role of vertical wind shear. They developed the "Layer Lifting Model of Convection" (LLMC) which places importance on the thermodynamic role of vertical wind shear on moist convection and describes how low-level vertical shear modulates the inflow of convectively unstable air and water vapour, determining latent heating. Recently Mulholland et al. (2021) have shown how in idealised numerical model simulations vertical shear decreases entrainment dilution of updraft cores in squall lines.

Over West Africa, the conditions necessary for intense MCSs may be created by a strong meridional temperature gradient between the hot Sahara and the cooler more humid Gulf of Guinea. Warming in the Sahara intensifies the SHL and increases the meridional temperature gradient (Nicholson 2013) which results in a stronger AEJ. The intense SHL causes a stronger monsoon flow (Lavaysse et al. 2009), creating a stronger 600-925 hPa wind shear which, along with a high CAPE and high CIN environment favours intense MCSs (Taylor et al. 2017; Klein et al. 2020).

Studies with observed brightness temperature data from satellites have revealed an association between an increase in frequency of extreme MCSs and vertical wind shear over the Sahel, SWA and the Congo (Taylor et al. 2017, 2018; Klein et al. 2020). A follow up study by Bickle et al. (2021) using an idealised simulation of squall lines showed that an increased shear led to intense storms, although the thermodynamic changes dominated the effects of shear. An additional study indicated that, the LLMC might be too simple to accurately capture the effects of thermodynamic changes (Bickle et al. 2022). In contrast, studies using a convection-permitting climate model with a 4.4 km grid-spacing show no response of rain-rates to vertical wind shear (Fitzpatrick et al. 2020a; Senior et al. 2021). These findings raise the question of how best to use such state-of-the-art models for projections of changes in extremes. A better understanding of the processes that lead to intense storms from observations is therefore needed to constrain climate models. Improving our understanding of the effect of vertical shear on the dynamics of MCSs in the different sub-regions of West Africa is key to addressing the challenges associated with MCS prediction across time-scales.

We focus on mature West African MCSs and investigate the effect of vertical shear on cloud-top temperatures and rainfall rates of observed MCSs under different environmental conditions in the different West African sub-regions. We address whether vertical shear affects observed cloud top heights by investigating the effect of vertical shear on the difference between the cloud top heights and level of neutral bouyancies (LNBs) from reanalysis. The relationships between low-level vertical wind shear, MCS speed and lifetimes are also investigated. Section 5.2 provides a description of the study regions and the different datasets used in this study. The effect of vertical wind shear on MCSs is addressed in Section 5.3. The main results are summarised and conclusions are given in Section 5.4.

## 5.2 Study area and data source

The study area is divided into six sub-regions: Sahel, SWA, Coast, the North Atlantic ("N. Atlantic"), the Gulf of Guinea ("Gulf") and the Congo area (Figure 5.1). A 10-year MCSs data set (1998-2007) of MCS tracks was generated from Cloud Archive User Service (CLAUS) brightness temperatures using the algorithm introduced by Huang et al. (2018). The Huang et al. (2018) tracking algorithm combines the traditional area overlap method with Kalman filter enabling small and fast moving MCSs to be tracked. An area threshold of 5000 km$^2$ and a brightness temperature threshold of 233 K were used.

The effect of vertical wind shear on West African MCSs is investigated by studying the relationship between shear and the brightness temperature, associated CAPE, CIN and temperature at the LNB of mature MCSs, defined here as the point in the lifetime of an MCS where its brightness temperature is coldest. CAPE and CIN were calculated from ERA-Interim profiles based on the definitions in Wallace and Hobbs (1977):

$$CAPE = -R_d \int_{LFC}^{EL} (T_{parcel} - T_{env}) dln(p); \tag{5.1}$$

$$CIN = -R_d \int_{SFC}^{LFC} (T_{parcel} - T_{env}) dln(p); \tag{5.2}$$

where $LFC$ is the pressure at the level of free convection, $EL$ is the pressure at the equilibrium level, $SFC$ is the level of the surface, $R_d$ is the gas constant, $g$ is the grav-

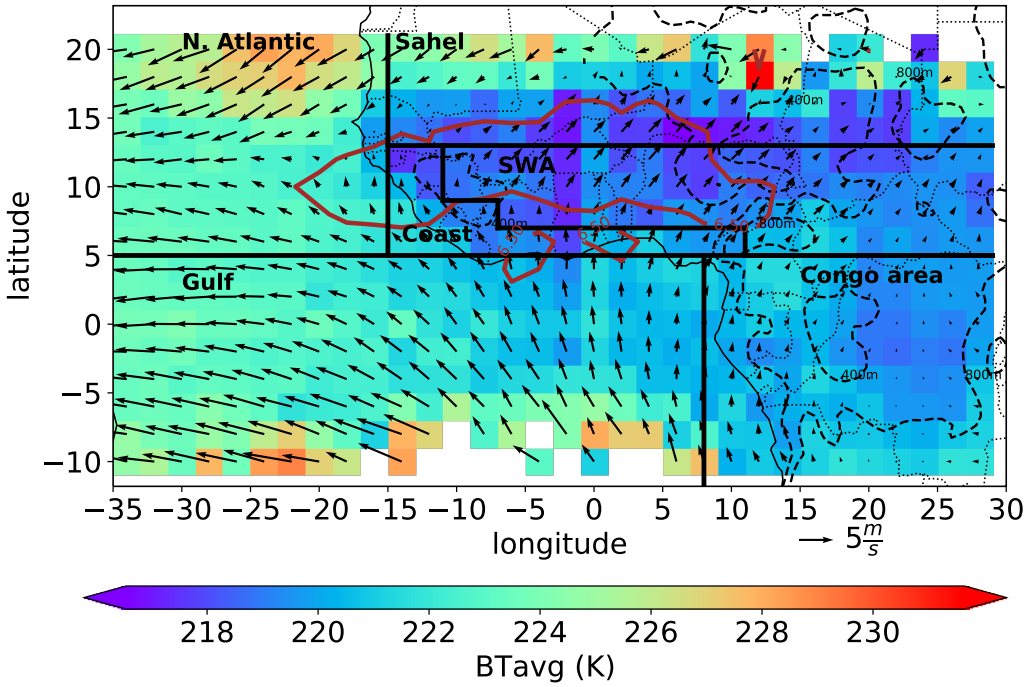


Figure 5.1: Mean brightness temperatures (BTavg, $^{o}$C) associated with MCSs (1998-2007) are shown in shading. The average 925-hPa horizontal wind (m s$^{-1}$, arrows) and the 600-hPa wind speed greater than 6.5 m s$^{-1}$ (burgundy contours) are overlaid. The black boxes indicate the sub-regions used: Gulf, N. Atlantic, Congo area, Sahel, SWA and Coast. The elevations greater than 400 m above sea level are displayed as dashed contours.

itational acceleration, $T_{parcel}$ is the temperature of the parcel, $T_{env}$ is the temperature of the environment, and $p$ is the atmospheric pressure.

The rain-rates and (thermo)-dynamic environments of each MCS were selected from TRMM 3B42 and ERA-Interim respectively at the time of the occurrence of the matured storm. ERA-Interim reanalysis data is used for the investigation of the (thermo-) dynamic environments of the MCSs studied. In this study we use ERA-Interim upper air data and TRMM 3B42 version 7 for the period 1998-2007. Vertical wind shear was calculated by computing the vector difference between the wind at 925 hPa and 600 hPa.

## 5.3 Effect of vertical wind shear on MCSs

### 5.3.1 The relationship between vertical wind shear and storms with coldest brightness temperatures

The relationship between the 925-hPa wind, wind speed at 600-hPa and the mean MCS brightness temperature is investigated (Figure 5.1). It is worth noting that the brightness temperature used here is the average brightness temperature (BTavg) of the entire storm anvil and not the minimum brightness temperature (overshooting top). Colder BTavgs are found over land, with the coldest values over the Sahel and SWA, which have strong shear between 925 and 600-hPa. Storms over the Coast and Congo have relatively warmer brightness temperatures and have either lower 925-hPa winds, lower 600-hPa winds, or both.

To further investigate the relationship between vertical wind shear and MCS brightness temperatures, Figure 5.2 (a-d) separates out the thermodynamic factors: CAPE, CIN and the temperature at the LNB. The regions with the strong vertical wind shear (greater than $8\,\mathrm{m\,s^{-1}}$) and coldest observed average brightness temperature (Figure 5.2a) are not the regions with high CAPE values (Figure 5.2c) or low CIN values (Figure 5.2d). High CAPE does not explain the colder observed brightness temperatures in West Africa. Similarly, the areas of lowest average brightness temperatures (Figure 5.2a) are not simply explained by the coldest (predicted) temperatures at the LNB (Figure 5.2b). The results show colder brightness temperatures over the Sahel than the Congo, despite a colder LNB and higher CAPE in the Congo, suggesting that the high vertical shear found in the Sahel is important for the storms to achieve the low brightness temperatures seen there.

In order to compare the observe MCS brightness temperatures with those expected if the anvils were to detrain at the theoretical LNB, Figure 5.2e was created which shows the relationship between the brightness temperature difference (hereafter "BT_diff"), i.e. the observed average brightness temperature (BTavg) minus the theoretical temperature at the LNB. Generally, the BT_diff is positive over almost the entire land domain studied (Figure 5.2e) indicating that the observed cloud top heights are lower (have warmer brightness temperatures) than their (theoretical) LNBs (consistent with Takahashi and Luo (2012); Takahashi et al. (2017); Wang et al. (2020); Mullendore et al. (2013)). The few regions with negative BT_diff are found in areas with few

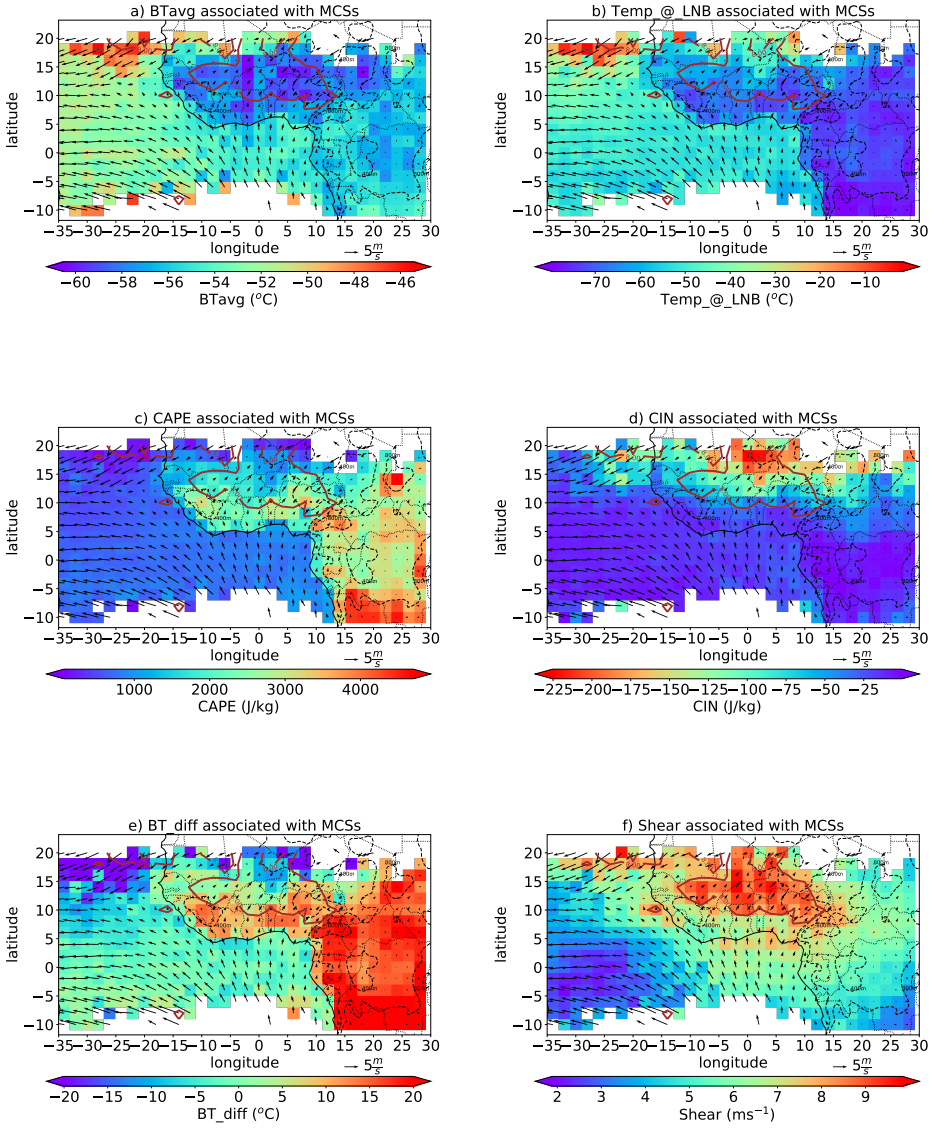


Figure 5.2: (a) Mean brightness temperature (BTavg, $^o$C) (b) temperature at the LNB ($^o$C), (c) CAPE (J kg$^{-1}$), (d) CIN (J kg$^{-1}$) (e), brightness temperature difference (BTavg - temperature at the LNB, $^o$C) and (f) vertical wind shear associated with MCSs (1998-2007; m s$^{-1}$). The associated 925-hPa winds (arrows, m s$^{-1}$) and the wind shear of 8 m s$^{-1}$ (burgundy contours) are overlaid. Bins with a standard error of the mean greater than the 95th percentile are eliminated.

storms and are consistent with the emissivities of clouds being less than 1 and do not necessarily show anvils located higher than the LNB (Allen 1971; Protopapadaki et al. 2017), or over the Sahara errors in analysed low-level water vapour may give underestimation of LNBs (Trzeciak et al. 2017). Furthermore, BT_diffs are higher over the Congo than over the Sahel, with the low BT_diffs in the Sahel collocated with regions of high vertical wind shear (Figure 5.2f). The brightness temperatures used are of the whole anvil, not just the overshooting top, and therefore the results are consistent with high vertical shear allowing decreased entrainment (Peters et al. 2019; Mulholland et al. 2021) and therefore anvils that reach higher altitudes relative to their LNB. This effect was further confirmed with an $r$ value of -0.16 and $p$ value less than 0.01.

The observed cloud top heights of storms over the oceans are closer to their LNBs compared to their land counterparts on the same latitudes. We hypothesise that entrainment of drier air over land, and possibly higher entrainment rates over land (Becker and Hohenegger 2021), resulting in higher entrainment-driven dilution of updraft cores prevents storms from reaching as high cloud top heights relative to their LNBs compared with oceanic storms. Further studies are required to identify the exact role of these mechanisms on the cloud-top height of MCS.

### 5.3.2 Vertical wind shear and MCS properties

Here we assess how vertical wind shear affects MCS speeds, brightness temperature, rain-rate and lifetime. We hypothesise that long-lived fast-moving storms occur in strongly sheared environments (Bunkers et al. 2006; Yang et al. 2017). Figure 5.3 shows the mean MCS size, brightness temperatures, rain-rate, lifetime, BT_diffs and the relative humidity at 600 hPa for West African land storms (Sahel, SWA and the Coast) as a function of the vertical wind shear and MCS speed. Slow moving storms tend to be short-lived and small in size compared with other MCSs (Figures 5.3a and d). Fast moving storms tend to be larger (Figures 5.3a), but the longest-lived storms are found for moderate speeds 10 to 25 $\mathrm{m\,s^{-1}}$) and high vertical shear (Figure 5.3d). Moderate–speed (10 - 30 $\mathrm{m\,s^{-1}}$) long-lived systems give the coldest brightness temperatures (Figures 5.3b) with vertical shear giving colder brightness temperatures for this range of storm speeds.

Figure 5.3e confirms the results of the preceding sub-section, showing that for any MCS speed, higher vertical shear tends to give colder cloud-tops relative to the LNB, except perhaps for the fastest storms, where the sample size is reduced and there are no cases of high vertical shear. The lowest brightness temperature differences, i.e. the storms that reach higher altitudes relative to their LNBs, are seen for the largest vertical shear values, which are found for MCS speeds of 5 to 30 $\mathrm{m\,s^{-1}}$.

The overall effects of mid-level moisture are unclear. Figure 5.3e and f shows that for moderate shear there is some increase in BT_diff with specific humidity, i.e. lower cloud tops with moist mid-levels, and that dry mid-levels are associated both with low vertical shear high BT_diff storms, and high shear low BT_diff storms. Vertical shear also gives higher rain rates for all but the fastest and slowest storms (Figure 5.3c), with the heaviest rain rates coming from long lived storms, which tend to have moderate speeds (5 to 25 $\mathrm{m\,s^{-1}}$). It is important to note that the TRMM 3B42 product makes use of infrared imagery, so impacts of shear on cloud-top height may be falsely converted to rain rates.

The most intense MCSs in West Africa have lifetimes greater than 15 hours, speed between 15 - 30 ms $\mathrm{h^{-1}}$, BT's colder than -58.15$^{o}$C, size between 100,000 - 250,000 $\mathrm{km^2}$, rain-rates between 5 - 12 mm $\mathrm{h^{-1}}$ and shear greater than 8 $\mathrm{m\,s^{-1}}$. Highly sheared storms with speeds and lifetimes greater than 13 $\mathrm{m\,s^{-1}}$ and 20 hours respectively results in colder, more organised storms. Highly sheared storms with speeds less than 13 $\mathrm{m\,s^{-1}}$ and lifetimes greater than 20 hours might be less organised with relatively warmer BTs but might have higher rain-rates.

We conclude that, the longest lived storms have a moderate speed ($\sim$15 $\mathrm{m\,s^{-1}}$) and are associated with the highest vertical shear values (Figure 5.3d). For any speed, the longest-lived storms are associated with the coldest brightness temperatures (Figure 5.3b), colder brightness temperatures relative to their LNB (Figure 5.3e) and high vertical wind shear.

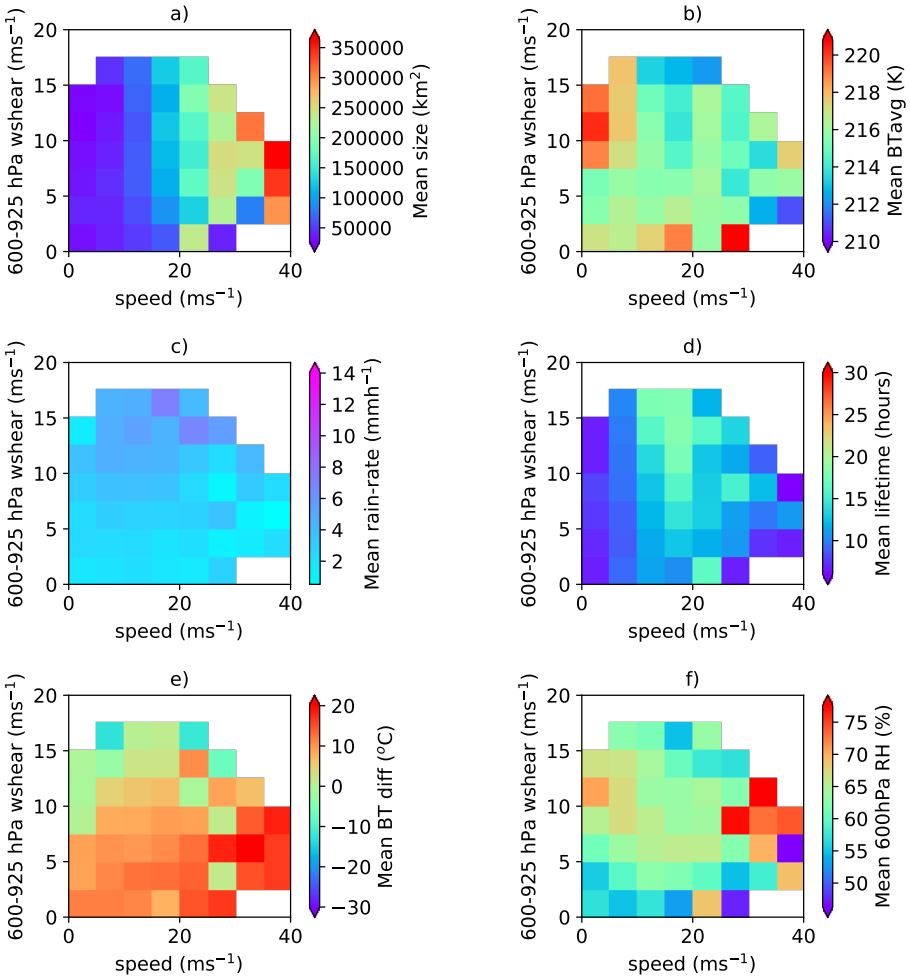


Figure 5.3: Vertical wind shear against speed for (a) MCS size, (b) mean brightness temperature (c) rain-rate, (d) lifetime, (e) brightness temperature difference, and (f) relative humidity at 600-hPa over the period 1998-2007.

#### 5.3.2.1 Relationship between vertical wind shear, specific humidity, brightness temperature difference and rainfall rate in each sub-region

The effect of vertical wind shear on brightness temperature difference as seen in Figure 5.3e is investigated in detail in Figure 5.4. Here, we examine if the effect of vertical wind shear on BT_diff is the same in all the sub-regions over land. High vertical wind shear corresponds to minimised BT_diff over all the land regions. For lower vertical wind shear values, fast moving MCSs are associated with higher BT_diff mainly over the Coast, SWA and the Congo area. Over the Coast, increasing shear with increasing speed seem to generally result in higher BT_diff (Figure 5.4a). In SWA and Sahel, increasing vertical wind shear results in minimised BT_diff for all storm speeds (Figure 5.4b and c). In the Congo area, higher vertical wind shear values generally result in minimised BT_diff. The difference between the brightness temperatures and the LNBs is further minimised for fast moving storms (Figure 5.4d).

In Figures 5.5 and 5.6 we assess the effect of vertical wind shear and 600-hPa relative humidity (mid-level specific humidity) on brightness temperature difference and rainfall rate of MCSs. In addition to the findings from the previous section, we find that higher vertical wind shear values generally result in minimised BT_diff in all the sub-regions (including the oceans) but its effect on rainfall rates is mainly seen over West Africa land regions (Sahel, SWA, and the Coast, Figure 5.6). The BT_diff is further minimised for higher mid-level relative humidity storms over the Sahel, SWA and the Coast (Figures 5.5a,b and c respectively) and results in higher rainfall rates over these regions (Figures 5.6a,b and c) due to the generally higher vertical wind shear values in these regions. The effect of vertical wind shear on the BT_diff and rainfall rates of storms over the Congo area and the oceans (Figure 5.6 d, e and f) is not as significant as compared to the West Africa land regions possibly due to the generally low vertical wind shear values in the Congo area and the oceans.

Examining the effects of mid-level humidity by region shows that this complex picture may be a result of impacts that vary by region. For the Coast, the Congo area, Gulf of Guinea and N. Atlantic there is some evidence that moist mid-levels, for any value of vertical shear, favour colder cloud-tops, possibly from reduced drying through entrainment. Conversely for the Sahel and SWA there is perhaps some hint of the reverse, i.e. dry mid-levels favouring cold cloud tops and low BT_diff, possibly through favouring

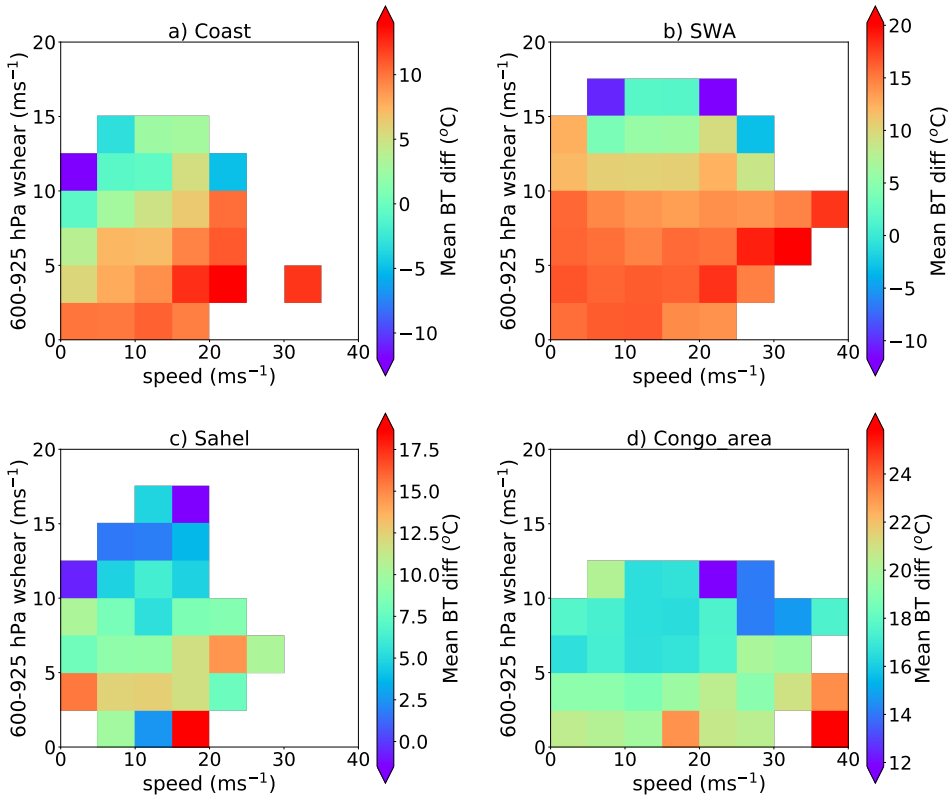


Figure 5.4: Vertical shear against speed for brightness temperature difference (BT_diff) for (a) the Coast, (b) SWA, (c) the Sahel and (d) the Congo area (1998-2007). Bins within latitudes greater than 15$^o$N and bins with less than 2 storms have been eliminated.

strong cold pools and so convective organization (James and Markowski 2010; Fitzpatrick et al. 2020a). The strong cold pools may also influence the speed of MCSs as the cold pool speeds get balanced by vertical wind shear. New cells may initiate ahead of the dissipating mother cell as a result of this balance making the storm self-sustaining (Rotunno et al. 1988). We conclude that it is plausible that effects of mid-level moisture vary by region, due to effects on both entrainment drying and cold pool production, and that this requires further research.

## 5.4 Conclusions

The observed impact of vertical wind shear on MCSs has been investigated over West and Central Africa, using the 10-year dataset of MCS tracks from Huang et al. (2018).

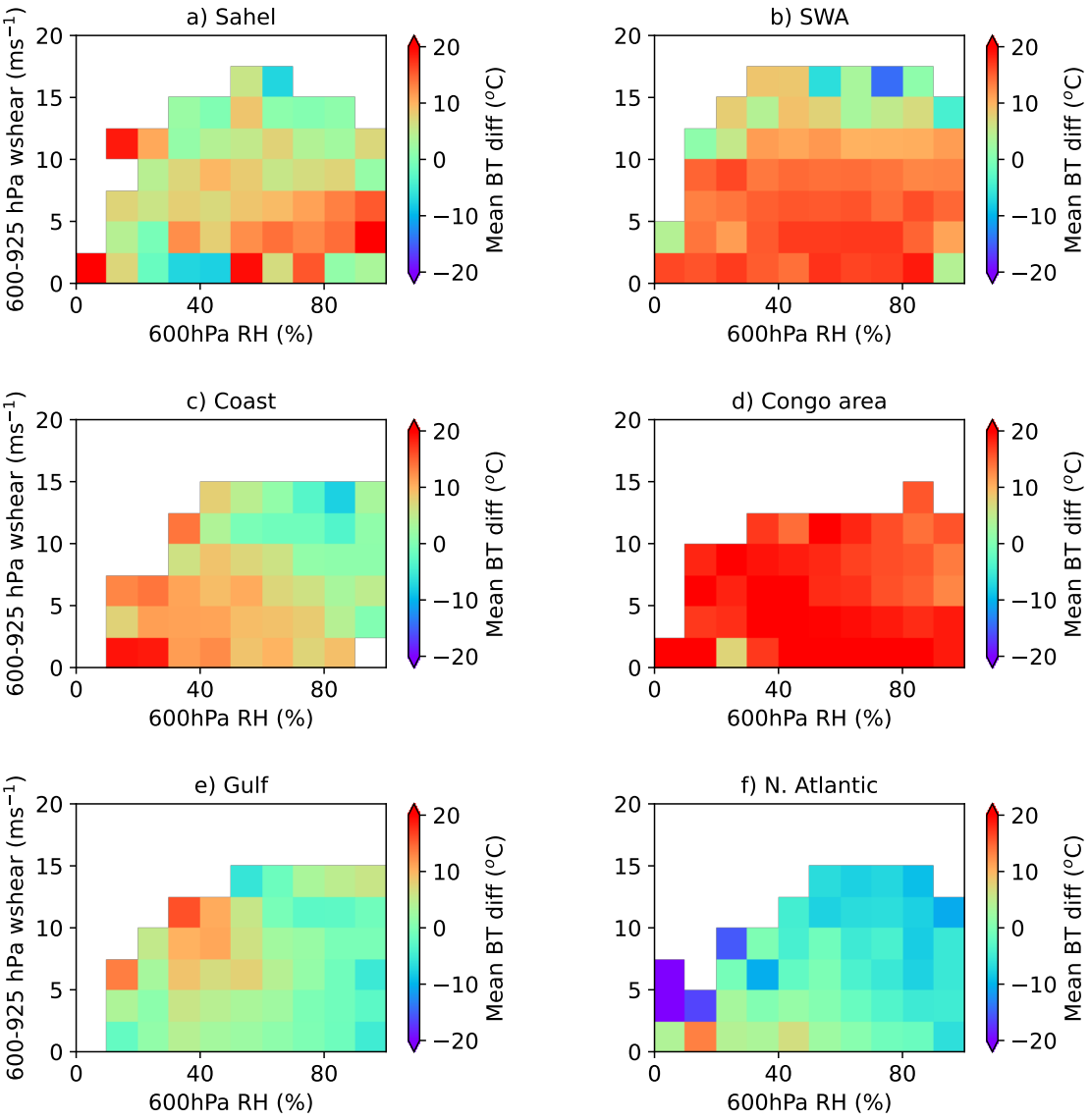


Figure 5.5: Vertical shear against relative humidity at 600-hPa for brightness temperature difference (BT_diff) for (a) Sahel, (b) SWA, (c) Coast, (d) Congo area, (e) Gulf and (f) N. Atlantic (1998-2007). Bins within latitudes greater than 15$^o$N and bins with less than 2 storms have been eliminated.

The associated environments and rain-rates of the MCSs were taken from ERA-Interim and TRMM 3B42 datasets, at the time of storm maturity, defined as the time of coldest

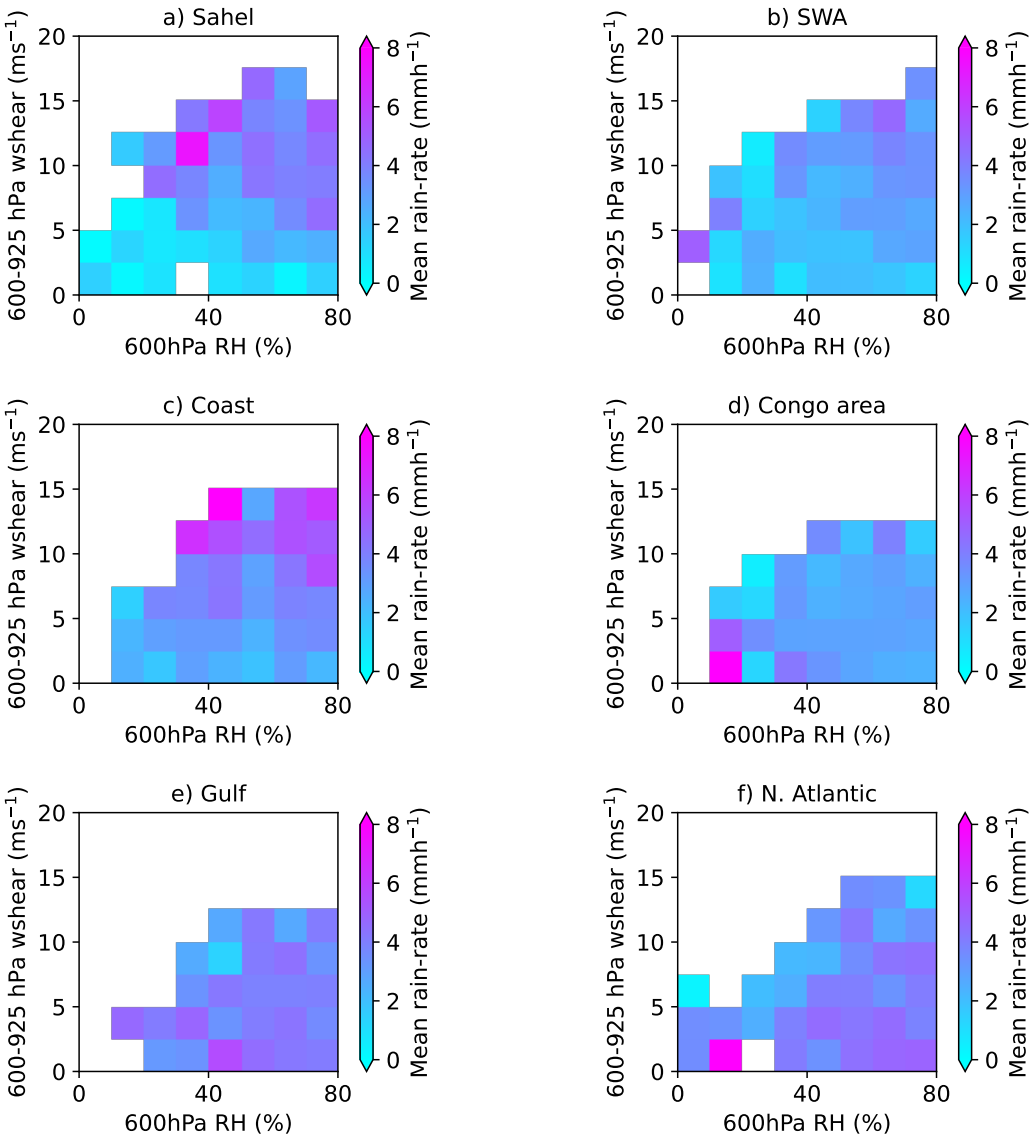


Figure 5.6: Vertical shear against relative humidity at 600-hPa for rainfall rate for (a) Sahel, (b) SWA, (c) Coast, (d) Congo area, (e) Gulf and (f) N. Atlantic (1998-2007). Bins within latitudes greater than 15$^o$N and bins with less than 2 storms have been eliminated.

mean brightness temperature in the life-cycle of a storm.

The results show that, a strong vertical wind shear is associated with long-lived, moderate speed and size storms with colder brightness temperatures. Over West Africa land regions, these storms were also associated with high rain-rates.

To isolate the effects of vertical wind shear on cloud-top height from the effect of the thermodynamic profile temperatures we compare the storm brightness temperatures with the temperatures at the LNB. It was found that storms over the oceans could reach higher relative to their LNBs compared to storms over land, which we hypothesise may be due to greater entrainment of drier air over land (Becker and Hohenegger 2021). Greater vertical shear gives clouds that are higher relative to the LNB. Storms are observed to reach higher heights relative to their LNB in the presence of larger shear. Notably storms reach higher relative to their LNB in the Sahel, where vertical shear is strong, compared to storms over the Congo, where vertical shear is weaker but CAPE and LNBs are both higher. This impact of vertical shear on cloud-top heights relative to the LNB is consistent with recent idealized numerical model simulations showing that vertical shear can reduce entrainment dilution in both supercells and squall-lines (Mulholland et al. 2021; Peters et al. 2019). However, assuming storms move with mid-level winds increased vertical shear will tend to give greater system-relative inflow of low-level air compared with mid-level air, which may also increase the mean positive buoyancy of the inflow in the Alfaro (2017) layer lifting model of convection. The exact balance of mechanisms by which vertical wind shear controls cloud-top heights and rainfall rates is left to future work.

We conclude that, not only is it important to capture the role of vertical shear in modelling the organisation of convection and high impact weather, but that vertical shear is also important for the climatology of anvil heights, therefore affecting the profile of diabatic heating from storms and the earth's radiation budget. We hypothesise that a poor representation of vertical shear impacts on entrainment might be one reason why 4.4 km grid spacing convection-permitting models struggle to capture the observed effects of vertical shear on rain rates over Africa (Fitzpatrick et al. 2020a; Senior et al. 2021). Since grid spacings less than or around 100 m are needed to model entrainment (Bretherton et al. 1999), the poor representation of the effect of vertical wind shear on entrainment in the models raises challenges for modelling and predicting future high impact weather from squall-lines, which we expect to be impacted by future changes in vertical shear, as well as thermodynamics (Taylor et al. 2017).

# Chapter 6

# Evaluation of the Met Office Tropical Africa Model

## 6.1 Introduction

The (thermo-)dynamic environments of MCSs in the sub-regions of West Africa and their relationship with vertical wind shear have been investigated in chapters 4 and 5. This chapter focuses on the evaluation of the performance of the Met Office Tropical Africa Model (TAM) in simulating rain-rates over each sub-region. Forecasting of MCSs in the tropics has been a major challenge because global models parameterise convection. As the resolution of global models is usually coarser than that required for simulating storm initiations, the models struggle to simulate the exact location of initiated storms. Moreover, the sensitivity of the earth's atmosphere to small perturbations in initial conditions (the butterfly effect) means that, models with coarser resolution or parametrized models might easily miss storm initiations, their evolution and propagation as initial errors grow. However, CP models provide a step-change in forecasting convective storms (Clark et al. 2016).

The UK Met Office runs a CP model at a 4.4 km horizontal resolution over tropical Africa known as the TAM. The output from the model is currently made available to African operational forecasters as part of the Met Office's contribution to the WMO Voluntary Cooperation Programme (VCP) (Hanley et al. 2021). Little work has been done on the evaluation of these products and as a result there is limited guidance on how forecasters should interpret the outputs of the models for particular weather situations. With the access to the TAM output provided to forecasters comes the need to

increase understanding of the model performance in different times of the day, seasons and locations as well as different lead times. This is necessary for the model to truly serve its purpose.

A detailed evaluation of an earlier version of the TAM model has been performed over Lake Victoria and its surrounding regions in East Africa (Woodhams et al. 2018). However, no published detailed evaluation has been performed over West Africa. Given that MCSs and their associated winds affects lives and the economy of most West African countries (since they contribute to much of the annual rainfall in the region), evaluating the model performance is essential to address this forecasting challenge.

Figure 6.1 shows plots from the Met Office website that compares the operational Global model, TAM and GPM rainfall for the 29th October, 2021. This case reveals the typical disparity between the two models. Figure 6.2 shows this disparity further by revealing the representation of the diurnal cycle of convection in the models. The 3 hourly rainfall from the models versus GPM demonstrates that the Global Model has poor representation of the diurnal cycle compared to the TAM. Both models however struggle to represent rainfall. The Global model seems to represent large-scale features well but has few thunderstorm-like features and a lot of widespread rain of low intensities. It rains too early in the day and too little in the evening. The TAM on the other hand simulates more realistic thunderstorms that occur at the right time of the day. The storms are, however, too fragmented and have too high rain-rates resulting in misses in some areas. Point to point verification of the TAM will therefore likely lead to the double penalty problem mentioned in section 3.2.4. The TAM might get events roughly in the right area, but the timing or exact locations could be incorrect. Experienced operational meteorologists will look at the overall predictions coming from the models rather than point locations. A verification measure that lines up with their practices and does not unduly penalise models based on point accuracy is necessary. FSS is therefore used for the evaluation for the models as this skill score rewards behaviour that is more important for operational meteorology.

Section 6.2 compares the performance of the two models (the TAM and the Global model) for both daily and sub-daily (6 hourly) rainfall accumulation. It also assesses the impact of the spin-up problem in the TAM on the model skill by comparing the performance of the two models for both Day 1 and Day 2 forecasts using sub-daily

rainfall accumulation. Section 6.3 presents a detailed evaluation of Day 2 forecast using sub-daily rainfall accumulations. The detailed evaluation of the Day 2 forecasts was done by comparing the Localised Fractional Skill Score (LFSS), the FSS versus neighbourhood sizes, FSS for different rainfall intensities and the FSS for different lead times and times of the day. The model's ability to represent the effect vertical wind shear on storms as found in chapter 5 is evaluated in section 6.3.5 and finally the discussion and conclusions from the chapter are presented in section 6.4.

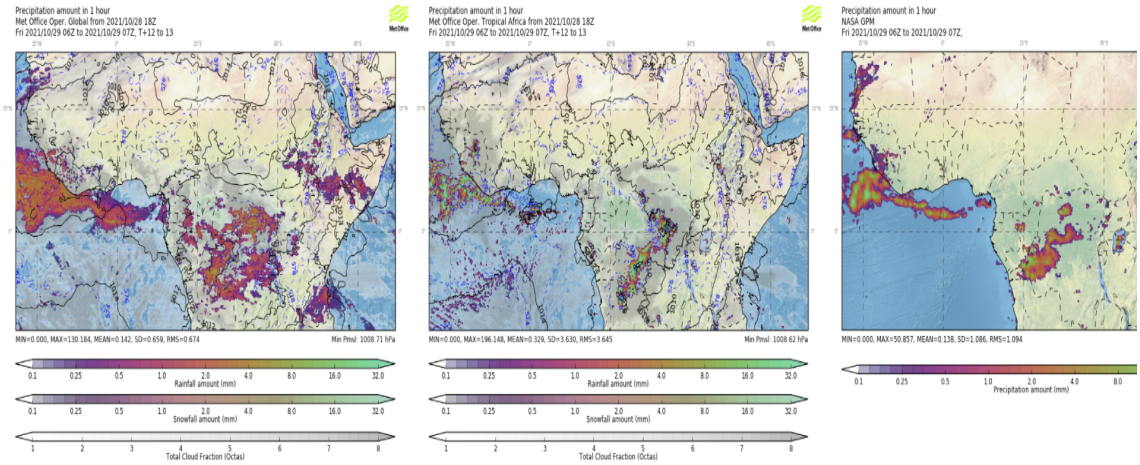


Figure 6.1: Met Office operational Global (left), TAM (middle) and GPM rainfall (right) on 29.10.2021 (06Z-07Z), T+12 - T+13.

## 6.2 Comparison of model skill of daily and sub-daily rainfall accumulation for Day 1 and Day 2

Figure 6.3 compares the skill of the TAM to that of the Global model for daily rainfall accumulation by comparing the FSS for different neighbourhood sizes of the daily rainfall amounts accumulated over the period of study (December 2019 - November 2020). A detailed description of the comparison of FSS with the neighbourhood sizes and its significance will be discussed in section 6.3.2. Here we focus on the general difference in skill between the TAM and the Global model with emphasis on the benefit of using sub-daily against daily accumulations. The Global model outperforms the TAM over almost all regions and for all neighbourhood sizes when daily rainfall accumulations were used. This result means that there is no significant advantage of using the TAM for daily rainfall accumulation. However, when sub-daily (6 hourly) rainfall accumulations were used, a significant improvement in the skill was seen in the TAM (Figure 6.4)

indicating that, the TAM is more skilful in capturing the diurnal cycle of convection and rainfall as it simulates more realistic storms (Marsham et al. 2013).

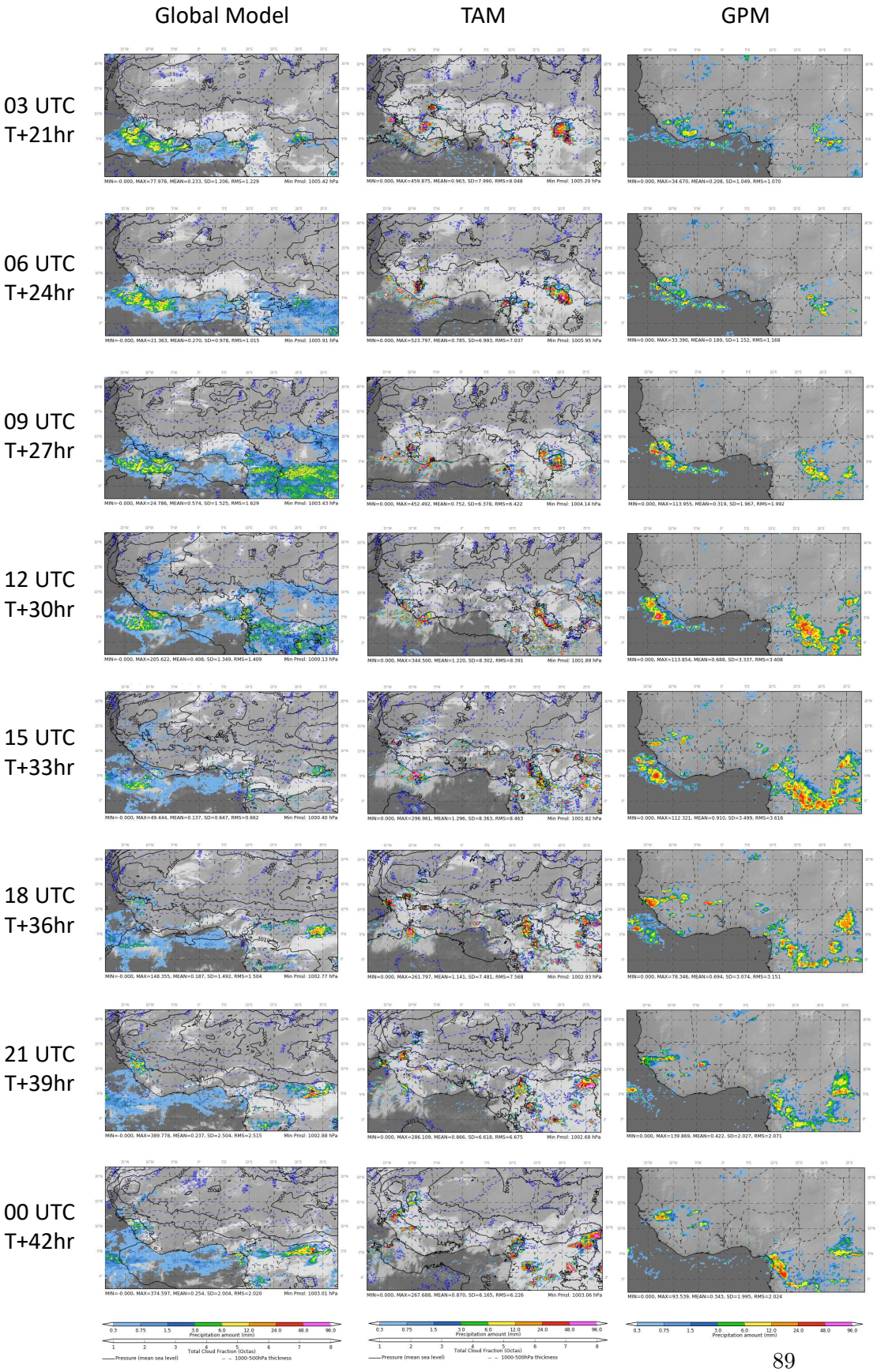




Figure 6.2: The representation of the diurnal cycle in the Met Office operational Global (left), TAM (middle) and GPM rainfall (right).

Despite the improvement in the skill of the TAM, the Global model continues to outperform the TAM in most sub-regions for day 1 forecasts. Interestingly, the skill of the TAM improves significantly when day 2 forecasts are used for the comparison although the skill of all the models decrease generally for Day 2 (as is expected with the growth of errors from initial conditions). Particularly, the TAM outperforms the Global model for the whole domain of study (West Africa), the Coast, the Congo area, and SWA for neighbourhood sizes less than 400 km. This intriguing result may be attributed to the long spin-up period of the TAM and high-resolution NWP models in general (Warner et al. (2022, in preparation), (Short and Petch 2022)). Warner et al. (in preparation) showed that, about a 12-hour spin-up period was associated with forecasts from the TAM. A 12-hour spin-up period significantly affects the skill of the TAM for the day 1 forecast. We therefore focus on evaluating day 2 forecast in the remaining parts of the work.

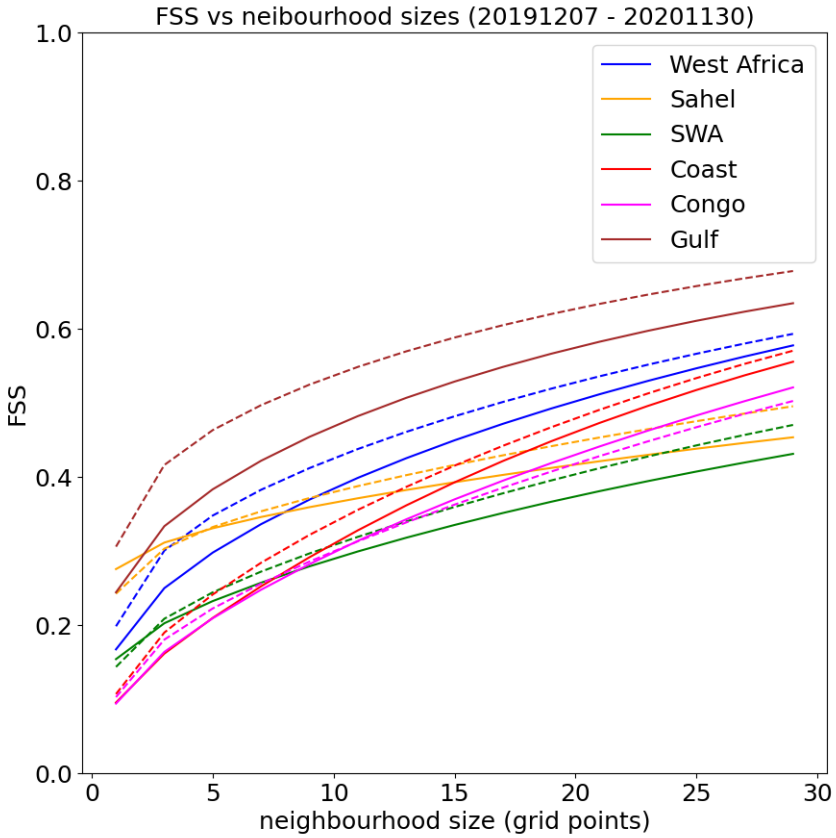


Figure 6.3: FSS versus neighbourhood size for daily rainfall accumulation (Dec 2019-Nov 2020). The Global Model data is shown in dashed line and the TAM data as solid lines. Note: each grid point is 0.1°(11.1 km) as the models were regridded to the resolution of the GPM.

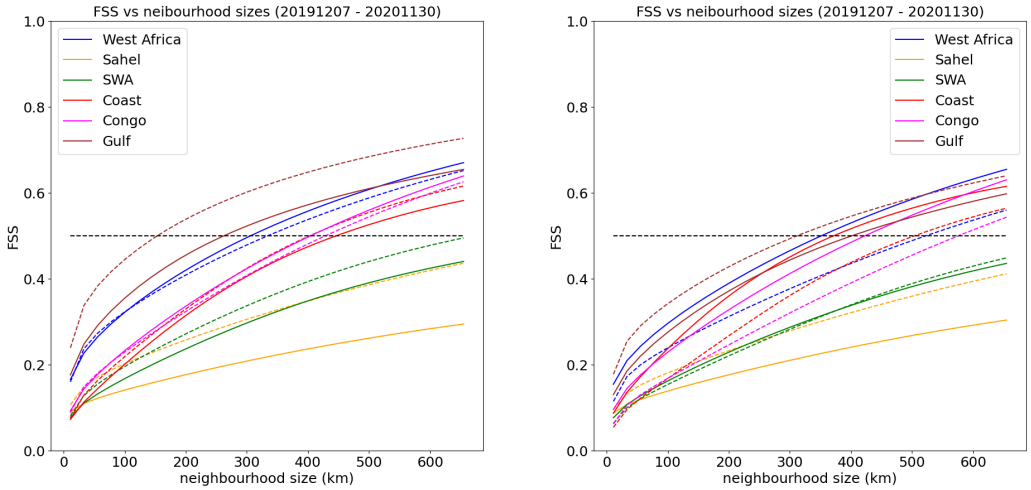


Figure 6.4: FSS versus neighbourhood size for sub-daily rainfall accumulation (Dec 2019- Nov 2020) for day 1 (left) and day 2 (right). The Global Model data is shown in dashed line and the TAM data as solid lines.

## 6.3 Evaluation of model performance for Day 2 forecast

### 6.3.1 LFSS results over West Africa

A spatial verification of the TAM is first performed using the LFSS as defined and used in Woodhams et al. (2018). Figure 6.5 compares the LFSS for both the Global model and the TAM for the entire study period (December 2019 - November 2020) using sub-daily (6 hourly) rainfall accumulation for the Day 2 forecast. The LFSS was computed using the neighbourhood size of 33 grid points (366.3 km) which is the smallest neighbourhood size for which the TAM has skill over the entire West Africa domain (also consistent with Hanley et al. (2021)). It is worth noting that, the models were regridded to the resolution of the GPM data (0.1°). The TAM shows higher skill over the mountainous regions in the Congo area as well as northern Nigeria. There is also higher skill along the coastal areas where the near surface winds are generally perpendicular to the land. This result shows the model's ability to represent orographic effects as well as sea-land breeze circulations. These features remain persistent throughout all seasons.

In DJF, the two models simulate rainfall over larger parts of the Gulf of Guinea and with dominantly high intensities compared to the observed (Figure 6.6). The Global

model particularly has rain spread out over most parts of the Gulf, creating false alarms over most areas. SWA and the Sahel are generally dominated by low intensity rainfall events as this is the main dry season of these regions. The TAM outperforms the Global model in most parts of the region. There is pronounced high skill over the western side of the Gulf of Guinea close to the coast of Liberia. High skill is also seen around the mountainous regions of the Congo area as seen from the results of the entire year's evaluation.

In MAM, the latitudinal band of rainfall shifts slightly northward as shown by the GPM (Figure 6.7). Both the Global and the TAM simulates this quite well. The Global however gets much of the rainy areas over the oceans well but with a band of rain over land which leads the actual rain latitude in the observed. The TAM likewise simulates the northward shift of the rain band but with higher intensities and smaller extend compared to the observed. There is a pronounced decreased skill along the coast from Cote D'Ivoire to Nigeria in both the Global and the TAM. The TAM seems to struggle in simulating rainfall in these coastal areas in this season. The exact reason for this is not well understood yet, however, climatologies of the number of MCSs over West Africa (Figure 4.1 and 4.2) generally indicates lower number of MCSs in these regions. As the advantage of the TAM over the Global is its ability to simulate convective storms more accurately, the fewer number of MCSs in the above mentioned coastal regions could be the reason for the decrease in performance of the TAM in these places. Further research is encouraged in this region to understand the reason for the relatively fewer number of MCSs as well as the reason for the decreased skill of the TAM over these regions. The skill of the TAM is however generally higher in most parts of the land areas compared to the Global model in this season.

In JJA, both the Global model and the TAM simulates very high intense rainfall compared to the observed although it should be kept in mind that the GPM rainfall observations have biases of their own (Figure 6.8). The rain-rates of the TAM are however generally more intense. The TAM remains more skilful in the same areas described above (mountainous and coastal regions perpendicular to the near surface winds) with some extra hot spots in parts of the ocean. Very low intensity rainfall events are seen over the ocean in this season as the peak of convective activities is centred over the Sahel.

The rainfall events for the two models remain generally more intense even in SON when compared to the GPM (Figure 6.9). The most intense events are seen around the mountainous regions of the Congo area and the coastal areas. The FSS also remains generally higher in the TAM than the Global model. The skill over the Sahel is generally low in SON for the two models although the skill is a little better for the TAM.

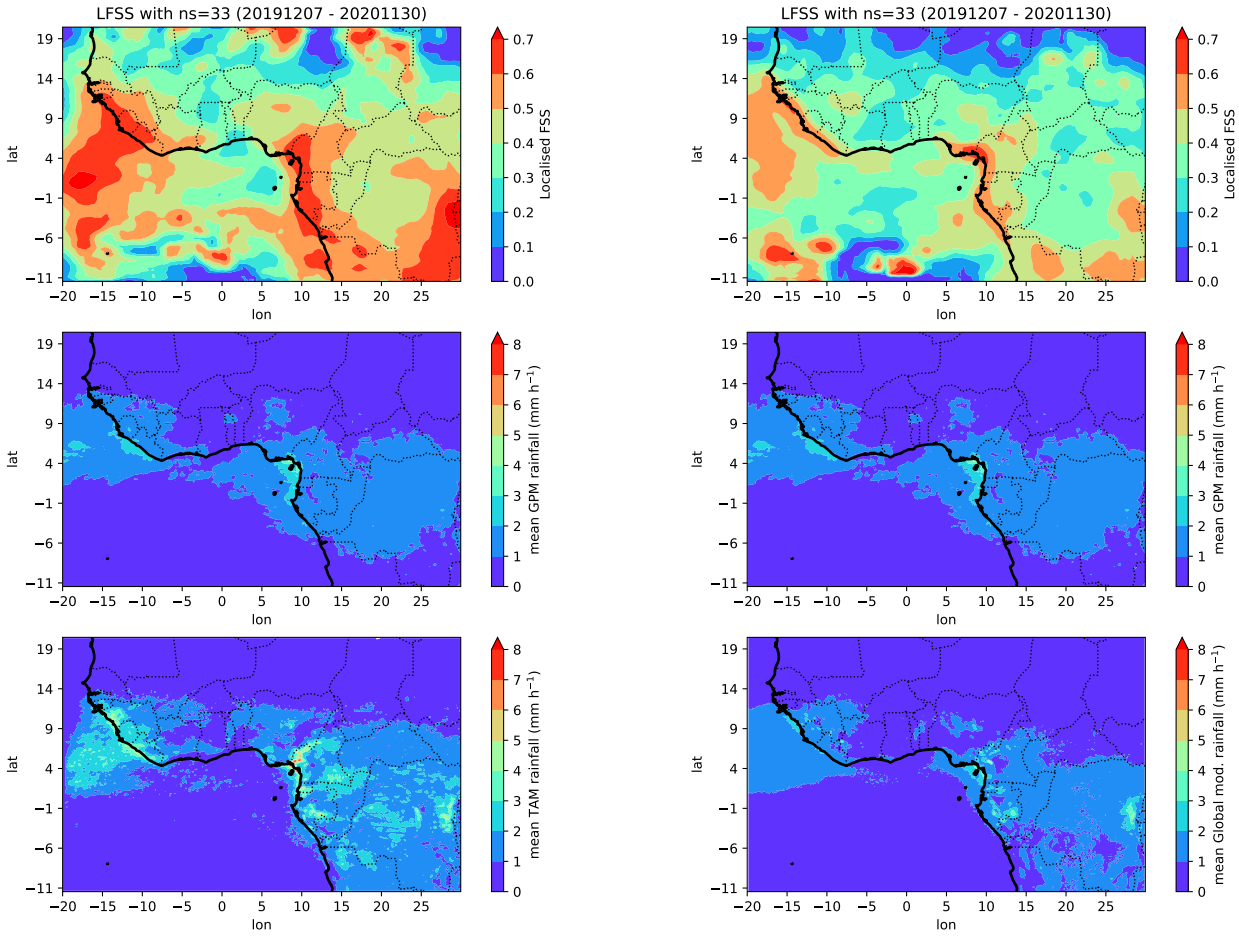


Figure 6.5: Localised FSS computed over West Africa using the neighbourhood size of 33 and the 97th percentile threshold. TAM (left), Global Model (right).

### 6.3.2 FSS versus neighbourhood sizes over West Africa

The greatest challenge of NWP models is predicting the location and timing of convective systems which are strongly controlled by local processes that are generally poorly represented and assimilated into model initial conditions. Moving to a higher resolution is the first step in the attempt to improve the prediction of convection. To assess

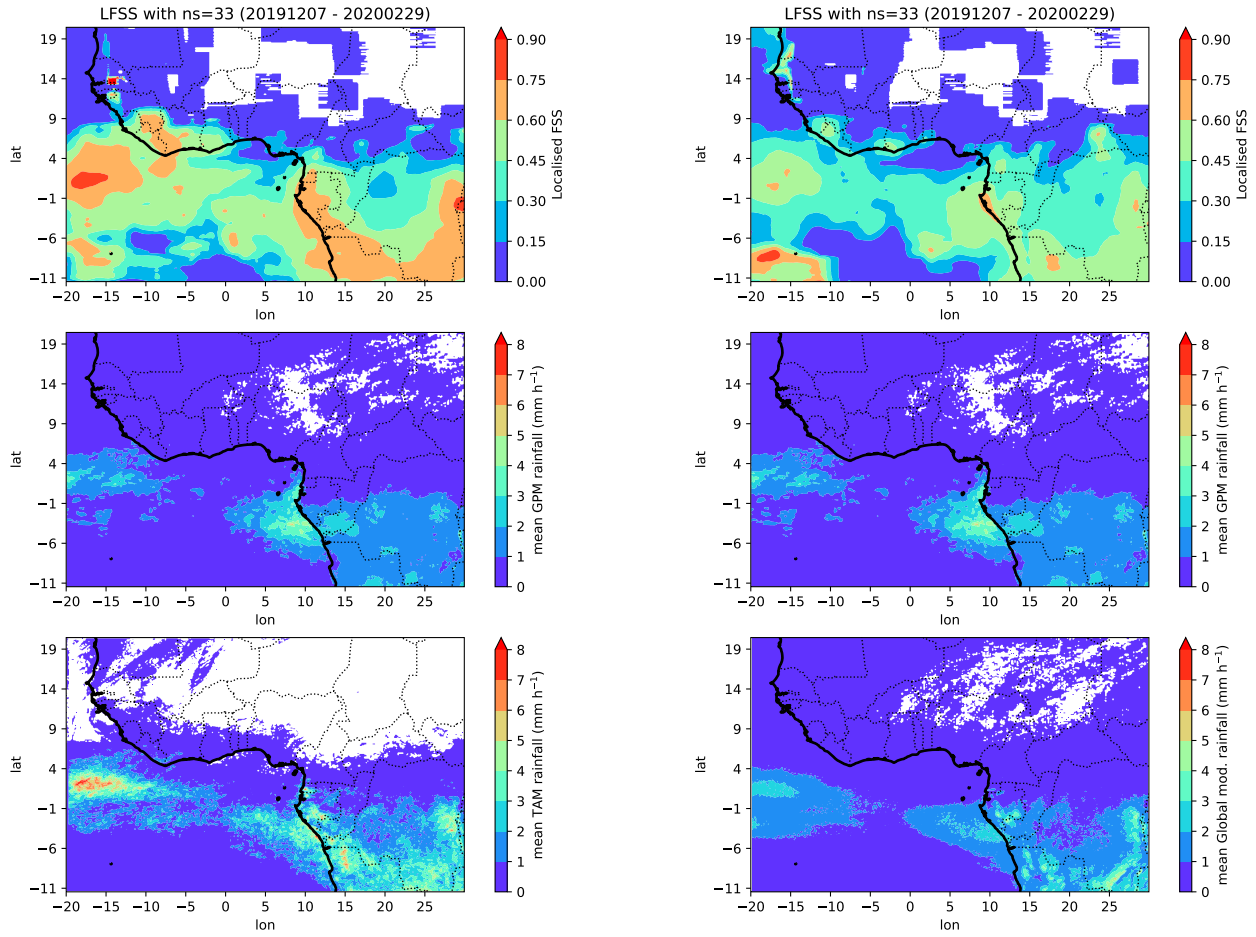


Figure 6.6: Same as Figure 6.5 but for the DJF season.

the TAM's ability to predict the location of storms, the FSS is computed for different neighbourhood sizes. The results for each of the sub-regions over the entire study period is compared in Figure 6.10.

The FSS generally increases with increasing neighbourhood size. For forecasters, the reliability of a model in any specific location will depend on the model's ability to simulate storms within the smallest radius (neighbourhood) possible. It is therefore very useful to determine the smallest neighbourhood size for which the model has skill. As suggested by Roberts and Lean (2008), an FSS $\geq 0.5$ is considered skilful enough for this purpose as it is halfway between random forecast (FSS = 0.0) and a perfect forecast (FSS = 1.0) (Burton et al. 2022).

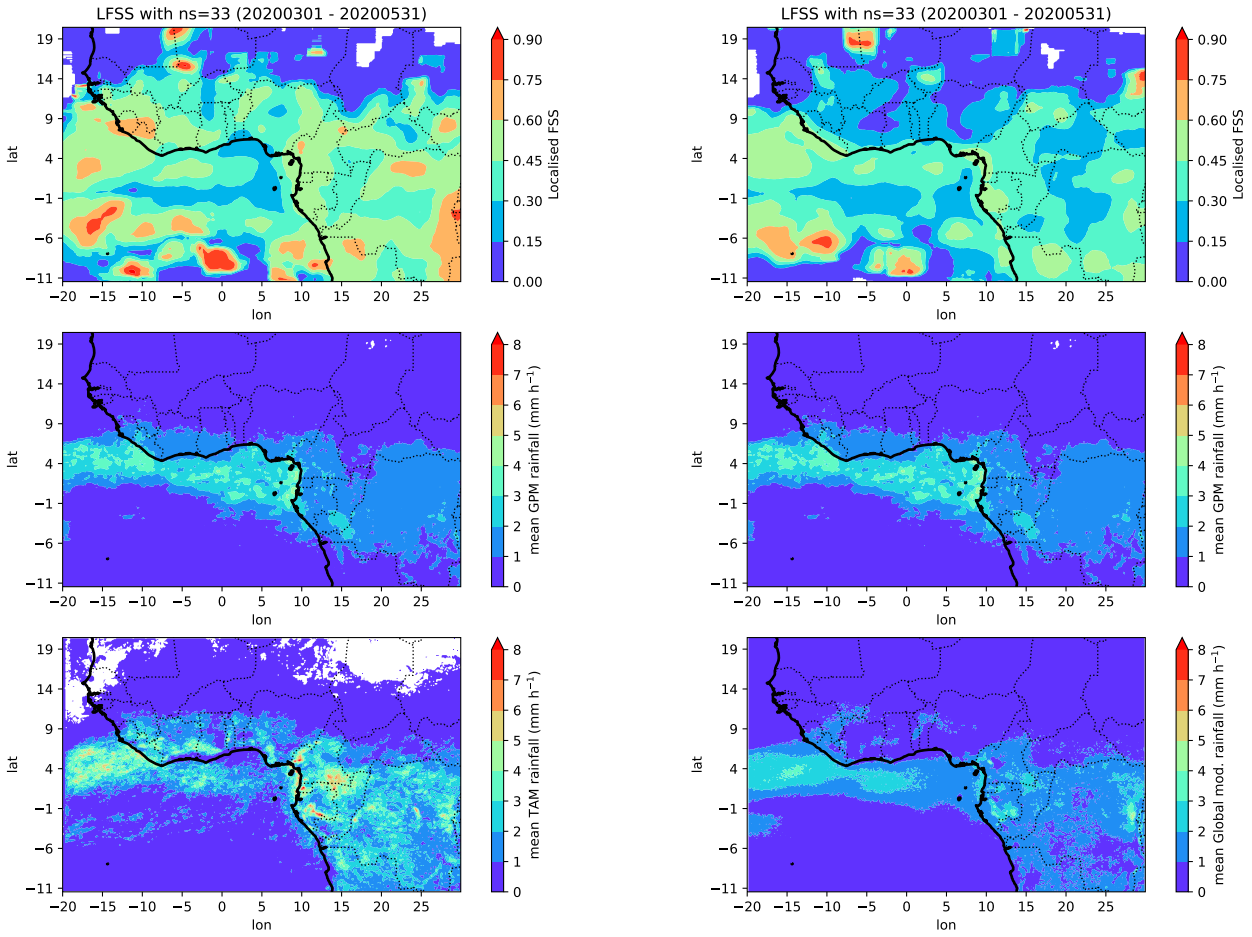


Figure 6.7: Same as Figure 6.5 but for the MAM season.

#### 6.3.2.1 What is the smallest neighbourhood size for which the model has skill in each sub-region?

Over the entire West Africa, the smallest neighbourhood size for which the TAM has skill is about ∼350 km. The Coast, the Gulf and the Congo area follow with ∼390, 420 and 430 km respectively. SWA and the Sahel show insignificant skill in both models for FSS threshold of 0.5. For the Global model, the Gulf showed the highest skill with the minimum neighbourhood size of 320 km. The Coast, West Africa and the Congo area follow with the least neighbourhood sizes of 500, 520 and 580 km respectively. The range of length scales seen over the various land regions of the Global model is therefore too wide to be useful for forecasters. A distance of ∼500 km means that, a forecaster who observes rain in Accra has to expect the rain to occur anywhere in-between Togo to Cote d'Ivoire.

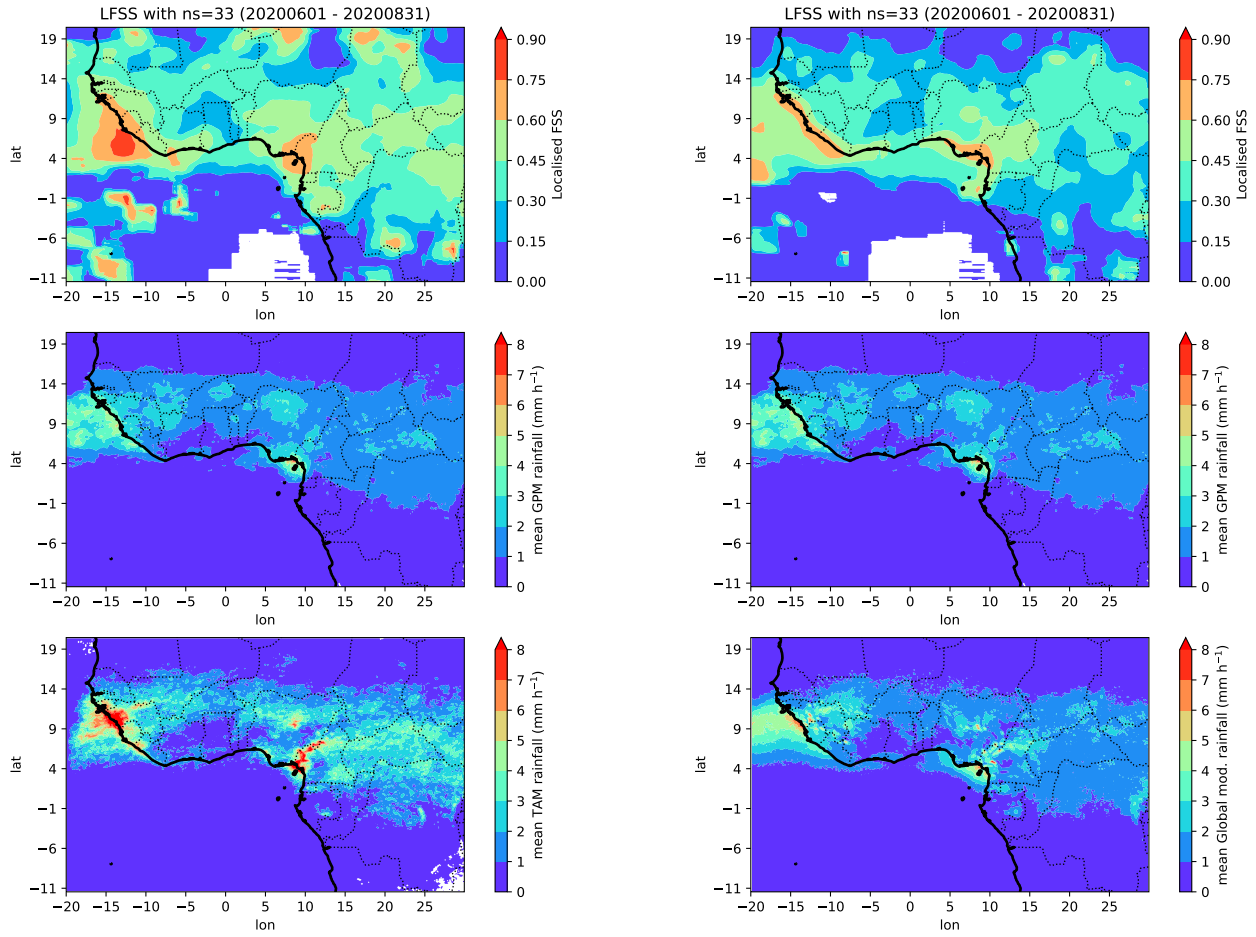


Figure 6.8: Same as Figure 6.5 but for the JJA season.

The TAM generally outperforms the Global model for all the sub-regions except for the Gulf and the Sahel where the Global model outperforms the TAM. The higher skill of the global model over the Gulf of Guinea is possibly because the advantage of a higher resolution model is to represent more accurately sub-grid scale processes such as orography, vegetation, rivers, lakes, land surface temperatures etc. These are mostly features peculiar to land surfaces rather than oceanic surfaces. The added value of high resolution models is therefore more on lands than over the oceans although a higher resolution also helps to improve model skill over oceans (Senior et al. 2021; Willetts et al. 2017). The skill over the Gulf is very high in both models. This high skill over the Gulf might be due to the models' ability to represent light rain (mainly from less organised convective systems) which occur mostly over the oceans and are associated

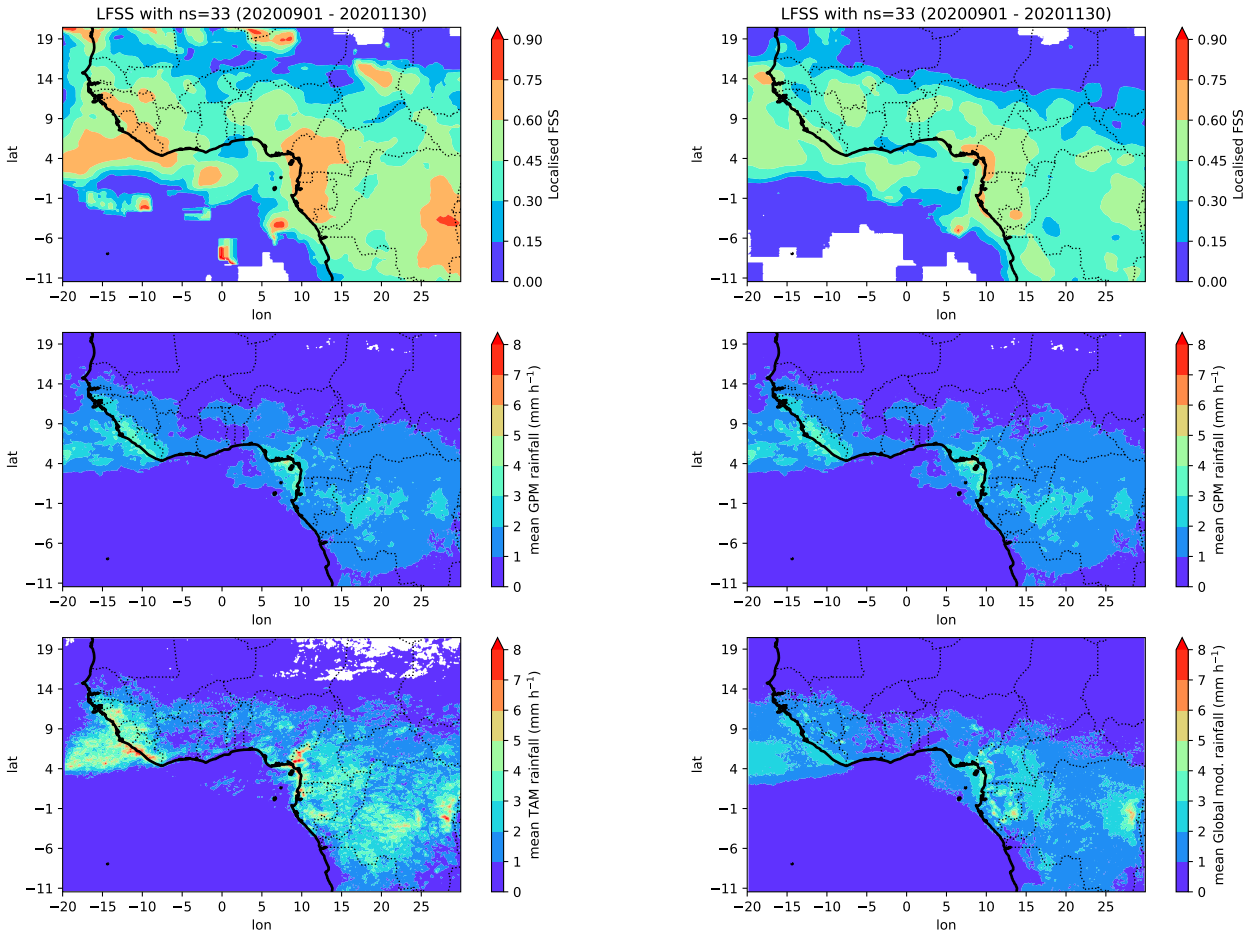


Figure 6.9: Same as Figure 6.5 but for the SON season.

with the well represented synoptic scale circulations.

For the different land regions, the coast showed the highest skill for the TAM possibly because of the TAM's ability to represent land-sea breeze circulations more accurately. This is consistent with Woodhams et al. (2019) who identified a better representation of lake-land breeze circulation in the CP model over the lake Victoria when simulated at 1.5 km. The Congo area, SWA and the Sahel follow respectively. The skill of the Global model over the Sahel outperforms the TAM for the entire period since the entire period is dominated by light rains which are well represented by the Global model. As shown in the next session, the skill of the TAM over the Sahel gets better for the JJA season where the region is dominated by well organised convective storms. This is indicative of the TAM's ability to simulate MCSs more accurately.

The skill over the Sahel is the lowest in both models as it has MCSs as the most dominant source of rain in the region (Maranan et al. 2018). The skill stays low as the simulation of organised convective systems is the greatest challenge of NWP models (Marsham et al. 2013; Woodhams et al. 2018). The skill of both models is significantly higher than the persistence forecast for the entire study domain (West Africa).

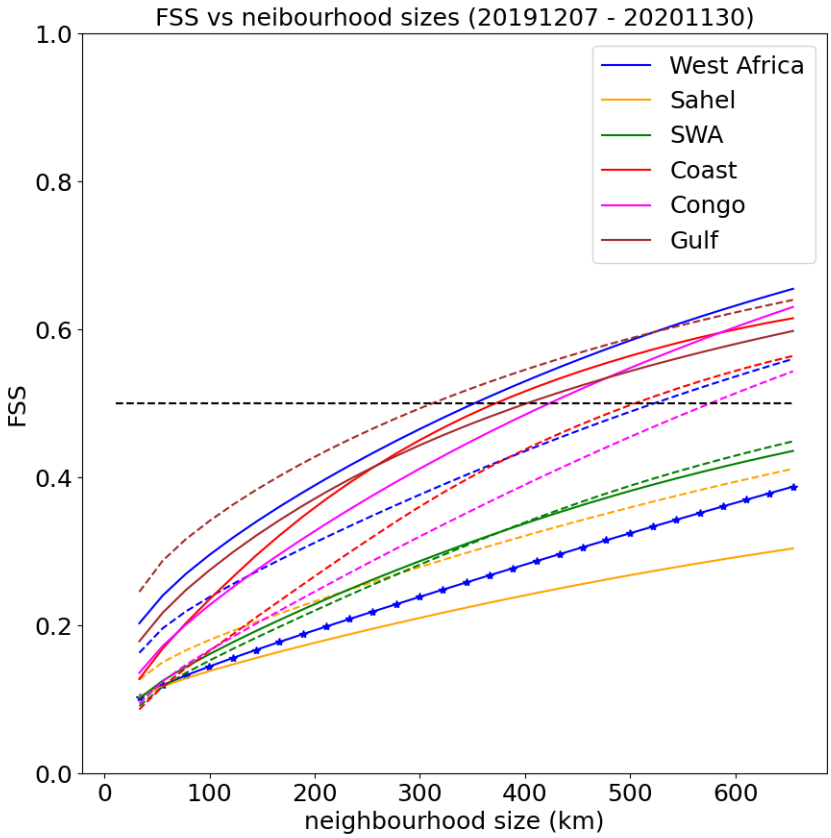


Figure 6.10: FSS versus neighbourhood sizes for the entire period (Dec 2019- Nov 2020). The Global Model data is shown in dashed line, the TAM data as solid lines and the persistence forecast as line with star.

#### 6.3.2.2 FSS versus neighbourhood sizes over West Africa -seasons

Figure 6.11 shows the variation of FSS skill with neighbourhood sizes for the different seasons. The TAM outperforms the Global model for almost all the sub-regions in all seasons. The skill of the TAM seems to be highest for the region of intense convective

activity in each season. In DJF, where convective activities are dominant over the Gulf, the skill of the TAM is highest in this region. In MAM and SON where convective activities are concentrated along the coast, the skill of the TAM is highest along the coast. In JJA where convective activities are mostly over the Sahel and parts of SWA, the skill of the TAM for the Sahel is highest. The difference in skill between the TAM and the Global model over the Congo area seems not to change much across the seasons as this region is known for consistent convective activities. However the skill of the TAM over the Congo area is highest in DJF and JJA.

The Global model outperforms the TAM over the Gulf (in JJA and SON) and the Sahel (in MAM and SON). As mentioned above, minimal convective activities in these regions during these seasons may be the reason for the poor performance of the TAM as the advantage of the TAM over the Global is its ability to predict convective storms more accurately. The Global model generally performs well in simulating the synoptic scale circulations which is mostly associated with weakly organised smaller sized systems associated with the presence of a cyclonic vortex (Maranan et al. 2018). The Global model however fails to simulate organised convective systems accurately as they parameterise these storms. The TAM therefore shows higher skill for these same regions during the season of their peak convective activity; DJF and MAM for the Gulf and JJA for the Sahel. These peak seasons are characterised by the presence of a strong meridional temperature gradient; leading to a strong AEJ, a strong low level winds; resulting in a strong vertical wind shear which favour more intense MCSs (as described in chapter 5).

The two models outperform the persistence forecast in all seasons over the entire domain of study (labelled as West Africa on the plots). Note, the Sahel and SWA had to be removed from the DJF plots as the rainfall recorded in these region were very low in this (dry) season.

### 6.3.3 FSS for different percentiles

The performance of the two models in simulating rainfall of different intensities is investigated. This was done by computing the FSS for varying rainfall thresholds (percentiles) for a fixed neighbourhood size (33 grid points). Figure 6.12 shows the results over the entire year of study. The two models generally show higher skill for light rains

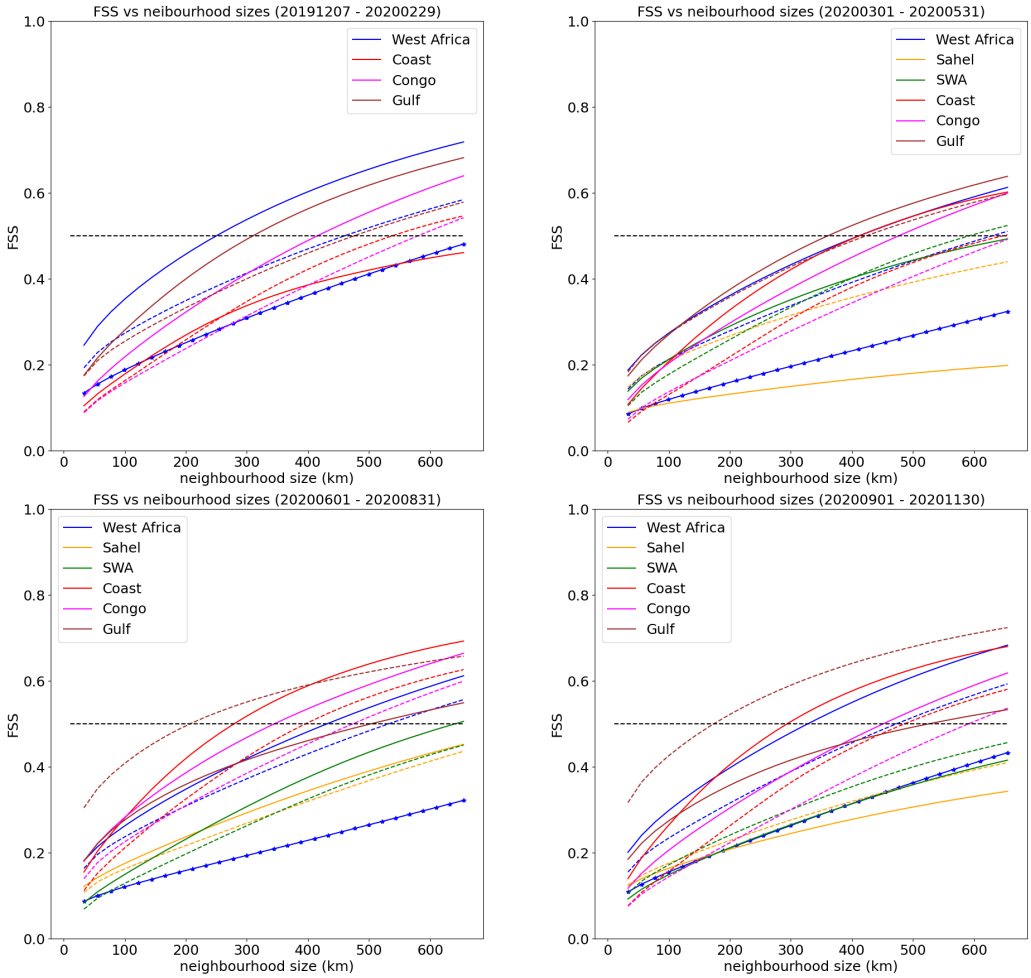


Figure 6.11: FSS versus neighbourhood sizes for different seasons: DJF (top left), MAM (top right), JJA (bottom left) and SON (bottom right). The Global Model data is shown in dashed line, the TAM data as solid lines and the persistence forecast as line with star.

(lower rainfall intensities) compared to heavy rains (higher rainfall intensities). The difference plot at the bottom reveals the difference in skill between the TAM and the Global model for the varying rainfall intensities. Generally, the TAM outperforms the Global model in most regions apart from the Sahel and the Gulf. The skill of the TAM increases with increasing rainfall intensities for almost all regions. The result for the entire study domain (W. Africa) summarises the relationship between the TAM and the Global clearly. The Global model outperforms the TAM for lower rainfall intensities while the TAM outperforms the global for higher rainfall intensities. This confirms the TAM ability to simulate very organised convective storms more accurately; which are

mostly high rain-rate storms.

The Global model outperforms the TAM over the Gulf but this difference decreases with increasing rainfall intensity. This might be due the the dominance of low intensity rain events over the Gulf which is generally well simulated by the Global model as they are mostly associated with large (synoptic) scale tropical convergence. Over the Sahel, the Global outperforms the TAM since this is a study over the entire year and not JJA only where highly organised convective systems dominates the Sahel. The breakdown of this plot into different seasons as seen in the next section sheds more light on this.

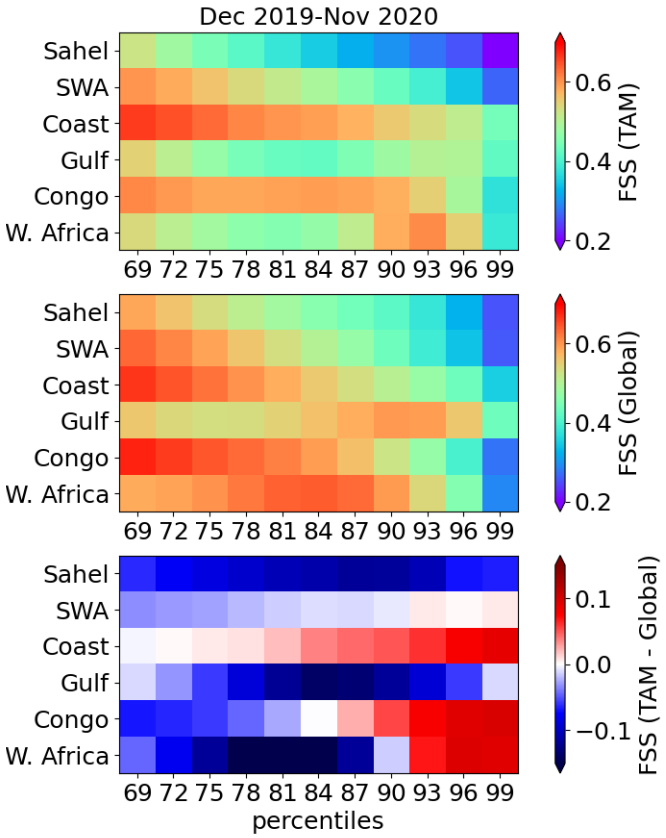


Figure 6.12: FSS for different percentiles using neighbourhood size of 33 for the entire period. Top - TAM, Middle - Global, Bottom - Difference (TAM-Global).

**FSS for different percentiles -seasons**

A detailed investigation of Figure 6.12 is done in this section by breaking it down into the different seasons (Figure 6.13). The ability of the models to simulate lower rainfall intensities as seen in the previous section is persistent in all seasons. This confirms the

skill of the models in simulating light rains which are associated with larger and synoptic scale systems. The Global models have shown good performance over the years for large scale circulations as the geostrophic approximation holds for these systems. The difference the convection permitting model makes here is its ability to simulate sub-grid scale systems more accurately. The TAM proves this ability to some extent by showing an improved skill for increasing rainfall intensities for almost all regions and all seasons.

In DJF the skill for lower intensity rainfall is generally very high especially for SWA and the Sahel (which are usually in their dry season in this period) in both models. But this decreases for higher intense events as these events are mostly contributed by very organised convective storms. The TAM shows an improved skill for these events in this season as expected in all the sub-regions except for the Sahel where the Global outperforms the TAM. The lower skill of the TAM compared to the Global model in the Sahel during this season might be due to the absence of highly organised convective systems in in the Sahel in this season as the Sahel is the driest region in the season. The TAM shows consistently higher skill over the Coast and even the Gulf for almost all rainfall intensities. This is likely due the concentration of organised convective systems in this regions during this time of the year as the ITD is at it's southernmost position in this period. The TAM continue to outperform the Global model in the Congo region for high rainfall intensities. This is likely because intense convective activities continue to occur in the Congo region in this season. The average skill over the entire West Africa generally shows higher skill of the TAM for both low intensity rainfall events and high intensity events. The global however outperforms the TAM for rainfall intensities between the 84th - 90th percentiles mainly due the the contribution from the Gulf.

In MAM convective storms begin to dominate the Coast and SWA. The skill of the TAM begin to improve for higher rainfall intensities in these regions. As organised convective storms leave the Gulf, the skill of the TAM begins to weaken during the transition from DJF to MAM. However, the TAM continues to outperform the Global for intense rainfall as expected over the Gulf, Congo and the entire West Africa. Over the Sahel, the Global model outperforms the TAM in this season for all rainfall intensities as rainfall in this season over the Sahel is normally contributed by less organised systems.

In JJA, convective activities dominates the Sahel as this region is characterised by the

presence of a strong AEJ, a strong vertical wind shear and drier mid levels. The TAM therefore shows high skill for intense rain events over the Sahel (particularly events greater than the 96th percentile). SWA, the Coast and the Congo exhibit similar characteristic. Over SWA, the TAM outperforms the Global model for rainfall intensities greater than the 78th percentile. Over the Coast the TAM outperforms the Global model for all rainfall intensities. The Global model outperforms the TAM for lower rainfall intensities over the Congo area however this switches in favour of the TAM after the 87th percentile. A similar situation is seen when averaged over the entire West Africa, the TAM outperforms the global for rainfall intensities greater than the 87th percentile. Over the Gulf however, the reverse appears to be the case. The TAM outperforms the the Global model for lower rainfall intensities but the skill switches in favour of the Global model for high rainfall intensities. This is probably because intense convective activities dominates the Sahel in this season as the ITD is further north in this season. Rainfall over the Gulf in this season is likely a contribution from mainly less organised systems which are simulated better by the Global model.

This skill of the TAM is however weakened over the Sahel and SWA in SON as the band of intense convective activities (located at about $10^oS$ of the ITD as shown in chapter 4) begins to retreat. This results in the dominance of convective activities mainly over the Coast resulting in a higher skill seen in the TAM over the Coast in this season especially as rainfall intensities get higher. The Gulf however continues to show lower skill in the TAM for higher rainfall intensities as storms over the ocean remains less organised. Over the Congo and the entire West Africa, the the skill of the TAM remains high for higher rainfall intensities consistent with the association of high rainfall intensities with well organised convective systems.

### 6.3.4 FSS for different times of day

The skill of the models for different times of the day is investigated (Figure 6.14). The TAM outperforms the Global model for most of the regions at almost all times except for the Gulf, the Sahel and SWA. Over the Gulf of Guinea, the TAM outperforms the Global model only in the early hours of the morning (00-06 UTC) where MCS activities peak over the ocean (as mentioned in chapter 4). Rainfall over the ocean during the remaining hours of the day are mainly light rain associated with the less organised convective systems described in Maranan et al. (2018) and are well simulated by Global models. Over SWA, the TAM outperforms the Global model during the

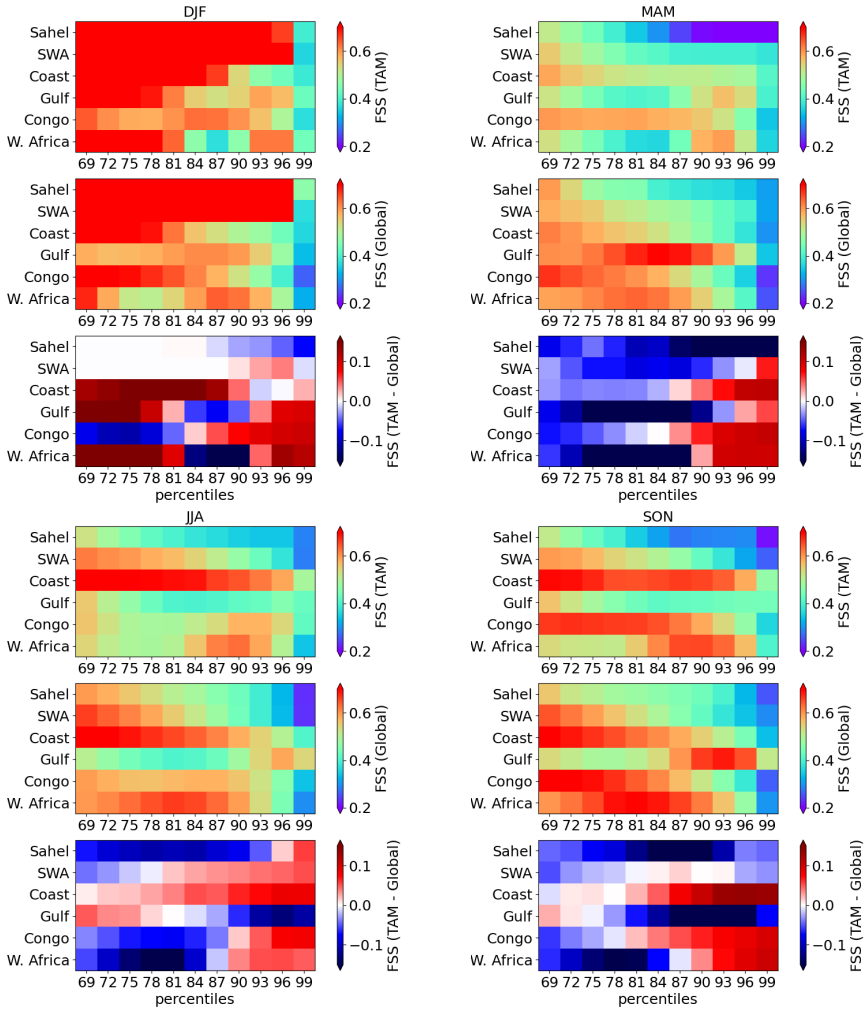


Figure 6.13: FSS for different percentiles using neighbourhood size of 33 for different seasons. Top - TAM, Middle - Global, Bottom - Difference (TAM-Global).

00-06 UTC and 12-18 UTC. The Global however outperforms the TAM over the SWA domain during 06-12 UTC and 18-24 UTC. Similarly, over the Sahel domain, the Global model seem to outperform the TAM during all the periods of the day. These appear so mainly because annual averages are considered here. Breaking the results into seasons (Figures 6.15 - Figures 6.18) reveal that the skill of the TAM over the Sahel or SWA is mostly high during the JJA season. In JJA season, the TAM outperformed the Global model over the Sahel and SWA in the early hours of the morning (00-06 UTC) and especially in the evenings (12-18 and 18-24 UTC) where organised convective activities dominates over the region (Figure 6.17). The 06-12 UTC is the period of the poorest performance of the TAM over these regions (Sahel and SWA) since convective activities

are minimal over these regions during these times.

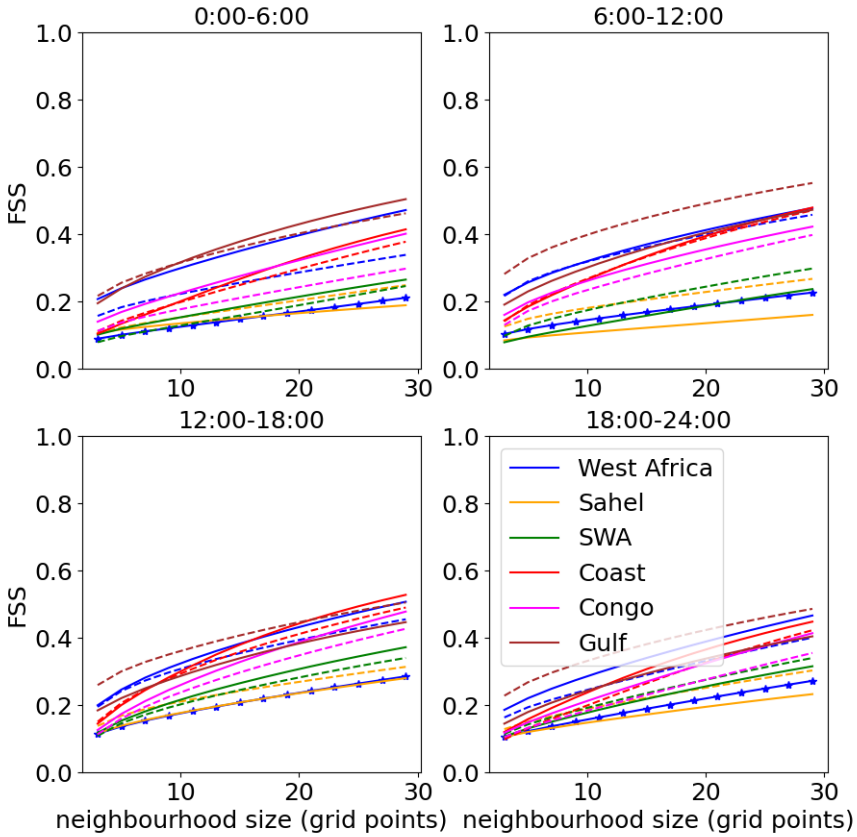


Figure 6.14: FSS versus neighbourhood sizes for different times of the day. The Global Model data is shown in dashed line, the TAM data as solid lines and the persistence forecast as line with star.

### 6.3.5 Evaluating the representation of the effects of vertical wind shear on storms

The model's ability to represent the effects of vertical wind shear on storms as found in chapter 5 is evaluated and discussed in this section. Figure 6.19 compares the relationship between Outgoing Long-wave Radiation (OLR) and vertical wind shear in both the TAM and the Global model using data for JJA 2021. OLR values are lower in TAM compared to the Global model (top plots) suggesting the presence of more convective storms in the TAM than the Global model. The area covered by strong 600-hPa wind speeds (using $8\,\mathrm{m\,s^{-1}}$ as a threshold) is slightly larger in the Global model compared to the TAM. The mean OLR in the TAM exhibit a wavy pattern suggesting the model's

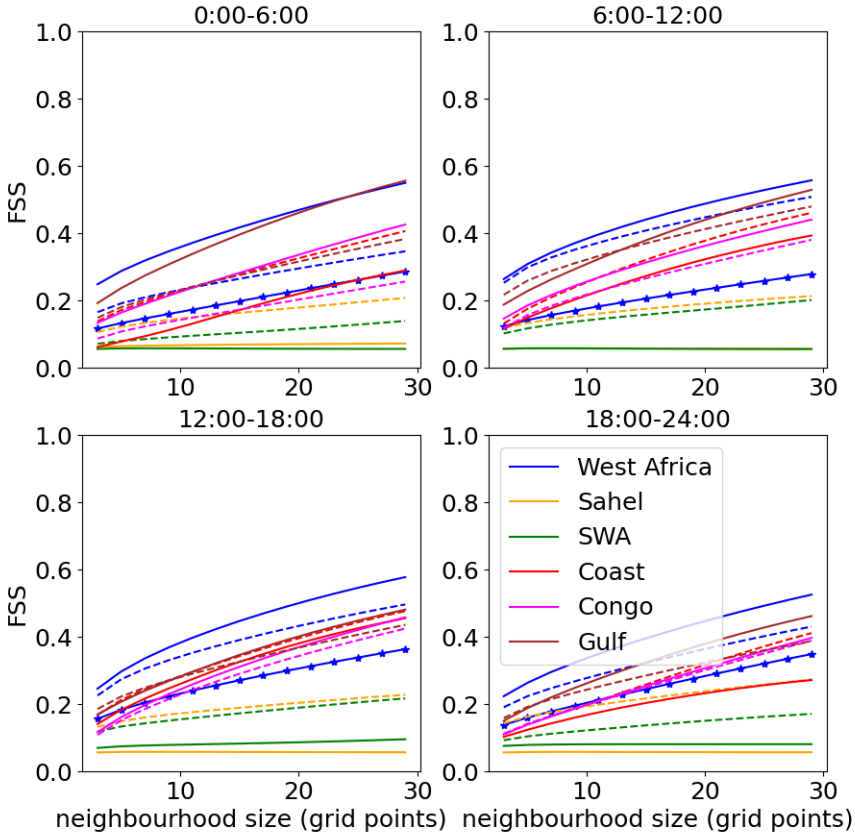


Figure 6.15: Same as Figure 6.14 but for DJF.

ability to represent the response of the OLR (convective storms) to the AEW. The mean 925-hPa winds does not differ in the two models. The regions with strong vertical wind shear values in the two models also do not differ (Figure 6.19 bottom plots).

The OLR in TAM exhibits a strong response to vertical wind shear as compared to that of the Global model (Figure 6.19 middle). This effect is mainly seen in the north western parts of the Sahel as well as parts of the north east. Relatively warmer storms (characterised by high OLR values) dominates the Gulf, southern parts of the Congo area and the North of the Sahel region which are also the regions with the lowest vertical wind shear values. The Global model struggles to represent the effect of vertical wind shear on storms in the region. There is a good relationship between low OLR values and vertical wind shear in the north-western side of the Sahel and parts of the the extreme east of the Sahel. However, most of the remaining regions with high shear do not show an association with lower OLR values.

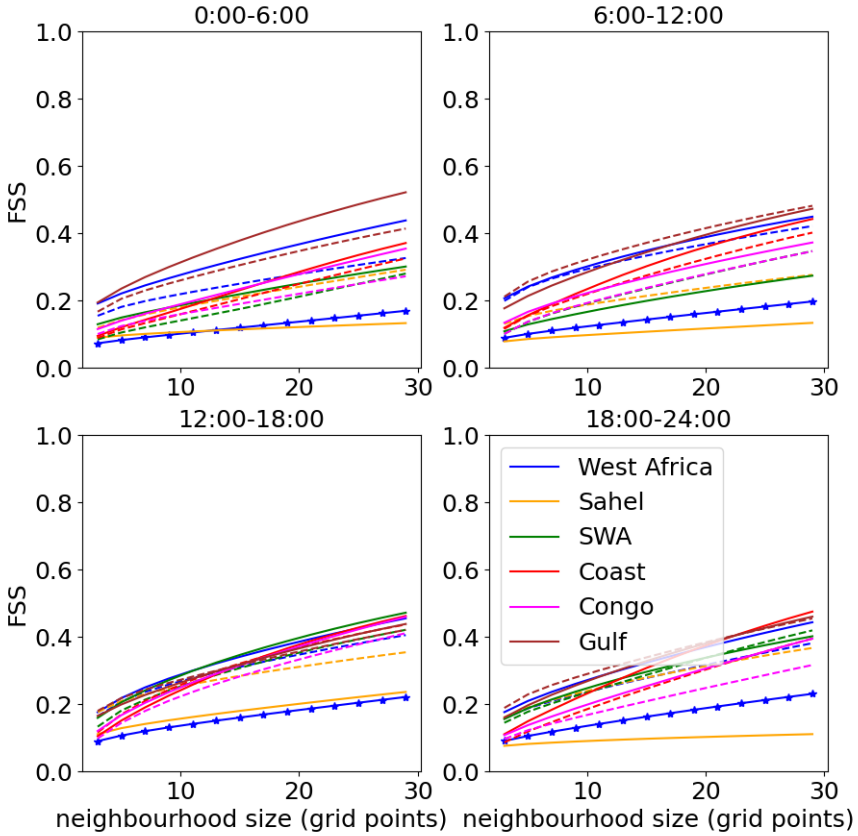


Figure 6.16: Same as Figure 6.14 but for MAM.

This results demonstrates a better representation of the effects of vertical wind shear on storms in the TAM compared to the Global model. It should be noted that, this analyses is only based on the model climatologies and not tracked storms during the period. A detailed investigation based on environments associated with tracked storms within the model will be a very useful future work.

## 6.4 Discussion and conclusions

The performance of the Met Office TAM has been evaluated over the entire West African domain using the FSS. The model's ability to represent the effect of vertical wind shear on storms as found in chapter 5 has also been evaluated using the model's OLR and associated 600 - 925-hPa winds. The skill of the TAM was compared with

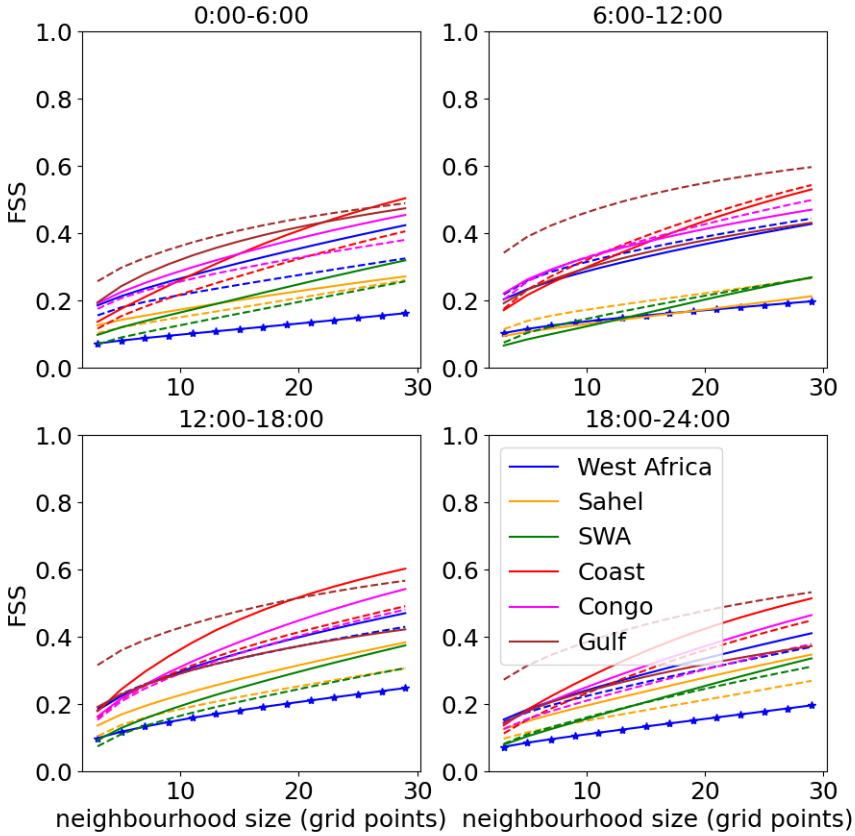


Figure 6.17: Same as Figure 6.14 but for JJA.

the skill of the Met Office Global model. GPM rainfall was used as the observations in this evaluation. The effect of the TAM's ability to simulate more realistic storms and to represent the diurnal cycle of convection and it's associated rainfall more accurately on the forecast skill was assessed by comparing the skill for daily rainfall accumulations to that of sub-daily (6 hourly) rainfall accumulations. The effect of the long spin-up period associated with the TAM on the forecast skill was also accessed by comparing the model skill of day 1 forecast to Day 2. A detailed evaluation of Day 2 forecast has also been performed. The LFSS has been used to investigate the spatial variation of the model skill. The ability of the model to simulate the closest location of observed convective activities has also been investigated by comparing the FSS of the models with different neighbourhood sizes. The ability of the model to simulate organised convective storms (high rain-rate storms) has also been assessed by comparing the skill of the model for different rainfall intensities. And finally, the performance of the model for different times of the day has also been investigated.

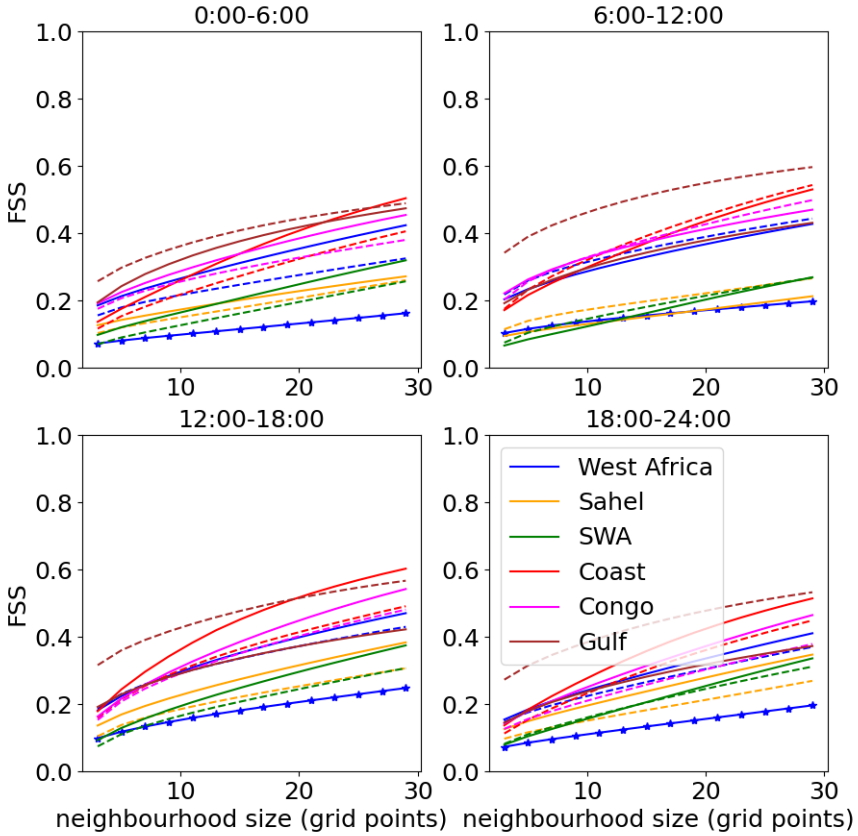


Figure 6.18: Same as Figure 6.14 but for SON.

The TAM simulates smaller storms with high rainfall intensities which is consistent with Woodhams et al. (2018); Hanley et al. (2021) who found excessive rain-rates in the earlier version of the model over east Africa (CP for East Africa). Woodhams et al. (2018) attributed this to the semi-Lagrangian advection used in the MetUM which does not conserve mass. The current version of the model however uses the Regional Atmosphere and Land version 1 science configuration (RAL1) which was expected to improve this bias. Not much improvements to the rainfall intensities have been made although this configuration compares better with GPM observations (Hanley et al. 2021). The updated configuration RAL2 is expected to be better at representing rainfall in the tropics. A useful future analysis would be to compare the RAL1 and RAL2 configurations. Percentile thresholds were used in the computation of the FSS and LFSS instead of absolute rain-rates. Using percentile threshold was useful in accounting for uncertainties associated with the GPM rainfall which was used as the observed data in this evaluation.

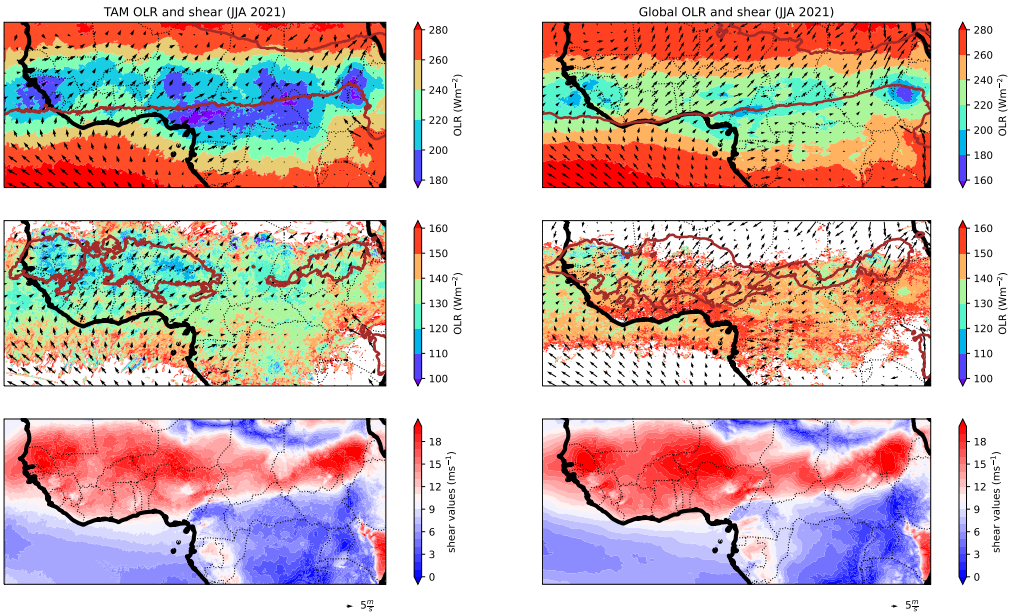


Figure 6.19: Mean OLR (shaded, top and middle) and vertical wind shear values (bottom) for both the TAM (left) and the Global model (right) during JJA 2021. The 925-hPa winds are overlaid in arrows. The 600-hPa wind speed contour at $8\,\mathrm{m\,s^{-1}}$ and the vertical wind shear contour at $16\,\mathrm{m\,s^{-1}}$ are overlaid on the top and middle plots respectively. OLR greater than $170\,\mathrm{W\,m^{-2}}$ are masked out of the middle plots.

Both models performed better than the persistence forecast which confirms the findings of Woodhams et al. (2018) that the models are valuable forecasting tools. The skill of the TAM is better for sub-daily rainfall compared to daily rainfall accumulations confirming the improved diurnal cycle and simulation of more realistic storms found in earlier studies of CP models (Marsham et al. 2013; Birch et al. 2015; Woodhams et al. 2018; Hanley et al. 2021). The high skill of the TAM when the FSS was compared for different times of the day also confirms this. The performance of the TAM is also better for Day 2 forecast compared to Day 1. This is due to the long spin-up associated with the TAM (12-18 hours) (Hanley et al. 2021). Exploring the use of warm-starts may therefore be useful in minimising this effect (Warner et al. (in preparation)).

The LFSS showed higher skill of the TAM over mountainous areas and coastal areas where near surface convergence is strongest confirming an improved ability of the TAM to capture convergence associated with orography as well as sea-land breeze circulation more effectively (Birch et al. 2014, 2015; Woodhams et al. 2019). Birch et al. (2015)

showed that the Met Office Global model with parameterised convection couldn't capture convection associated with convergence from sea-land breeze circulations although it is able to reproduce the main rain-forming sea-breeze circulation. This is because convective parameterisation causes rain events to occur too early in the models, cooling the boundary layer and reducing the the land-sea temperature contrast required for sea-land breeze circulation. The global model however performed better generally over the oceans (consistent with Woodhams et al. (2018)) mainly because rainfall over the oceans is generally dominated by less organised convective systems which are associated with the synoptic scale circulations. Evaluations from forecasters in the region suggest that most global models capture large scale systems well. Although there is improvement in skill over the oceans during the main seasons of convective activities (mainly DJF and MAM), the improvement in skill seen in the TAM is stronger over land than over the oceans. The TAM performs better over land than the oceans because, the advantage of a high resolution simulation is to better represent the sub-grid scale features like orography, vegetation, lakes and rivers which are generally land features than oceanic. Moreover, the response of convection to low-level convergence (which is a key feature associated with the initiation and sustenance of convection as seen in section 4 and well represented in CP models (Birch et al. 2014)) is seen more over lands due to the presence of orography and other local features.

The assessment of the closest radius (neighbourhood size) within which the TAM is able to simulate rainfall revealed that, the smallest neighbourhood size for which the TAM has skill for West Africa is ∼350 km as against ∼510 km of the Global model. A distance of ∼510 km as seen in the Global model means that, a forecaster who observes a rain in Accra has to expect the rain to occur anywhere in-between Togo to Cote d'Ivoire. The closest neighbourhood size suggested by the Global model is therefore not useful for forecasters in the region. The skill of the TAM for the various sub-region showed that, the coast had the smallest neighbourhood size of ∼390 km. The Gulf and the Congo area followed with ∼420 and 430 km respectively. The skill of SWA and the Sahel were however insignificant as FSS threshold of 0.5 was used. Lowering the FSS threshold could show significant skills over the SWA and the Sahel, however 0.5 was used according to the suggestion of Roberts and Lean (2008). The results therefore indicates that, a 0.5 FSS threshold is not useful for all regions. It is therefore useful to investigate the most appropriate threshold for each region.

The TAM generally outperforms the global model for high rainfall intensities. The Global model performs better for low rainfall intensities. Light rain is well simulated

generally by all models (in all seasons) as light rain is normally associated with synoptic scale cyclonic vortices which is believed by forecasters to be well represented in most models. The skill for high intensity rainfall events (mainly associated with very organised convective systems) is generally low in both models (due to the scales on which they occur - a sub grid scale systems). The TAM however showed a higher skill for high rainfall intensities which suggests the TAM's ability to simulate organised convective systems more accurately. This is consistent with earlier works that have demonstrated the TAM's ability to represent both the diurnal cycle of convection as well as it's response to orography, sea-land breeze circulation and the associated low-level convergence as described above (Marsham et al. 2013; Birch et al. 2014, 2015; Woodhams et al. 2019). Particularly the skill of the TAM was highest during the season where organised convective systems dominates each region.

The assessment of the model skill for different times of the day revealed that, the performance of the TAM over the ocean was highest in the early hours of the morning but late evenings over land when convective storms dominates in each of these regions. The TAM outperforms the Global for most times of the day in almost all regions except for the Gulf. Over the Gulf, the TAM only outperforms the Global during the early hours of the morning (00-06 UTC) as convective activities peak at this period over the ocean. Over the Sahel and SWA, the TAM outperforms the Global model during the peak monsoon season (JJA) for all times of the day except the 06-12 UTC period where convective activity is minimal over these regions. The skill of the TAM over the Global model for the Sahel in JJA is highest in the evenings (12-18 UTC and 18-24 UTC) since convective activities peak over this region during this period. This result is consistent with Woodhams et al. (2018) who found that the FSS in the earlier version of the TAM over the lake Victoria peaked at 1500, 1800 and 2100 LT. These correspond to the peak times of initiation and sustenance of matured storms over land.

The TAM exhibited a better representation of the effects of vertical wind shear on the convective storms (regions with lower OLR values) as compared to the Global model. Regions with lower OLR values were associated with high vertical wind shear values. The Global model however struggled to represent this effect. The mean OLR in the TAM also exhibited a wavy nature suggesting a response of the model's storms to the large scale AEW.

Generally, an improved skill has been seen in the TAM compared to the Global suggesting an improved representation of MCSs and it's response to vertical wind shear and the AEW in the TAM compared to the Global model. It should however be noted that, GPM overestimates the size of storms. It also underestimates heavy rain and overestimates light rain, therefore biases in the TAM may be exaggerated (Tian et al. 2018). The evaluation of the effect of vertical wind shear in the model's was also done using the models' climatologies within for the period of JJA 2021 and not environments associated with tracked storms in the models. Further investigation comparing tracked storms within the models would be a useful extension of this work in the future.

# Chapter 7

# Conclusions and recommendations

## 7.1 Conclusions

The aim of this thesis was to address the problem of tropical weather forecasting by improving our understanding of the (thermo-)dynamic environments of MCSs in West Africa and evaluating their representation in high-resolution NWP models, and so inform the use of NWP models in forecasting rainfall in West Africa. This study is important because HIW systems pose threats to farmers, fishermen, industries, and many lives and properties in West Africa. MCSs were the main storm type studied here because they are one of the most devastating type of HIWs in West Africa. MCSs remain poorly represented and therefore poorly predicted in parameterised and even convection-permitting NWP models due to the sparse nature of observations in the region and our limited understanding of the (thermo-)dynamics of MCSs. Therefore, it is necessary to improve our understanding of the (thermo-)dynamic environments of MCSs and investigate the accuracy of the forecasts of their associated precipitation in NWP models.

Given that the climate of West Africa exhibits a high spatial variability from the Gulf of Guinea in the south to the Sahel in the North, the (thermo-)dynamic environments of MCSs in the region were investigated by demarcating the study region into 6 subregions (the Gulf, Coast, SWA, Sahel North Atlantic and the Congo area). The unique environments of matured MCSs were investigated in chapter 4. The reason why some storms live longer and propagate faster than others was also investigated by grouping

the storms according to their various lifetimes and speeds. The environmental conditions associated with long-lived fast moving MCSs as against those of short-lived slow moving MCSs were then analysed. Long-lived storms were found to be associated with highly sheared environments. The effects of vertical wind shear on MCS intensity was investigated in detail in chapter 5. Finally, the ability of a convection permitting model to forecast rainfall rates in West Africa was evaluated over the various sub-regions of West Africa in chapter 6 by using the FSS. The 4.4 km Met Office TAM was the main model used as products from this model are made available to African forecasters as part of the Met Office's contribution to the WMO's Voluntary Cooperation Programme. The TAM was evaluated against the Met Office Global model to ascertain the advantages or disadvantages of the convection-permitting model against the Global model with the aim of providing a hint of the TAM's ability to simulate convection more accurately.

The observed MCSs studied in this thesis were obtained from the MCSs tracked from CLAUS brightness temperatures using the Huang et al. (2018) algorithm which combines a Kalman filter with the traditional area overlap method; therefore small and fast moving MCSs are tracked more accurately. The associated environments and rain-rates of the MCSs were selected from ERA-Interim and TRMM 3B42 respectively. Mature MCSs were used here which was defined as the stage in the lifetime of an MCS where the associated brightness temperature was coldest. GPM rain-rate data were also used as the observed data for the evaluation of the Met Office TAM.

The typical environments of matured MCSs included regions of strong surface convergence and high orography (chapter 4). Matured MCSs were also associated with highly sheared environments characterised by the presence of a strong mid-level AEJ core, 925-hPa winds, a near surface convergence south of the ITD region, and a mid-level relative vorticity maxima. The analysed strong near surface convergence precedes the arrival of an observed matured storm. The convergence leads to strong vertical velocities that supports the development of an intense MCS and an upper level divergence that compensates the near surface convergence. A strong outflow from the storm results in surface divergence over the Sahel and SWA right after the passage of the storm. Maranan et al. (2018) found this post-storm surface divergence to be associated with most of the rainfall types in SWA (especially storms with broad stratiform regions, deep convective cores and wide convective cores).

Long-lived storms had moderate speeds (10 - 25 $ms^{-1}$), associated with a strong vertical wind shear ($> 8\ m\,s^{-1}$) which led to moderate size storms ($\sim$125000 - 190000 $km^2$) with high rain-rates ($> 4\ mmh^{-1}$) and colder BTs (<210K). The long-lived storms were also associated with the presence of AEWs. The sizes of the storms generally increased with lifetime and speed. This result is consistent with Maranan et al. (2018) who showed that long-lived storms had colder BTs and Tomasini et al. (2006) who also showed that long-lived fast moving storms had the largest sizes. Short-lived slow moving storms were associated with weaker vertical wind shear ($< 8\ ms^{-1}$), smaller in sizes ($< 125000\ km^2$), low rain rates ($< 5\ mmh^{-1}$) and warmer BTs (< 213K). Consistent with Lafore et al. (2017), the short-lived storms were the most numerous but had low rain rates and were often located near mountainous areas.

Generally oceanic storms were associated with the highest mean rain-rates (4.5 - 5.4 $mmh^{-1}$) compared to land storms (2.4 - 4.5 $mmh^{-1}$). The highest mean rain-rate associated with land MCSs was found along the Coast (4.5 $mmh^{-1}$). The Congo, SWA, and Sahel followed with decreasing mean rain-rates of 3.6, 3.2 and 2.4 $mmh^{-1}$ respectively. Sahelian storms were the fastest with the average speed of 13.9 $ms^{-1}$ as they were associated with the strongest vertical wind shear and steering level winds (AEJ). SWA, the Congo area, Coast and the oceans followed in decreasing order of mean storm speeds of 13.5, 12.0 and 11.5 $ms^{-1}$ respectively. The main factors that determine MCS speed in the region are not fully understood but we hypothesize that, MCS speeds are determined by the steering level winds and also modified by the vertical wind shear. The higher rain rates and stronger surface convergence associated with oceanic storms compared with land storms suggests that, high rain rates results from a strong surface convergence and corresponding strong vertical velocities in a moist environment, leading to a strong influx of moisture into the storms. While a near surface wind convergence is associated with the oceanic and coastal storms, the convergence associated with land MCSs generally initiates from the surface but it elevates and maximises around 800 - 700 hPa level.

A detailed investigation of the effect of vertical wind shear on MCSs showed that, a strong vertical wind shear results in colder BTs relative to their temperatures at their LNB (chapter 5). Since this BT, is the BT of the anvil and not just the over-shooting top, it was hypothesized that this happens by increasing the updraft and minimising entrainment. This is consistent with a recent idealised model simulations showing that vertical wind shear can reduce entrainment dilution of squall-lines (Mulholland et al. 2021). Storms over oceans get closer to their LNBs compared to storms over the land

suggesting that higher entrainment rates of drier air over land compared to the ocean prevents storms from reaching their LNBs (Becker and Hohenegger 2021). This speculation was investigated further by comparing the vertical shear and mid level specific humidity to their associated BT_diffs and rain-rates. In almost all the sub-regions apart from some samples over the Sahel and the Gulf, higher mid-level specific humidity with high vertical wind shear resulted in minimised BT_diffs. Over the West Africa land regions (Sahel, SWA and the Coast), higher mid-level specific humidity with high vertical wind shear did not only result in minimised BT_diff but also high rain rates. The effect of vertical wind shear shown in this study provides some observational evidence supporting an earlier work by Peters et al. (2019) that entrainment dilution of storm updraft cores prevents storms from reaching their LNBs. Some high sheared storms over the Sahel and the Gulf showed dry mid-levels giving cold cloud tops which could be attributed to the balance between the strong shear and the downdrafts from a storm resulting in strong (more vertical) updrafts as proposed by Rotunno et al. (1988).

Finally, the performance of the Met Office TAM for rainfall was evaluated over the entire West African domain using the FSS (chapter 6). The model's ability to represent the effect of vertical wind shear on storms as found in chapter 5 was also evaluated. The LFSS defined and used in Woodhams et al. (2018) was used to investigate the spatial variation of the model skill. The ability of the model to simulate the right location of a rain event was also investigated by comparing the FSS of the models with different neighbourhood sizes. The ability of the model to simulate high rain-rate events (organised convective storms) was also assessed by comparing the skill of the model for different rainfall intensities. Here, high rain-rate events were considered as a proxy for organised convective storms as most cold BT storms have large sizes and are associated with high rain-rates (Figure 4.15). The TAM simulates smaller storms with high rainfall intensities. The skill of the TAM is highest over coastal areas and mountainous regions likely indicating the model's ability to simulate sea-land breeze and orographic effects more accurately. The skill of the TAM is better than the Global for sub-daily rainfall compared to daily rainfall accumulations as the diurnal cycle of convection is better represented in convection permitting models (Zhang et al. 2016; Crook et al. 2019; Li et al. 2020; Scaff et al. 2020). The performance of the TAM is again better than the Global for Day 2 forecast compared to Day 1 due to the long spin up period associated with the TAM. Over the entire West Africa, the smallest neighbourhood size for which the TAM has skill using an FSS threshold of 0.5 was ∼350 km. The TAM generally outperforms the global model for high rainfall intensities while the Global model performs better for low rainfall intensities. The

higher skill of the TAM for high rainfall intensities demonstrates its ability to simulate organised convective systems more accurately which is very useful for forecasters and model developers. The TAM also exhibited a strong response of the model storms to vertical wind shear and the AEW. This is a useful added value of the CP model since the Global model struggles to represent these effects.

## 7.2 Discussion and implication of results

The environmental conditions associated with matured MCSs in West Africa and the reasons why some storms live longer and propagate faster than others have been investigated. The effect of vertical wind shear on the intensities of MCSs has also been investigated. And finally the representation of rainfall in the Met Office convection-permitting TAM has been evaluated.

Matured MCSs in West Africa are generally associated with environments of strong near surface convergence which mostly occur around regions of high orography; especially elevated regions along the coast. The strong near surface convergence lead to strong vertical velocities and resulted in cold cloud top MCSs in the presence of a strong vertical wind shear. Unlike the oceans and the coast where the convergence is confined to the surface, the convergence associated with inland MCS elevates and maximises between 800 - 700 hPa where strong vertical velocities follow. The convergence of moisture at these levels enhances the coupling of moist diabatic processes and circulation in the propagation of the AEW through latent heating (Tomassini et al. 2017). Birch et al. (2013) showed that the synoptic scale convergence and circulation were important for a successful simulation of an MCS.

Over SWA and the Sahel, a strong outflow from the storm is seen after the passage of the storm which might be associated with the strong downdrafts and cold pools from an MCS. This outflow is significant over SWA and Sahel compared to the oceans and the remaining land regions probably because storms over SWA and the Sahel are generally more organised and have colder BTs compared to storms in the remaining regions. The strongly organised and colder BT MCSs over the Sahel and SWA is due to the presence of a strong vertical wind shear resulting from the dominance of a strong mid-level AEJ and near surface winds over these regions as compared to the other regions.

A detailed investigation of the effect of vertical wind shear on MCSs in West Africa has revealed that, a strong vertical wind shear results in MCSs with colder cloud tops relative to the temperature at their LNBs and high rain rates. This likely happens by increasing updrafts and minimising entrainment (Mulholland et al. 2021). Land MCSs struggle to reach their LNBs compared to oceanic MCSs probably due to a higher entrainment rate of drier air over land compared to moister air over the oceans (Becker and Hohenegger 2021). The entrainment dilution of updraft cores as suggested by Peters et al. (2019) in their study of supercells is likely what prevents storms from reaching their LNBs.

High rain rates associated with West African MCSs likely result from an influx of moisture through a strong surface convergence and associated high vertical velocities as inferred from the high rain rates and strong surface convergence associated with oceanic storms as compared to land storms. High rain rates of West African land MCSs is also associated with the presence of a strong vertical wind shear which contributes to the inflow of moisture into the storms (Alfaro 2017).

West African MCSs live longer when they are located in an environment of strong vertical wind shear or when they get coupled with the AEWs as most long-lived storms are located ahead of the wave trough (Mathon et al. 2002a; Tomassini et al. 2017; Tomassini 2018). These storms, however propagate faster than the AEWs (Dieng et al. (in preparation)) and the AEJ (not shown). The fast moving long-lived storms have the largest sizes suggesting that, the most organised long-lived storms (larger sizes) propagated faster than the AEW and the AEJ probably due to strong cold pool outflows from the storms which lead to secondary initiation of new cells as the storms propagated. Two main hypothesis can be deduced from this result: (i) storms live longer when they get coupled with he AEWs or associated with strong vertical wind shear; (ii) the most organised long-lived storms have larger sizes and propagates faster than the AEW and the AEJ due to high vertical wind shear and cold pool outflow from the storms enhancing the development of new cells as the storms propagates.

Using high resolution NWP models with permitted moist convection does not only improve the diurnal cycle of convection but also improves the representation of MCSs as inferred from the higher skill of the TAM for high intensity rain events compared to the Global model. The representation of orographic effects as well as sea-land breeze

circulation is probably also improved as inferred from the high skill over areas of high orography and coastal areas. The model's ability to represent the right location of convection is significantly improved as the nearest neighbourhood size for which the TAM has skill over the entire West Africa is ∼350 km compared to ∼510 km of the Global model based on an FSS threshold of 0.5. However, forecasters in the region are advised to take forecasts of the first 12 - 18 hours with a pinch of salt as the long spin up period of the TAM affects the model skill. Day 2 forecasts are generally better than Day 1 forecasts as a result, although the model skill generally decreases with increasing lead time. There is an improvement in the representation of the effects of vertical wind shear on the cloud top temperatures of MCSs in the TAM. Convection-permitting models better represents the relationship between vertical wind shear and the cloud top temperatures of storms but might not represent well the relationship between vertical wind shear and rainfall (Fitzpatrick et al. 2020a,b; Senior et al. 2021). The poor representation of the effect of vertical wind shear on entrainment might be the reason why convection-permitting climate models struggle to capture the relationship between vertical wind shear and rainfall.

## 7.3 Limitations of the work

### 7.3.1 The environment, characteristic lifetime and speed of Mesoscale Convective Systems in West Africa

Inadequate observations in the region (especially upper air observations) may have an impact on the accuracy of the reanalysis data used in the region. Reanalysis data were used as they were the only available data that could be considered as close enough to the observed. However, given that reanalysis data are largely model data with assimilated observations, the limited observed data in the region raises a great concern about the accuracy of reanalysis data in the region. Moreover, the analysed fields heavily depend on the convective parameterisation as few observations are assimilated, this introduces biases in processes such as the diurnal cycle. Lavers et al. (2022) showed that, ERA5 struggles to simulate observed precipitation totals although it generally captures their location and patterns. ERA5 was also found to be more skilful in the extratropics than the tropics. The performance of ERA-interim and other reanalysis products in representing rainfall in West Africa has been poor compared to satellites and other gauge based products (Manzanas et al. 2014). ERA Interim struggles to represent storms in some cases. However, using composites of MCSs seems to minimize

this deficiency. The storm environments are reasonably well represented as can be seen in this study. For instance Figure 4.5 shows ERA-interim's ability to correctly represent pre-post convective environments and its association with rainfall from TRMM 3B42.

The Huang et al. (2018) MCS data being 3-hourly means that, short lived storms (including storms with 4-5 h duration) can easily be missed. In the case of several simultaneous cells, individual tacks may have unrealistic jumps as a result of this temporal resolution. Such storms are more frequent over the Congo area and southern West Africa but might not be frequent over the Sahel where storms are mostly long-lived.

### 7.3.2 Observed effects of vertical wind shear on the intensities of Mesoscale Convective Systems over West and Central Africa

- Previous theories explaining the mechanism through which vertical wind shear affects storm intensities could not be verified in this study. Theories such as the Rotunno et al. (1988) theory and the Alfaro (2017) layer lifting model of convection were proposed based on idealised model experiments. These theories have been tested to some extent by Bickle (2021) over the Sahel but through an idealised experiment with large eddy simulation. Investigating these theories with observations will be a useful way to validate these theories. However, the inability of ERA interim data to resolve sub-km features associated with MCSs as explained earlier and inadequate observations in the region limited the ability to test these theories.

- To test the Rotunno et al. (1988) theory, it will be useful for the depth of vertical wind shear to be selected to be equal to the depth of the cold pool. Not much studies have specifically measured and compared the depth of West African cold pools over the ocean versus that over land. However, Bryan and Parker (2010) investigated the characteristics of a squall line from a rawinsonde data collected during the passage of a storm in Oklahoma using 9 soundings. The sounding showed cold pool depth to be $\sim$4 km deep. In this study, vertical wind shear was calculated from 600 hPa which is equivalent to $\sim$4.2 km. This might not be exactly equivalent to the cold pool depth of a typical West African squall line but 600-hPa seems a reasonable level as 4.2 km is a good estimate of cold pool depth based on Bryan and Parker (2010). 600-hPa also seem a reasonable level for all the sub-regions as the steering level winds (the AEJ) occur at this level.

As storms over the ocean are normally less organised compared to land storms, it is recommended that, in future works, an accurate test of the Rotunno et al. (1988) theory can be done by measuring the cold pool depth of storms over West African land and oceanic regions.

- The relationship between vertical wind shear and mid-level humidity needs to be investigated in detail. While the results over the Sahel seem to support earlier studies of drier mid-levels favouring most intense storms, most other sub-regions of West Africa showed a relationship between high vertical wind shear, and high mid-level humidity resulting in colder storms (Figure 5.5). The minimised BT_diff resulting from high vertical wind shear and moist mid-levels however confirms findings from an earlier work which showed that, drier air increases entrainment dilution of updraft cores (Peters et al. 2019). The Sahelian storms which rather showed minimised BT_diff for drier mid-levels in the presence of a strong vertical wind shear could be a confirmation of the Rotunno et al. (1988) theory which states that, strong (more vertical) updrafts could result from the balance between the horizontal vorticity generated by the cold pool outflow from a storm and that generated by vertical wind shear. As the intrusion of mid-level dry air results in stronger cold pools, drier mid-levels in the Sahel is likely to result in stronger cold pools required to balance the strong vertical wind shear in the region for strong updrafts to occur leading to colder BTs. This effect might be more pronounced in the Sahel than other regions because of the dominance of very organised convective storms in the Sahel (a region of high CAPE and CIN) compared to other regions in West Africa.

- The effect of shear on the intensities of MCSs in West Africa has been studied in this work. However, it will be useful to confirm if this effect remains the case over other tropical regions around the globe. This will be useful in providing a more robust explanation of the effect of shear on MCSs.

### 7.3.3 Evaluation of the Met Office Tropical Africa Model

- Only one year of data was studied which which was not long enough for a robust FSS computation for high rain-rates as a function of location. A longer dataset could not be used as the model was upgraded from RAL1 to RAL2 in December 2020.

- Since the work has been MCS focused, it would have been beneficial if a de-

tailed evaluation of the representation of MCSs in the TAM had been performed, however, there was not enough time to perform these in detail. Although high intensity rain events were considered as events associated with MCSs, a direct tracking of MCSs in the TAM and the subsequent selection of it's associated rainfall would be a valuable next step.

- A detailed investigation of the TAM's ability to represent the (thermo-)dynamic environments associated with MCSs as well as the representation of the effects of vertical wind shear on the storms as seen in chapters 4 and 5 is needed for a thorough evaluation of the model skill. However, this could not be performed in detail due to the limited time and funding available.

- Finally, the impact of ensemble forecasting over the region as suggested by Woodhams et al. (2018); Cafaro et al. (2021) could not be explored within the time available.

## 7.4 Recommendations

### 7.4.1 Recommendations for a short time scale (∼6 months - a year)

A useful continuation of the work within a short time scale will be to investigate the representation of the processes in the TAM and the Global model to ascertain the reason for the low and high skill in different regions.

- Track MCSs simulated within the TAM and the Global and investigate the skill to test the hypotheses raised in chapter 6:

  - *Does the TAM's ability to simulate high intensity rainfall indicate its ability to represent MCSs more accurately?*

- Select the (thermo-)dynamic environments of the tracked storms and investigate the model's representation of the mean storm environments as done with observation in chapter 4:

  - *How well do the models represent the (thermo-)dynamic environment of matured MCSs?*

  - *Are long-lived fast moving storms in the models' associated with a strong*

*vertical wind shear and the AEWs?*

- *How well do the models represent the (thermo-)dynamic environment before, during and after the passage of a matured MCS?*

- Select the associated outgoing longwave radiation, the rain-rates, the low level humidity, the mid level humidity, mid and low level winds and investigate the model's representation of the observed effect of vertical wind shear on storm intensities (as found in chapter 5):

  - *How well do the models represent the effect of vertical wind shear on BTs, BT_diffs and associated rain-rates?*

  - *How accurate is the models' representation of the response of BTs, BT_diffs and rain-rates to high vertical wind shear and mid-level humidity?*

  - *How well do the models represent the effect of vertical wind shear on BT_diff over the oceans and lands?*

  - *Does a better representation shear mean a higher skill?*

Other investigations that could be done in the short term include: A comparison between the runes initialised at 06 UTC and 18 UTC. This comparison will help to potentially investigate the spin-up problem in detail. As storms initialised at 06 UTC are more likely to spin up faster than storms initialised at 18 UTC as there is no solar radiation at 18 UTC to initiate convection.
A comparison between the RAL1 and RAL2 would also be useful in understanding the added value of RAL2. The RAL1 comes with two sub configurations, RAL-M for the mid-latitudes and RAL-T for the tropics (Bush et al. 2020). These sub configurations are useful for ensuring that the unique model configuration suitable for the tropics or mid-latitudes is used unlike its predecessors that used the same configuration tuned for the mid-latitudes for the tropics. The RAL2-T is expected to improve upon biases associated the RAL1 configuration as it comes with an improved model physics. Steptoe et al. (2021) found that simulations with the RAL2-T showed a better representation of tropical cyclone wind speed, gust speed and mean sea level pressure than that of ERA5 when compared with data from the International Best Track Archive for Climate Stewardship. The improved simulations with RAL2-T found in other works like Boutle et al. (2021) supports the need to properly evaluate the added value of RAL2-T configuration over Tropical Africa.

### 7.4.2 Recommendation for a longer time scale (∼ 3 years)

Exploring the use of ensembles over the region could help to improve the skill and quantify uncertainties within the model as a study over East Africa suggests (Cafaro et al. 2021). Cafaro et al. (2021) evaluated the skill of probabilistic rainfall forecasts from convection-permitting ensembles, convection-permitting deterministic, the global model ensembles and global model deterministic using the FSS. The convection-permitting ensembles provided more skilful forecasts than the convection-permitting deterministic, the global model ensemble and global model deterministic forecasts. As the Cafaro et al. (2021) study was conducted with the older RAL1-T and over East Africa which has entirely different climatic conditions and topographical features, repeating this work over West Africa using the TAM with the improved RAL2-T will be a very useful work. Moreover, given that the smallest neighbourhood size for which the TAM has skill over West Africa was ∼350 km using the FSS threshold of 0.5 which is still too coarse for forecasters to make useful decisions, testing the FSS of ensembles generated from the TAM will likely result in a smaller neighbourhood size that will be useful for decision making.

Testing the mechanism through which vertical wind shear affect the BT_diff of MCSs as hypothesised in chapter 5 will address a key source of uncertainty in our understanding of the (thermo-)dynamics of MCSs and their representation in NWP models. In chapter 5, it was hypothesised that vertical wind shear causes storm anvils to reach higher heights relative to their LNBs by increasing updrafts and minimising entrainment consistent with Mulholland et al. (2021). By using measurements from a field campaign or some of the previous campaigns over the region, this hypothesis can be tested by comparing differences in updraft strengths for cases of weakly sheared storms and highly sheared storms. Measurements of updrafts is difficult, ERA 5 reanalysis data will be unable to quantify updrafts as the they parameterise storms. However, using the the Huang et al. (2018) algorithm to track MCSs, a proxy for updrafts could be created by estimating the heights of overshooting tops in each storm using the difference between the temperature of the overshooting top and the average temperature of the storm anvil (BTmin-BTavg).

It will also be interesting to go ahead to investigate the effect of entrainment of drier air versus that of moist air into storms as suggested in chapter 5. Consistent with Peters et al. (2019) who found that entrainment dilution of squall line updrafts prevents

storms from reaching higher heights, it was found that, storms over the ocean could reach their LNBs compared to storms over the land. It was speculated that the higher entrainment rate of drier air into land storms is what prevents them from reaching their LNBs as compared to oceanic storms. However, a minimised BT_diff was also found for some Sahelian storms which we speculate could be a result of a process similar to the Rotunno et al. (1988) theory described earlier. By estimating the cold pools, vertical wind shear, mid-level humidity and updrafts associated with tracked MCSs, this hypothesis could be tested by comparing the effects of the entrainment of dry and moist air in an environment for cases of strong cold pools versus weak cold pools and the effects on the corresponding updraft strength.

Experiments to test the Alfaro (2017) theory of the effect of vertical wind shear on MCSs as well as Alfaro (2017)'s theory for rain-rates using observed data would help to confirm these theories. An attempt to test these theories over West Africa was done by Bickle (2021) but using an idealised large eddy simulation over the Sahel. The results showed that the Alfaro (2017)'s theory works well for squall line average ascent and rain-rates but doesn't show a good correlation with the maximum values. The poor correlations were attributed to variations in storm organisation due to differences in cold pool structure. Experimenting with passive tracers revealed that the LLMC might be an inaccurate representation of how the system relative inflow may account for storm rainfall. This raises the need for further testing and experimenting with observations will likely help to answer the outstanding questions raised in the Bickle (2021) idealised test. Bickle (2021) however gave a hint of a reconciliation between the Alfaro (2017) and the Rotunno et al. (1988) theories as storms with strong cold pools and vertical wind shear were more intense and had high rain-rates.

The Alfaro (2017) LLMC can be tested by comparing composites of tracked observed storms with strong vertical wind shear to weakly sheared ones in environments of strong low level moisture flux versus weak low level moisture flux. The relative effect of these two composites on the corresponding BTs, BT_diff, BT_min and rain-rates of the storms will then be analysed. The BT_diff, BT_min and rain-rates will be used as parameters to help quantify the impact of the increased latent heating resulting from the increased inflow of convectively unstable air on storm intensities as proposed by Alfaro (2017). The Alfaro (2017) theory for rain-rates will also be tested by comparing theoretically estimated rain-rates (using the CAPEs and vertical velocities associated with the storms) with the observed rain-rates from TRMM.

Simulations of specified cases with the TAM will be very useful for a detailed investigation of the model's ability to represent MCSs more accurately. A couple of cases of extreme weather events could be selected and the model's ability to simulate these storms investigated by evaluating the representation of the right environments and processes that lead to the initiation, growth, propagation and dissipation of MCSs. In addition, the effect of vertical wind shear on storm sizes, speed, and BTs as well as it's effect on the forecast skill can also be investigated. Such detailed evaluation of the effect of vertical wind shear on storm characteristics in the TAM will provide useful additions to earlier works done by Birch et al. (2013, 2014); Crook et al. (2019) who although made useful contribution to our understanding of the representation of MCSs in convection-permitting MetUM simulations over West Africa, did not provide a detailed evaluation of the representation of the effects of vertical wind shear on West African MCSs.

The performance of the TAM could be compared to other high resolution models such as the WRF model. This can involve the comparison of the simulation of some extreme cases with observed tracked storms. The representation of the storm environments and their effect on the storm intensity as well as the forecast skill can be compared. The representation of rainfall using FSS can also be investigated. Finally, the impact of the models' ability to simulate vertical wind shear on the forecast skill can also be compared.

Current projections from convection-permitting models over Africa are likely underestimating future extremes as they struggle to capture the effects of vertical wind shear on rainfall (Fitzpatrick et al. 2020a,b; Senior et al. 2021). The above listed future works which further investigates the mechanism through which vertical wind shear impact on the updraft strength, entrainment and resulting rainfall of MCSs as well as their representation in high resolution NWP models is crucial for more accurate future climate projections over Africa.

This thesis has improved our understanding of the (thermo-)dynamic environments of MCSs, the effects of vertical wind shear on MCSs and the added value of convection-permitting models in forecasting rainfall and representing the environments of MCSs over West Africa as well as the limitations of the model. The thesis has also highlighted key areas for further research needed to address the limitations that have been iden-

tified. The availability of convection-permitting NWP and climate models, large eddy simulations, and observations provides opportunities for the further research needed to improve MCS simulation over West Africa.

# References

Abdou, K., Parker, D. J., Brooks, B., Kalthoff, N., and Lebel, T. (2010). The diurnal cycle of lower boundary-layer wind in the West African monsoon. *Quarterly Journal of the Royal Meteorological Society*, 136(S1):66–76.

Alestalo, M. and Savijärvi, H. (1985). Mesoscale circulations in a hydrostatic model: coastal convergence and orographic lifting. *Tellus A: Dynamic Meteorology and Oceanography*, 37(2):156–162.

Alfaro, D. A. (2017). Low-tropospheric shear in the structure of squall lines: Impacts on latent heating under layer-lifting ascent. *Journal of the Atmospheric Sciences*, 74(1):229–248.

Alfaro, D. A. and Khairoutdinov, M. (2015). Thermodynamic constraints on the morphology of simulated midlatitude squall lines. *Journal of the Atmospheric Sciences*, 72(8):3116–3137.

Allen, J. (1971). Measurements of cloud emissivity in the 8–13 $\mu$ waveband. *Journal of Applied Meteorology and Climatology*, 10(2):260–265.

Amekudzi, L., Yamba, E., Preko, K., Asare, E., Aryee, J., Baidu, M., and Codjoe, S. (2015). Variabilities in rainfall onset, cessation and length of rainy season for the various agro-ecological zones of Ghana. *Climate*, 3(2):416–434.

Aryee, J., Amekudzi, L., Quansah, E., Klutse, N., Atiah, W., and Yorke, C. (2018). Development of high spatial resolution rainfall data for Ghana. *International Journal of Climatology*, 38(3):1201–1215.

Bader, J. and Latif, M. (2003). The impact of decadal-scale Indian Ocean sea surface temperature anomalies on Sahelian rainfall and the North Atlantic Oscillation. *Geophysical Research Letters*, 30(22).

Bader, J. and Latif, M. (2011). The 1983 drought in the West Sahel: a case study. *Climate Dynamics*, 36(3-4):463–472.

Baidu, M., Amekudzi, L. K., Aryee, J. N., and Annor, T. (2017). Assessment of long-term spatio-temporal rainfall variability over Ghana using wavelet analysis. *Climate*, 5(2):30.

Baidu, M., Schwendike, J., Marsham, J. H., and Bain, C. (2022). Effects of vertical wind shear on intensities of mesoscale convective systems over West and Central Africa. *Atmospheric Science Letters*, page e1094.

Bain, C., Williams, K., Milton, S., and Heming, J. (2014). Objective tracking of African easterly waves in Met Office models. *Quarterly Journal of the Royal Meteorological Society*, 140(678):47–57.

Bain, C. L., Parker, D. J., Taylor, C. M., Kergoat, L., and Guichard, F. (2010). Observations of the nocturnal boundary layer associated with the West African monsoon. *Monthly Weather Review*, 138(8):3142–3156.

Becker, T. and Hohenegger, C. (2021). Entrainment and its dependency on environmental conditions and convective organization in convection-permitting simulations. *Monthly Weather Review*, 149(2):537–550.

Berrisford, P., Dee, D., Fielding, K., Fuentes, M., Kallberg, P., Kobayashi, S., and Uppala, S. (2009). The ERA-Interim archive. ERA Report series. No. 1. Technical (ERA) report. European Centre for Medium-range Weather Forecasting, Shinfield Park. *ERA Report Series*, (1):1–16.

Berthou, S., Rowell, D. P., Kendon, E. J., Roberts, M. J., Stratton, R. A., Crook, J. A., and Wilcox, C. (2019). Improved climatological precipitation characteristics over West Africa at convection-permitting scales. *Climate Dynamics*, 53(3):1991–2011.

Biasutti, M., Sobel, A. H., and Camargo, S. J. (2009). The role of the sahara low in summertime Sahel rainfall variability and change in the CMIP3 models. *Journal of Climate*, 22(21):5755–5771.

Bickle, M., Marsham, J. H., Griffiths, S. D., Ross, A. N., and Crook, J. (2022). The Influence of the Diurnal Cycle in Wind Shear and Thermodynamics on Squall Lines in the West African Monsoon. *Journal of the Atmospheric Sciences*, 79(8):2125–2143.

Bickle, M. E. (2021). *The Role of Wind Shear in Organised Deep Moist Convection in the West African Monsoon*. PhD thesis, University of Leeds.

Bickle, M. E., Marsham, J. H., Ross, A. N., Rowell, D. P., Parker, D. J., and Taylor, C. M. (2021). Understanding mechanisms for trends in Sahelian squall lines: Roles of thermodynamics and shear. *Quarterly Journal of the Royal Meteorological Society*,

147(735):983–1006.

Birch, C., Parker, D., O'Leary, A., Marsham, J., Taylor, C., Harris, P., and Lister, G. (2013). Impact of soil moisture and convectively generated waves on the initiation of a West African mesoscale convective system. *Quarterly Journal of the Royal Meteorological Society*, 139(676):1712–1730.

Birch, C. E., Marsham, J. H., Parker, D. J., and Taylor, C. M. (2014). The scale dependence and structure of convergence fields preceding the initiation of deep convection. *Geophysical Research Letters*, 41(13):4769–4776.

Birch, C. E., Roberts, M. J., Garcia-Carreras, L., Ackerley, D., Reeder, M. J., Lock, A. P., and Schiemann, R. (2015). Sea-breeze dynamics and convection initiation: The influence of convective parameterization in weather and climate model biases. *Journal of Climate*, 28(20):8093–8108.

Bony, S., Stevens, B., Frierson, D. M., Jakob, C., Kageyama, M., Pincus, R., Shepherd, T. G., Sherwood, S. C., Siebesma, A. P., Sobel, A. H., et al. (2015). Clouds, circulation and climate sensitivity. *Nature Geoscience*, 8(4):261–268.

Boutle, I. A., Moore, S., and Turner, R. (2021). Moving earth (not heaven): A novel approach to tropical cyclone impact modelling, demonstrated for New Zealand. *Weather and Climate Extremes*, 34:100395.

Bretherton, C. S., MacVean, M. K., Bechtold, P., Chlond, A., Cotton, W. R., Cuxart, J., Cuijpers, H., Mhairoutdinov, M., Kosovic, B., Lewellen, D., Moeng, C.-H., Siebesma, P., Stevens, B., Stevens, D., and Sykes, I. ansd Wyant, M. (1999). An intercomparison of radiatively driven entrainment and turbulence in a smoke cloud, as simulated by different numerical models. *Quarterly Journal of the Royal Meteorological Society*, 125(554):391–423.

Bryan, G. H., Knievel, J. C., and Parker, M. D. (2006). A multimodel assessment of RKW theory's relevance to squall-line characteristics. *Monthly Weather Review*, 134(10):2772–2792.

Bryan, G. H. and Parker, M. D. (2010). Observations of a squall line and its near environment using high-frequency rawinsonde launches during vortex2. *Monthly weather review*, 138(11):4076–4097.

Bryan, G. H., Wyngaard, J. C., and Fritsch, J. M. (2003). Resolution requirements for

the simulation of deep moist convection. *Monthly Weather Review*, 131(10):2394–2416.

Bunkers, M. J., Johnson, J. S., Czepyha, L. J., Grzywacz, J. M., Klimowski, B. A., and Hjelmfelt, M. R. (2006). An observational examination of long-lived supercells. Part II: Environmental conditions and forecasting. *Weather and Forecasting*, 21(5):689–714.

Burton, R., Blyth, A., Cui, Z., Groves, J., Lamptey, B., Fletcher, J., Marsham, J., Parker, D., and Roberts, A. (2022). Satellite-based nowcasting of west african mesoscale storms has skill at up to four hours lead time. *Weather and Forecasting*.

Bush, M., Allen, T., Bain, C., Boutle, I., Edwards, J., Finnenkoetter, A., Franklin, C., Hanley, K., Lean, H., Lock, A., et al. (2020). The first met office unified model–jules regional atmosphere and land configuration, ral1. *Geoscientific Model Development*, 13(4):1999–2029.

Cafaro, C., Woodhams, B. J., Stein, T. H., Birch, C. E., Webster, S., Bain, C. L., Hartley, A., Clarke, S., Ferrett, S., and Hill, P. (2021). Do convection-permitting ensembles lead to more skillful short-range probabilistic rainfall forecasts over tropical East Africa? *Weather and Forecasting*, 36(2):697–716.

Carlson, T. N. (1969a). Some remarks on african disturbances and their progress over the tropical atlantic. *Mon. Wea. Rev*, 97(10):716–726.

Carlson, T. N. (1969b). Synoptic histories of three african disturbances that developed into atlantic hurricanes. *Monthly Weather Review*, 97(3):256–276.

Casenave, A. and Valentin, C. (1992). A runoff capability classification system based on surface features criteria in semi-arid areas of West Africa. *Journal of Hydrology*, 130(1-4):231–249.

Chamberlain, J., Bain, C., Boyd, D., McCourt, K., Butcher, T., and Palmer, S. (2014). Forecasting storms over lake victoria using a high resolution model. *Meteorological Applications*, 21(2):419–430.

Charba, J. (1974). Application of gravity current model to analysis of squall-line gust front. *Monthly Weather Review*, 102(2):140–156.

Chauvin, F., Roehrig, R., and Lafore, J.-P. (2010). Intraseasonal variability of the

saharan heat low and its link with midlatitudes. *Journal of Climate*, 23(10):2544–2561.

Chen, T.-C. (2005). Maintenance of the midtropospheric North African summer circulation: Saharan high and African easterly jet. *Journal of climate*, 18(15):2943–2962.

Chen, T.-C. and van Loon, H. (1987). Interannual variation of the tropical easterly jet. *Monthly Weather Review*, 115(8):1739–1759.

Chen, Y., Ebert, E. E., Walsh, K. J., and Davidson, N. E. (2013). Evaluation of TRMM 3B42 precipitation estimates of tropical cyclone rainfall using PACRAIN data. *Journal of Geophysical Research: Atmospheres*, 118(5):2184–2196.

Cheng, C.-P. and Houze Jr, R. A. (1979). The distribution of convective and mesoscale precipitation in gate radar echo patterns. *Monthly Weather Review*, 107(10):1370–1381.

Chong, M. and Hauser, D. (1989). A tropical squall line observed during the COPT 81 experiment in West Africa. Part ii: Water budget. *Monthly Weather Review*, 117(4):728–744.

Chung, C. E. and Ramanathan, V. (2006). Weakening of North Indian SST gradients and the monsoon rainfall in India and the Sahel. *Journal of Climate*, 19(10):2036–2045.

Clark, P., Roberts, N., Lean, H., Ballard, S. P., and Charlton-Perez, C. (2016). Convection-permitting models: A step-change in rainfall forecasting. *Meteorological Applications*, 23(2):165–181.

Coniglio, M. C., Hwang, J. Y., and Stensrud, D. J. (2010). Environmental factors in the upscale growth and longevity of mcss derived from rapid update cycle analyses. *Monthly weather review*, 138(9):3514–3539.

Cook, K. H. (1999). Generation of the African easterly jet and its role in determining West African precipitation. *Journal of Climate*, 12(5):1165–1184.

Corfidi, S., Meritt, J., and Fritsch, J. (1996). Predicting the movement of mesoscale convective complexes. *Weather and Forecasting*, 11(1):41–46.

Cornforth, R. J., Hoskins, B. J., and Thorncroft, C. D. (2009). The impact of moist processes on the african easterly jet–african easterly wave system. *Quarterly Journal*

*of the Royal Meteorological Society*, 135(641):894–913.

Couvreux, F., Guichard, F., Bock, O., Campistron, B., Lafore, J.-P., and Redelsperger, J.-L. (2010). Synoptic variability of the monsoon flux over West Africa prior to the onset. *Quarterly Journal of the Royal Meteorological Society*, 136(S1):159–173.

Couvreux, F., Rio, C., Guichard, F., Lothon, M., Canut, G., Bouniol, D., and Gounou, A. (2012). Initiation of daytime local convection in a semi-arid region analysed with high-resolution simulations and amma observations. *Quarterly Journal of the Royal Meteorological Society*, 138(662):56–71.

Crook, J., Klein, C., Folwell, S., Taylor, C. M., Parker, D. J., Stratton, R., and Stein, T. (2019). Assessment of the representation of West African storm lifecycles in convection-permitting simulations. *Earth and Space Science*, 6(5):818–835.

Dalu, G., Gaetani, M., and Baldi, M. (2009). A hydrological onset and withdrawal index for the West African monsoon. *Theoretical and Applied Climatology*, 96(1-2):179–189.

Dee, D. P., Uppala, S., Simmons, A., Berrisford, P., Poli, P., Kobayashi, S., Andrae, U., Balmaseda, M., Balsamo, G., Bauer, d. P., Bechtold, P., Beljaars, A. C. M., van de Berg, L., Bidlot, J., Bormann, N., Delsol, C., Dragani, R., Fuentes, M., Geer, A. J., Haimberger, L., Healy, S. B., Hersbach, H., Hólm, E. V., Isaksen, L., Kållberg, P., Köhler, M., Matricardi, M., McNally, A. P., Monge-Sanz, B. M., Morcrette, J.-J., Park, B.-K., Peubey, C., de Rosnay, P., Tavolato, C., Thépaut, J.-N., and Vitart, F. (2011). The ERA-Interim reanalysis: Configuration and performance of the data assimilation system. *Quarterly Journal of the Royal Meteorological Society*, 137(656):553–597.

Delworth, T. L., Zhang, R., and Mann, M. E. (2007). Decadal to centennial variability of the atlantic from observations and models. *Geophysical Monograph-American Geophysical Union*, 173:131.

Dembélé, M. and Zwart, S. J. (2016). Evaluation and comparison of satellite-based rainfall products in Burkina Faso, West Africa. *International Journal of Remote Sensing*, 37(17):3995–4014.

Dezfuli, A. K. and Nicholson, S. E. (2011). A note on long-term variations of the african easterly jet. *International Journal of Climatology*, 31(13):2049–2054.

Dinku, T., Connor, S. J., and Ceccato, P. (2010). Comparison of cmorph and trmm-

3b42 over mountainous regions of africa and south america. In *Satellite rainfall applications for surface hydrology*, pages 193–204. Springer.

Drager, A. J. and Van den Heever, S. C. (2017). Characterizing convective cold pools. *Journal of Advances in Modeling Earth Systems*, 9(2):1091–1115.

Druyan, L. M., Fulakeza, M., and Lonergan, P. (2006). Mesoscale analyses of west african summer climate: focus on wave disturbances. *Climate Dynamics*, 27(5):459–481.

Ebert, E. E., Janowiak, J. E., and Kidd, C. (2007). Comparison of near-real-time precipitation estimates from satellite observations and numerical models. *Bulletin of the American Meteorological Society*, 88(1):47–64.

Edwards, J. M., Beljaars, A., Holtslag, A. A., and Lock, A. P. (2020). Representation of boundary-layer processes in numerical weather prediction and climate models. *Boundary-Layer Meteorology*, 177(2):511–539.

Ferguson, W. (1985). Integrating crops and livestock in West Africa. *FAO Animal Production and Health Paper*, 41.

Fink, A. H., Agustí-Panareda, A., Parker, D. J., Lafore, J.-P., Ngamini, J.-B., Afiesimama, E., Beljaars, A., Bock, O., Christoph, M., Didé, F., et al. (2011). Operational meteorology in west africa: observational networks, weather analysis and forecasting. *Atmospheric Science Letters*, 12(1):135–141.

Fink, A. H., Engel, T., Ermert, V., van der Linden, R., Schneidewind, M., Redl, R., Afiesimama, E., Thiaw, W. M., Yorke, C., and Evans, M. (2017). Mean climate and seasonal cycle. *Meteorology of Tropical West Africa: The Forecasters' Handbook*, pages 1–39.

Fiolleau, T. and Roca, R. (2013). An algorithm for the detection and tracking of tropical mesoscale convective systems using infrared images from geostationary satellite. *IEEE transactions on Geoscience and Remote Sensing*, 51(7):4302–4315.

Fitzpatrick, R. G., Bain, C. L., Knippertz, P., Marsham, J. H., and Parker, D. J. (2015). The West African monsoon onset: A concise comparison of definitions. *Journal of Climate*, 28(22):8673–8694.

Fitzpatrick, R. G., Bain, C. L., Knippertz, P., Marsham, J. H., and Parker, D. J. (2016). On what scale can we predict the agronomic onset of the West African Monsoon?

*Monthly Weather Review*, 144(4):1571–1589.

Fitzpatrick, R. G., Parker, D. J., Marsham, J. H., Rowell, D. P., Guichard, F. M., Taylor, C. M., Cook, K. H., Vizy, E. K., Jackson, L. S., Finney, D., Crook, J., Stratton, R., and Tucker, S. (2020a). What drives the intensification of mesoscale convective systems over the West African Sahel under climate change? *Journal of Climate*, 33(8):3151–3172.

Fitzpatrick, R. G., Parker, D. J., Marsham, J. H., Rowell, D. P., Jackson, L. S., Finney, D., Deva, C., Tucker, S., and Stratton, R. (2020b). How a typical west african day in the future-climate compares with current-climate conditions in a convection-permitting and parameterised convection climate model. *Climatic Change*, pages 1–30.

Flaounas, E., Janicot, S., Bastin, S., and Roca, R. (2012a). The West African monsoon onset in 2006: sensitivity to surface albedo, orography, SST and synoptic scale dry-air intrusions using WRF. *Climate Dynamics*, 38(3-4):685–708.

Flaounas, E., Janicot, S., Bastin, S., Roca, R., and Mohino, E. (2012b). The role of the indian monsoon onset in the west african monsoon onset: observations and agcm nudged simulations. *Climate Dynamics*, 38(5-6):965–983.

Foelsche, U., Kirchengast, G., Fuchsberger, J., Tan, J., Petersen, W. A., et al. (2017). Evaluation of gpm imerg early, late, and final rainfall estimates using wegener-net gauge data in southeastern austria. *Hydrology and Earth System Sciences*, 21(12):6559–6572.

Folland, C. K., Palmer, T. N., and Parker, D. E. (1986). Sahel rainfall and worldwide sea temperatures, 1901–85. *Nature*, 320(6063):602.

Fontaine, B., Garcia-Serrano, J., Roucou, P., Rodriguez-Fonseca, B., Losada, T., Chauvin, F., Gervois, S., Sijikumar, S., Ruti, P., and Janicot, S. (2010). Impacts of warm and cold situations in the mediterranean basins on the west african monsoon: observed connection patterns (1979–2006) and climate simulations. *Climate Dynamics*, 35(1):95–114.

Fontaine, B., Roucou, P., Gaetani, M., and Marteau, R. (2011). Recent changes in precipitation, ITCZ convection and northern tropical circulation over North Africa (1979–2007). *International Journal of Climatology*, 31(5):633–648.

Fritsch, J. and Forbes, G. (2001). Mesoscale convective systems. In *Severe convective storms*, pages 323–357. Springer.

Gaetani, M., Fontaine, B., Roucou, P., and Baldi, M. (2010). Influence of the mediterranean sea on the West African monsoon: Intraseasonal variability in numerical simulations. *Journal of Geophysical Research: Atmospheres*, 115(D24).

Giannini, A., Saravanan, R., and Chang, P. (2003). Oceanic forcing of Sahel rainfall on interannual to interdecadal time scales. *Science*, 302(5647):1027–1030.

Gleixner, S., Demissie, T., and Diro, G. T. (2020). Did era5 improve temperature and precipitation reanalysis over east africa? *Atmosphere*, 11(9):996.

Goff, R. C. (1976). Vertical structure of thunderstorm outflows. *Monthly Weather Review*, 104(11):1429–1440.

Goyens, C., Lauwaet, D., Schröder, M., Demuzere, M., and Van Lipzig, N. P. (2012). Tracking mesoscale convective systems in the sahel: Relation between cloud parameters and precipitation. *International Journal of Climatology*, 32(12):1921–1934.

Gray, M., Shutts, G., and Craig, G. (1998). The role of mass transfer in describing the dynamics of mesoscale convective systems. *Quarterly Journal of the Royal Meteorological Society*, 124(548):1183–1207.

Gregory, D. and Rowntree, P. (1990). A mass flux convection scheme with representation of cloud ensemble characteristics and stability-dependent closure. *Monthly Weather Review*, 118(7):1483–1506.

Grist, J. P. (2002). Easterly waves over Africa. Part i: The seasonal cycle and contrasts between wet and dry years. *Monthly Weather Review*, 130(2):197–211.

Grist, J. P. and Nicholson, S. E. (2001). A study of the dynamic factors influencing the rainfall variability in the west african sahel. *Journal of climate*, 14(7):1337–1359.

Grist, J. P., Nicholson, S. E., and Barcilon, A. I. (2002). Easterly waves over africa. Part II: observed and modeled contrasts between wet and dry years. *Monthly Weather Review*, 130(2):212–225.

Grodsky, S. A., Carton, J. A., and Nigam, S. (2003). Near surface westerly wind jet in the Atlantic ITCZ. *Geophysical Research Letters*, 30(19):1–4.

Gu, G. and Adler, R. F. (2004). Seasonal evolution and variability associated with the West African monsoon system. *Journal of Climate*, 17(17):3364–3377.

Guichard, F., Asencio, N., Peugeot, C., Bock, O., Redelsperger, J.-L., Cui, X., Garvert, M., Lamptey, B., Orlandi, E., Sander, J., et al. (2010). An intercomparison of simulated rainfall and evapotranspiration associated with a mesoscale convective system over West Africa. *Weather and Forecasting*, 25(1):37–60.

Hagen, M., Van Baelen, J., and Richard, E. (2011). Influence of the wind profile on the initiation of convection in mountainous terrain. *Quarterly Journal of the Royal Meteorological Society*, 137(S1):224–235.

Hall, N. M., Kiladis, G. N., and Thorncroft, C. D. (2006). Three-dimensional structure and dynamics of African easterly waves. Part II: Dynamical modes. *Journal of the Atmospheric Sciences*, 63(9):2231–2245.

Hamilton, R., Archbold, J., and Douglas, C. (1945). Meteorology of Nigeria and adjacent territory. *Quarterly Journal of the Royal Meteorological Society*, 71(309-310):231–264.

Hanley, K. E., Pirret, J. S., Bain, C. L., Hartley, A. J., Lean, H. W., Webster, S., and Woodhams, B. J. (2021). Assessment of convection-permitting versions of the unified model over the Lake Victoria basin region. *Quarterly Journal of the Royal Meteorological Society*, 147(736):1642–1660.

Hoerling, M., Hurrell, J., Eischeid, J., and Phillips, A. (2006). Detection and attribution of twentieth-century northern and southern African rainfall change. *Journal of Climate*, 19(16):3989–4008.

Hou, A. Y., Kakar, R. K., Neeck, S., Azarbarzin, A. A., Kummerow, C. D., Kojima, M., Oki, R., Nakamura, K., and Iguchi, T. (2014). The global precipitation measurement mission. *Bulletin of the American Meteorological Society*, 95(5):701–722.

Houze Jr, R. A. (1989). Observed structure of mesoscale convective systems and implications for large-scale heating. *Quarterly Journal of the Royal Meteorological Society*, 115(487):425–461.

Houze Jr, R. A. (2004). Mesoscale convective systems. *Reviews of Geophysics*, 42(4):doi: 10.1029/2004RG000150.

Houze Jr, R. A. (2012). Orographic effects on precipitating clouds. *Reviews of Geo-*

*physics*, 50(1):doi: 10.1029/2011RG000365.

Houze Jr, R. A. (2018). 100 years of research on mesoscale convective systems. *Meteorological Monographs*, 59:17–1.

Houze Jr, R. A., Smull, B. F., and Dodge, P. (1990). Mesoscale organization of springtime rainstorms in oklahoma. *Monthly Weather Review*, 118(3):613–654.

Hsieh, J.-S. and Cook, K. H. (2005). Generation of African easterly wave disturbances: Relationship to the African easterly jet. *Monthly Weather Review*, 133(5):1311–1327.

Hsieh, J.-S. and Cook, K. H. (2008). On the instability of the African easterly jet and the generation of African waves: Reversals of the potential vorticity gradient. *Journal of the Atmospheric Sciences*, 65(7):2130–2151.

Huang, X., Hu, C., Huang, X., Chu, Y., Tseng, Y.-h., Zhang, G. J., and Lin, Y. (2018). A long-term tropical mesoscale convective systems dataset based on a novel objective automatic tracking algorithm. *Climate Dynamics*, 51(7):3145–3159.

Huffman, G., Stocker, E., Bolvin, D., Nelkin, E., and Jackson, T. (2017). GPM IMERG Final Precipitation L3 Half Hourly 0.1 degree x 0.1 degree V05. *Goddard Earth Sciences Data and Information Services Center (GES DISC): Greenbelt, MD, USA*.

Huffman, G. J., Bolvin, D. T., Braithwaite, D., Hsu, K., Joyce, R., Xie, P., and Yoo, S.-H. (2015). NASA global precipitation measurement (GPM) integrated multi-satellite retrievals for GPM (IMERG). *Algorithm Theoretical Basis Document (ATBD) Version*, 4:26.

Huffman, G. J., Bolvin, D. T., Nelkin, E. J., Wolff, D. B., Adler, R. F., Gu, G., Hong, Y., Bowman, K. P., and Stocker, E. F. (2007). The TRMM multisatellite precipitation analysis (TMPA): Quasi-global, multiyear, combined-sensor precipitation estimates at fine scales. *Journal of Hydrometeorology*, 8(1):38–55.

James, R. P. and Markowski, P. M. (2010). A numerical investigation of the effects of dry air aloft on deep convection. *Monthly Weather Review*, 138(1):140–161.

Janiga, M. A. and Thorncroft, C. D. (2014). Convection over tropical africa and the east atlantic during the west african monsoon: Regional and diurnal variability. *Journal of Climate*, 27(11):4159–4188.

Jeevanjee, N. and Romps, D. M. (2013). Convective self-aggregation, cold pools, and

domain size. *Geophysical Research Letters*, 40(5):994–998.

Joly, M. and Voldoire, A. (2010). Role of the Gulf of Guinea in the inter-annual variability of the West African monsoon: what do we learn from CMIP3 coupled simulations? *International Journal of Climatology*, 30(12):1843–1856.

Joly, M., Voldoire, A., Douville, H., Terray, P., and Royer, J.-F. (2007). African monsoon teleconnections with tropical SSTs: validation and evolution in a set of IPCC4 simulations. *Climate Dynamics*, 29(1):1–20.

Keat, W. J., Stein, T. H., Phaduli, E., Landman, S., Becker, E., Bopape, M.-J. M., Hanley, K. E., Lean, H. W., and Webster, S. (2019). Convective initiation and storm life cycles in convection-permitting simulations of the Met Office Unified Model over South Africa. *Quarterly Journal of the Royal Meteorological Society*, 145(721):1323–1336.

Kendon, E. J., Roberts, N. M., Senior, C. A., and Roberts, M. J. (2012). Realism of rainfall in a very high-resolution regional climate model. *Journal of Climate*, 25(17):5791–5806.

Kessler, J. and Breman, H. (1991). The potential of agroforestry to increase primary production in the Sahelian and Sudanian zones of West Africa. *Agroforestry systems*, 13(1):41–62.

Khairoutdinov, M. and Randall, D. (2006). High-resolution simulation of shallow-to-deep convection transition over land. *Journal of the atmospheric sciences*, 63(12):3421–3436.

Kiladis, G. N., Thorncroft, C. D., and Hall, N. M. (2006). Three-dimensional structure and dynamics of African easterly waves. Part I: Observations. *Journal of the Atmospheric Sciences*, 63(9):2212–2230.

Kim, K., Park, J., Baik, J., and Choi, M. (2017). Evaluation of topographical and seasonal feature using GPM IMERG and TRMM 3B42 over Far-East Asia. *Atmospheric Research*, 187:95–105.

Klein, C., Nkrumah, F., Taylor, C. M., and Adefisan, E. A. (2020). Seasonality and trends of drivers of mesoscale convective systems in southern West Africa. *Journal of Climate*, 34(1):71–87.

Kniffka, A., Knippertz, P., Fink, A. H., Benedetti, A., Brooks, M. E., Hill, P. G.,

Maranan, M., Pante, G., and Vogel, B. (2020). An evaluation of operational and research weather forecasts for southern west africa using observations from the DACCIWA field campaign in June–July 2016. *Quarterly Journal of the Royal Meteorological Society*, 146(728):1121–1148.

Kubota, T., Ushio, T., Shige, S., Kida, S., Kachi, M., and Okamoto, K. (2009). Verification of high-resolution satellite-based rainfall estimates around Japan using a gauge-calibrated ground-radar dataset. *Journal of the Meteorological Society of Japan. Ser. II*, 87:203–222.

Lafore, J. P., Chapelon, N., Diop, M., Gueye, B., Largeron, Y., Lepape, S., Ndiaye, O., Parker, D. J., Poan, E., Roca, R., Roehrig, R., and Taylor, C. (2017). Deep convection. *Meteorology of Tropical West Africa: The Forecasters' Handbook*, pages 90–129.

Lafore, J.-P. and Moncrieff, M. W. (1989). A numerical investigation of the organization and interaction of the convective and stratiform regions of tropical squall lines. *Journal of the atmospheric sciences*, 46(4):521–544.

Laing, A. G., Carbone, R., Levizzani, V., and Tuttle, J. (2008). The propagation and diurnal cycles of deep convection in northern tropical Africa. *Quarterly Journal of the Royal Meteorological Society*, 134(630):93–109.

Lamb, P. J. (1978a). Case studies of tropical Atlantic surface circulation patterns during recent sub-Saharan weather anomalies: 1967 and 1968. *Monthly Weather Review*, 106(4):482–491.

Lamb, P. J. (1978b). Large-scale tropical atlantic surface circulation patterns associated with subsaharan weather anomalies. *Tellus*, 30(3):240–251.

Langhans, W. and Romps, D. M. (2015). The origin of water vapor rings in tropical oceanic cold pools. *Geophysical Research Letters*, 42(18):7825–7834.

Lau, K., Shen, S., Kim, K.-M., and Wang, H. (2006). A multimodel study of the twentieth-century simulations of sahel drought from the 1970s to 1990s. *Journal of Geophysical Research: Atmospheres*, 111(D7).

Laurent, H., d'Amato, N., and Lebel, T. (1998). How important is the contribution of the mesoscale convective complexes to the Sahelian rainfall? *Physics and Chemistry of the Earth*, 23(5-6):629–633.

Lavaysse, C., Flamant, C., and Janicot, S. (2010a). Regional-scale convection patterns during strong and weak phases of the saharan heat low. *Atmospheric Science Letters*, 11(4):255–264.

Lavaysse, C., Flamant, C., Janicot, S., and Knippertz, P. (2010b). Links between african easterly waves, midlatitude circulation and intraseasonal pulsations of the west african heat low. *Quarterly Journal of the Royal Meteorological Society*, 136(S1):141–158.

Lavaysse, C., Flamant, C., Janicot, S., Parker, D. J., Lafore, J.-P., Sultan, B., and Pelon, J. (2009). Seasonal evolution of the West African heat low: A climatological perspective. *Climate Dynamics*, 33(2-3):313–330.

Lavers, D. A., Simmons, A., Vamborg, F., and Rodwell, M. J. (2022). An evaluation of ERA5 precipitation for climate monitoring. *Quarterly Journal of the Royal Meteorological Society*.

Le Barbé, L., Lebel, T., and Tapsoba, D. (2002). Rainfall variability in West Africa during the years 1950–90. *Journal of climate*, 15(2):187–202.

Lean, H. W., Clark, P. A., Dixon, M., Roberts, N. M., Fitch, A., Forbes, R., and Halliwell, C. (2008). Characteristics of high-resolution versions of the Met Office Unified Model for forecasting convection over the United Kingdom. *Monthly Weather Review*, 136(9):3408–3424.

LeMone, M. A., Zipser, E. J., and Trier, S. B. (1998). The role of environmental shear and thermodynamic conditions in determining the structure and evolution of mesoscale convective systems during toga coare. *Journal of the Atmospheric Sciences*, 55(23):3493–3518.

Leroux, S. and Hall, N. M. (2009). On the relationship between African easterly waves and the African easterly jet. *Journal of the Atmospheric Sciences*, 66(8):2303–2316.

Leroux, S., Hall, N. M., and Kiladis, G. N. (2010). A climatological study of transient–mean-flow interactions over West Africa. *Quarterly Journal of the Royal Meteorological Society*, 136(S1):397–410.

Li, P., Furtado, K., Zhou, T., Chen, H., Li, J., Guo, Z., and Xiao, C. (2020). The diurnal cycle of East Asian summer monsoon precipitation simulated by the Met Office Unified Model at convection-permitting scales. *Climate Dynamics*, 55(1):131–

151.

Lin, J., Qian, T., Bechtold, P., Grell, G., Zhang, G. J., Zhu, P., Freitas, S. R., Barnes, H., and Han, J. (2022). Atmospheric convection. *Atmosphere - Ocean*, pages 1–55.

Lin, J.-L., Qian, T., and Shinoda, T. (2014). Stratocumulus clouds in southeastern pacific simulated by eight CMIP5–CFMIP global climate models. *Journal of Climate*, 27(8):3000–3022.

Losada, T., Rodríguez-Fonseca, B., Janicot, S., Gervois, S., Chauvin, F., and Ruti, P. (2010). A multi-model approach to the atlantic equatorial mode: impact on the West African monsoon. *Climate Dynamics*, 35(1):29–43.

Losada, T., Rodriguez-Fonseca, B., Mohino, E., Bader, J., Janicot, S., and Mechoso, C. (2012). Tropical SST and Sahel rainfall: A non-stationary relationship. *Geophysical Research Letters*, 39(12).

Lothon, M., Saïd, F., Lohou, F., and Campistron, B. (2008). Observation of the diurnal cycle in the low troposphere of West Africa. *Monthly Weather Review*, 136(9):3477–3500.

Lu, J. and Delworth, T. L. (2005). Oceanic forcing of the late 20th century Sahel drought. *Geophysical Research Letters*, 32(22):doi: 10.1029/2005GL023316.

Luo, Y. and Chen, Y. (2015). Investigation of the predictability and physical mechanisms of an extreme-rainfall-producing mesoscale convective system along the meiyu front in east china: An ensemble approach. *Journal of Geophysical Research: Atmospheres*, 120(20):10–593.

Manzanas, R., Amekudzi, L., Preko, K., Herrera, S., and Gutiérrez, J. M. (2014). Precipitation variability and trends in ghana: An intercomparison of observational and reanalysis products. *Climatic change*, 124(4):805–819.

Manzato, A. and Morgan Jr, G. (2003). Evaluating the sounding instability with the lifted parcel theory. *Atmospheric Research*, 67:455–473.

Maranan, M., Fink, A. H., and Knippertz, P. (2018). Rainfall types over southern West Africa: Objective identification, climatology and synoptic environment. *Quarterly Journal of the Royal Meteorological Society*, 144(714):1628–1648.

Markowski, P. (2007). Convective storm initiation and organization. In *Atmospheric*

*Convection: Research and Operational Forecasting Aspects*, pages 23–28. Springer.

Marsham, J. H., Dixon, N. S., Garcia-Carreras, L., Lister, G. M., Parker, D. J., Knippertz, P., and Birch, C. E. (2013). The role of moist convection in the west african monsoon system: Insights from continental-scale convection-permitting simulations. *Geophysical Research Letters*, 40(9):1843–1849.

Marteau, R., Moron, V., and Philippon, N. (2009). Spatial coherence of monsoon onset over western and central Sahel (1950–2000). *Journal of Climate*, 22(5):1313–1324.

Marwitz, J. D. (1983). The kinematics of orographic airflow during Sierra storms. *Journal of the Atmospheric Sciences*, 40(5):1218–1227.

Mathon, V., Diedhiou, A., and Laurent, H. (2002a). Relationship between easterly waves and mesoscale convective systems over the Sahel. *Geophysical research letters*, 29(8):57–1.

Mathon, V., Laurent, H., and Lebel, T. (2002b). Mesoscale convective system rainfall in the Sahel. *Journal of applied meteorology*, 41(11):1081–1092.

McIlveen, R. (1991). *Fundamentals of weather and climate*. Psychology Press.

Mekonnen, A., Thorncroft, C. D., and Aiyyer, A. R. (2006). Analysis of convection and its association with African easterly waves. *Journal of Climate*, 19(20):5405–5421.

Michot, V., Vila, D., Arvor, D., Corpetti, T., Ronchail, J., Funatsu, B. M., and Dubreuil, V. (2018). Performance of TRMM TMPA 3B42 V7 in replicating daily rainfall and regional rainfall regimes in the Amazon Basin (1998–2013). *Remote Sensing*, 10(12):1879.

Mishra, S. (1993). Nonlinear barotropic instability of upper-tropospheric tropical easterly jet on the sphere. *Journal of the atmospheric sciences*, 50(21):3541–3552.

Mishra, S. and Tandon, M. (1983). A combined barotropic-baroclinic instability study of the upper tropospheric tropical easterly jet. *Journal of the atmospheric sciences*, 40(11):2708–2723.

Mohino, E., Rodríguez-Fonseca, B., Losada, T., Gervois, S., Janicot, S., Bader, J., Ruti, P., and Chauvin, F. (2011). Changes in the interannual SST-forced signals on west African rainfall. AGCM intercomparison. *Climate Dynamics*, 37(9-10):1707–1725.

Moncrieff, M. W. and Waliser, D. E. (2015). Organized convection and the yotc project. *Seamless prediction of the earth system: from minutes to months*, 1156:283–291.

Morcrette, C., Lean, H., Browning, K., Nicol, J., Roberts, N., Clark, P., Russell, A., and Blyth, A. (2007). Combination of mesoscale and synoptic mechanisms for triggering an isolated thunderstorm: Observational case study of CSIP IOP 1. *Monthly Weather Review*, 135(11):3728–3749.

Mulholland, J. P., Peters, J. M., and Morrison, H. (2021). How does vertical wind shear influence entrainment in squall lines? *Journal of the Atmospheric Sciences*, 78(6):1931–1946.

Mullendore, G., Homann, A., Jorgenson, S., Lang, T., and Tessendorf, S. (2013). Relationship between level of neutral buoyancy and dual-doppler observed mass detrainment levels in deep convection. *Atmospheric Chemistry and Physics*, 13(1):181–190.

Ndehedehe, C. E., Awange, J. L., Kuhn, M., Agutu, N. O., and Fukuda, Y. (2017). Climate teleconnections influence on West Africa's terrestrial water storage. *Hydrological Processes*, 31(18):3206–3224.

Newton, C. W. and Rodebush Newton, H. (1959). Dynamical interactions between large convective clouds and environment with vertical shear. *Journal of Atmospheric Sciences*, 16(5):483–496.

Nicholson, S., Barcilon, A., and Challa, M. (2008). An analysis of west african dynamics using a linearized gcm. *Journal of the Atmospheric Sciences*, 65(4):1182–1203.

Nicholson, S., Barcilon, A., Challa, M., and Baum, J. (2007). Wave activity on the tropical easterly jet. *Journal of the Atmospheric Sciences*, 64(7):2756–2763.

Nicholson, S. E. (1985). Sub-saharan rainfall 1981–84. *Journal of climate and applied meteorology*, 24(12):1388–1391.

Nicholson, S. E. (2008). The intensity, location and structure of the tropical rainbelt over west Africa as factors in interannual variability. *International Journal of Climatology: A Journal of the Royal Meteorological Society*, 28(13):1775–1785.

Nicholson, S. E. (2009a). A revised picture of the structure of the monsoon and land ITCZ over West Africa. *Climate Dynamics*, 32(7-8):1155–1171.

Nicholson, S. E. (2009b). On the factors modulating the intensity of the tropical

rainbelt over west africa. *International Journal of Climatology: A Journal of the Royal Meteorological Society*, 29(5):673–689.

Nicholson, S. E. (2013). The West African Sahel: A review of recent studies on the rainfall regime and its interannual variability. *ISRN Meteorology*, 2013.

Nicholson, S. E. (2018). The itcz and the seasonal cycle over equatorial africa. *Bulletin of the American Meteorological Society*, 99(2):337–348.

Nicholson, S. E. and Grist, J. (2001). A conceptual model for understanding rainfall variability in the West African Sahel on interannual and interdecadal timescales. *International Journal of Climatology: A Journal of the Royal Meteorological Society*, 21(14):1733–1757.

Nicholson, S. E. and Grist, J. P. (2003). The seasonal evolution of the atmospheric circulation over West Africa and equatorial Africa. *Journal of Climate*, 16(7):1013–1030.

Nicholson, S. E. and Kim, J. (1997). The relationship of the El Niño–Southern oscillation to African rainfall. *International Journal of Climatology*, 17(2):117–135.

Nicholson, S. E., Some, B., McCollum, J., Nelkin, E., Klotter, D., Berte, Y., Diallo, B., Gaye, I., Kpabeba, G., Ndiaye, O., et al. (2003). Validation of TRMM and other rainfall estimates with a high-density gauge dataset for West Africa. Part II: Validation of TRMM rainfall products. *Journal of Applied Meteorology*, 42(10):1355–1368.

Nicholson, S. E. and Webster, P. J. (2007). A physical basis for the interannual variability of rainfall in the sahel. *Quarterly Journal of the Royal Meteorological Society*, 133(629):2065–2084.

Nolan, D. S., Zhang, C., and Chen, S.-h. (2007). Dynamics of the shallow meridional circulation around intertropical convergence zones. *Journal of the Atmospheric Sciences*, 64(7):2262–2285.

Parker, D., Burton, R., Diongue-Niang, A., Ellis, R., Felton, M., Taylor, C., Thorncroft, C., Bessemoulin, P., and Tompkins, A. (2005a). The diurnal cycle of the West African monsoon circulation. *Quarterly Journal of the Royal Meteorological Society*, 131(611):2839–2860.

Parker, D. J. (2017). *Meteorology of tropical West Africa: The forecasters' handbook.*

John Wiley & Sons.

Parker, D. J., Thorncroft, C. D., Burton, R. R., and Diongue-Niang, A. (2005b). Analysis of the african easterly jet, using aircraft observations from the jet2000 experiment. *Quarterly Journal of the Royal Meteorological Society*, 131(608):1461–1482.

Parker, D. J., Willetts, P., Birch, C., Turner, A. G., Marsham, J. H., Taylor, C. M., Kolusu, S., and Martin, G. M. (2016). The interaction of moist convection and mid-level dry air in the advance of the onset of the Indian monsoon. *Quarterly Journal of the Royal Meteorological Society*, 142(699):2256–2272.

Paxian, A., Sein, D., Panitz, H.-J., Warscher, M., Breil, M., Engel, T., Tödter, J., Krause, A., Cabos Narvaez, W., Fink, A., et al. (2016). Bias reduction in decadal predictions of west african monsoon rainfall using regional climate models. *Journal of Geophysical Research: Atmospheres*, 121(4):1715–1735.

Petch, J., Brown, A., and Gray, M. (2002). The impact of horizontal resolution on the simulations of convective development over land. *Quarterly Journal of the Royal Meteorological Society*, 128(584):2031–2044.

Peters, J. M., Morrison, H., Zhang, G. J., and Powell, S. (2021). Improving the physical basis for updraft dynamics in deep convection parameterizations. *Journal of Advances in Modeling Earth Systems*, 13(2):e2020MS002282.

Peters, J. M., Nowotarski, C. J., and Morrison, H. (2019). The role of vertical wind shear in modulating maximum supercell updraft velocities. *Journal of the Atmospheric Sciences*, 76(10):3169–3189.

Polo, I., Rodríguez-Fonseca, B., Losada, T., and García-Serrano, J. (2008). Tropical atlantic variability modes (1979–2002). part i: Time-evolving sst modes related to west african rainfall. *Journal of Climate*, 21(24):6457–6475.

Polo, I., Ullmann, A., Roucou, P., and Fontaine, B. (2011). Weather regimes in the Euro-Atlantic and Mediterranean sector, and relationship with West African rainfall over the 1989–2008 period from a self-organizing maps approach. *Journal of Climate*, 24(13):3423–3432.

Prakash, S., Mitra, A. K., AghaKouchak, A., Liu, Z., Norouzi, H., and Pai, D. (2018). A preliminary assessment of gpm-based multi-satellite precipitation estimates over a monsoon dominated region. *Journal of Hydrology*, 556:865–876.

Protopapadaki, S. E., Stubenrauch, C. J., and Feofilov, A. G. (2017). Upper tropospheric cloud systems derived from IR sounders: Properties of cirrus anvils in the tropics. *Atmospheric Chemistry and Physics*, 17(6):3845–3859.

Provod, M., Marsham, J., Parker, D., and Birch, C. (2016). A characterization of cold pools in the west african sahel. *Monthly Weather Review*, 144(5):1923–1934.

Pu, B. and Cook, K. H. (2010). Dynamics of the west african westerly jet. *Journal of Climate*, 23(23):6263–6276.

Pytharoulis, I. and Thorncroft, C. (1999). The low-level structure of African easterly waves in 1995. *Monthly Weather Review*, 127(10):2266–2280.

Raicich, F., Pinardi, N., and Navarra, A. (2003). Teleconnections between Indian monsoon and Sahel rainfall and the Mediterranean. *International Journal of Climatology*, 23(2):173–186.

Rasmussen, K., Hill, A., Toma, V., Zuluaga, M., Webster, P., and Houze, R. (2015). Multiscale analysis of three consecutive years of anomalous flooding in Pakistan. *Quarterly Journal of the Royal Meteorological Society*, 141(689):1259–1276.

Ricciardulli, L. and Sardeshmukh, P. D. (2002). Local time-and space scales of organized tropical deep convection. *Journal of climate*, 15(19):2775–2790.

Richardson, Y. P. (1999). *The influence of horizontal variations in vertical shear and low-level moisture on numerically simulated convective storms.* PhD thesis.

Richardson, Y. P., Droegemeier, K. K., and Davies-Jones, R. P. (2007). The influence of horizontal environmental variability on numerically simulated convective storms. Part I: Variations in vertical shear. *Monthly Weather Review*, 135(10):3429–3455.

Riehl, H. and Malkus, J. (1958). On the heat balance in the equatorial trough zone. geophysica (helsinki), 6, 503–538., and j. simpson, 1979: The heat balance of the equatorial trough zone, revisited. *Contributions to Atmospheric Physics*, 52:287–304.

Roberts, N. M. and Lean, H. W. (2008). Scale-selective verification of rainfall accumulations from high-resolution forecasts of convective events. *Monthly Weather Review*, 136(1):78–97.

Ropelewski, C. F. and Halpert, M. S. (1987). Global and regional scale precipitation

patterns associated with the El Niño/Southern Oscillation. *Monthly Weather Review*, 115(8):1606–1626.

Ropelewski, C. F. and Halpert, M. S. (1989). Precipitation patterns associated with the high index phase of the Southern Oscillation. *Journal of Climate*, 2(3):268–284.

Rotunno, R., Klemp, J. B., and Weisman, M. L. (1988). A theory for strong, long-lived squall lines. *Journal of the Atmospheric Sciences*, 45(3):463–485.

Rowell, D. P. (2001). Teleconnections between the tropical pacific and the sahel. *Quarterly Journal of the Royal Meteorological Society*, 127(575):1683–1706.

Rowell, D. P. (2003). The impact of mediterranean SSTs on the Sahelian rainfall season. *Journal of Climate*, 16(5):849–862.

Rowell, D. P. and Milford, J. R. (1993). On the generation of african squall lines. *Journal of Climate*, 6(6):1181–1193.

Rutledge, S. A. and Houze Jr, R. A. (1987). A diagnostic modelling study of the trailing stratiform region of a midlatitude squall line. *Journal of the Atmospheric Sciences*, 44(18):2640–2656.

Sanderson, B. M., Shell, K. M., and Ingram, W. (2010). Climate feedbacks determined using radiative kernels in a multi-thousand member ensemble of AOGCMs. *Climate Dynamics*, 35(7):1219–1236.

Sathiyamoorthy, V. (2005). Large scale reduction in the size of the Tropical Easterly Jet. *Geophysical Research Letters*, 32(14).

Scaff, L., Prein, A. F., Li, Y., Liu, C., Rasmussen, R., and Ikeda, K. (2020). Simulating the convective precipitation diurnal cycle in North America's current and future climate. *Climate Dynamics*, 55(1):369–382.

Schumacher, C. and Houze Jr, R. A. (2003). Stratiform rain in the tropics as seen by the TRMM precipitation radar. *Journal of Climate*, 16(11):1739–1756.

Schumacher, R. S. and Rasmussen, K. L. (2020). The formation, character and changing nature of mesoscale convective systems. *Nature Reviews Earth & Environment*, 1(6):300–314.

Senior, C. A., Marsham, J. H., Berthou, S., Burgin, L. E., Folwell, S. S., Kendon,

E. J., Klein, C. M., Jones, R. G., Mittal, N., Rowell, D. P., and Tomassini, L. (2021). Convection-permitting regional climate change simulations for understanding future climate and informing decision-making in Africa. *Bulletin of the American Meteorological Society*, 102(6):E1206–E1223.

Sharifi, E., Steinacker, R., and Saghafian, B. (2016). Assessment of GPM-IMERG and other precipitation products against gauge data under different topographic and climatic conditions in Iran: Preliminary results. *Remote Sensing*, 8(2):135.

Sherwood, S. C., Bony, S., and Dufresne, J.-L. (2014). Spread in model climate sensitivity traced to atmospheric convective mixing. *Nature*, 505(7481):37–42.

Short, C. J. and Petch, J. (2022). Reducing the spin-up of a regional NWP system without data assimilation. *Quarterly Journal of the Royal Meteorological Society*.

Simpson, J. (1969). A comparison between laboratory and atmospheric density currents. *Quarterly Journal of the Royal Meteorological Society*, 95(406):758–765.

Stein, T. H., Hogan, R. J., Clark, P. A., Halliwell, C. E., Hanley, K. E., Lean, H. W., Nicol, J. C., and Plant, R. S. (2015). The dymecs project: A statistical approach for the evaluation of convective storms in high-resolution nwp models. *Bulletin of the American Meteorological Society*, 96(6):939–951.

Stephens, G. L., L'Ecuyer, T., Forbes, R., Gettelmen, A., Golaz, J.-C., Bodas-Salcedo, A., Suzuki, K., Gabriel, P., and Haynes, J. (2010). Dreary state of precipitation in global models. *Journal of Geophysical Research: Atmospheres*, 115(D24).

Steptoe, H., Savage, N. H., Sadri, S., Salmon, K., Maalick, Z., and Webster, S. (2021). Tropical cyclone simulations over bangladesh at convection permitting 4.4 km & 1.5 km resolution. *Scientific Data*, 8(1):1–12.

Stern, R., Dennett, M., and Garbutt, D. (1981). The start of the rains in West Africa. *Journal of Climatology*, 1(1):59–68.

Sultan, B. and Janicot, S. (2000). Abrupt shift of the ITCZ over West Africa and intra-seasonal variability. *Geophysical Research Letters*, 27(20):3353–3356.

Sultan, B., Janicot, S., and Drobinski, P. (2007). Characterization of the diurnal cycle of the West African monsoon around the monsoon onset. *Journal of climate*, 20(15):4014–4032.

Sun, J., Wang, H., and Yuan, W. (2010). Linkage of the boreal spring antarctic oscillation to the west african summer monsoon. *Journal of the Meteorological Society of Japan. Ser. II*, 88(1):15–28.

Sungmin, O. and Kirstetter, P.-E. (2018). Evaluation of diurnal variation of gpm imerg-derived summer precipitation over the contiguous us using MRMS data. *Quarterly Journal of the Royal Meteorological Society*, 144:270–281.

Takahashi, H. and Luo, Z. (2012). Where is the level of neutral buoyancy for deep convection? *Geophysical Research Letters*, 39(15).

Takahashi, H., Luo, Z. J., and Stephens, G. L. (2017). Level of neutral buoyancy, deep convective outflow, and convective core: New perspectives based on 5 years of cloudsat data. *Journal of Geophysical Research: Atmospheres*, 122(5):2958–2969.

Tang, G., Ma, Y., Long, D., Zhong, L., and Hong, Y. (2016). Evaluation of GPM Day-1 IMERG and TMPA Version-7 legacy products over Mainland China at multiple spatiotemporal scales. *Journal of hydrology*, 533:152–167.

Tang, Y., Lean, H. W., and Bornemann, J. (2013). The benefits of the Met Office variable resolution NWP model for forecasting convection. *Meteorological Applications*, 20(4):417–426.

Taylor, C. M., Belušić, D., Guichard, F., Parker, D. J., Vischel, T., Bock, O., Harris, P. P., Janicot, S., Klein, C., and Panthou, G. (2017). Frequency of extreme Sahelian storms tripled since 1982 in satellite observations. *Nature*, 544(7651):475–478.

Taylor, C. M., Fink, A. H., Klein, C., Parker, D. J., Guichard, F., Harris, P. P., and Knapp, K. R. (2018). Earlier seasonal onset of intense mesoscale convective systems in the Congo Basin since 1999. *Geophysical Research Letters*, 45(24):13–458.

Taylor, C. M., Gounou, A., Guichard, F., Harris, P. P., Ellis, R. J., Couvreux, F., and De Kauwe, M. (2011). Frequency of sahelian storm initiation enhanced over mesoscale soil-moisture patterns. *Nature Geoscience*, 4(7):430.

Taylor, C. M., Klein, C., Dione, C., Parker, D. J., Marsham, J., Diop, C. A., Fletcher, J., Chaibou, A. A. S., Nafissa, D. B., Semeena, V. S., et al. (2022). Nowcasting tracks of severe convective storms in West Africa from observations of land surface state. *Environmental Research Letters*, 17(3):034016.

Thorncroft, C. and Blackburn, M. (1999). Maintenance of the African easterly jet.

*Quarterly Journal of the Royal Meteorological Society*, 125(555):763–786.

Thorncroft, C. and Hoskins, B. (1994). An idealized study of African easterly waves. I: A linear view. *Quarterly Journal of the Royal Meteorological Society*, 120(518):953–982.

Thorncroft, C. D., Hall, N. M., and Kiladis, G. N. (2008). Three-dimensional structure and dynamics of African easterly waves. Part III: Genesis. *Journal of the Atmospheric Sciences*, 65(11):3596–3607.

Thorncroft, C. D., Nguyen, H., Zhang, C., and Peyrillé, P. (2011). Annual cycle of the West African monsoon: regional circulations and associated water vapour transport. *Quarterly Journal of the Royal Meteorological Society*, 137(654):129–147.

Tian, F., Hou, S., Yang, L., Hu, H., and Hou, A. (2018). How does the evaluation of the gpm imerg rainfall product depend on gauge density and rainfall intensity? *Journal of Hydrometeorology*, 19(2):339–349.

Ting, M., Kushnir, Y., Seager, R., and Li, C. (2011). Robust features of Atlantic multi-decadal variability and its climate impacts. *Geophysical Research Letters*, 38(17).

Tomasini, M., Lafore, J., Piriou, C., Roca, R., Ramage, K., Laurent, H., Morel, C., and Senesi, S. (2006). Atlas on a climatology of west african mesoscale convective systems. *AMMA European Deliverable*.

Tomassini, L. (2018). Mesoscale circulations and organized convection in african easterly waves. *Journal of the Atmospheric Sciences*, 75(12):4357–4381.

Tomassini, L., Parker, D. J., Stirling, A., Bain, C., Senior, C., and Milton, S. (2017). The interaction between moist diabatic processes and the atmospheric circulation in African Easterly Wave propagation. *Quarterly Journal of the Royal Meteorological Society*, 143(709):3207–3227.

Tompkins, A., Cardinali, C., Morcrette, J.-J., and Rodwell, M. (2005). Influence of aerosol climatology on forecasts of the African Easterly Jet. *Geophysical Research Letters*, 32(10).

Tompkins, A. M. (2001). Organization of tropical convection in low vertical wind shears: The role of cold pools. *Journal of the atmospheric sciences*, 58(13):1650–1672.

Trzeciak, T. M., Garcia-Carreras, L., and Marsham, J. H. (2017). Cross-Saharan trans-

port of water vapor via recycled cold pool outflows from moist convection. *Geophysical Research Letters*, 44(3):1554–1563.

Vizy, E. K. and Cook, K. H. (2002). Development and application of a mesoscale climate model for the tropics: Influence of sea surface temperature anomalies on the West African monsoon. *Journal of Geophysical Research: Atmospheres*, 107(D3):2.

Vizy, E. K. and Cook, K. H. (2017). Seasonality of the observed amplified sahara warming trend and implications for sahel rainfall. *Journal of Climate*, 30(9):3073–3094.

Vogel, P., Knippertz, P., Fink, A. H., Schlueter, A., and Gneiting, T. (2020). Skill of global raw and postprocessed ensemble predictions of rainfall in the tropics. *Weather and Forecasting*, 35(6):2367–2385.

Walker, D. P., Birch, C. E., Marsham, J. H., Scaife, A. A., Graham, R. J., and Segele, Z. T. (2019). Skill of dynamical and ghacof consensus seasonal forecasts of east african rainfall. *Climate Dynamics*, 53(7):4911–4935.

Wallace, J. M. and Hobbs, P. (1977). Atmospheric science-an introductory survey. *Academic Press*, page V.

Walters, D., Baran, A. J., Boutle, I., Brooks, M., Earnshaw, P., Edwards, J., Furtado, K., Hill, P., Lock, A., Manners, J., et al. (2019). The Met Office Unified Model global atmosphere 7.0/7.1 and JULES global land 7.0 configurations. *Geoscientific Model Development*, 12(5):1909–1963.

Walters, D., Boutle, I., Brooks, M., Melvin, T., Stratton, R., Vosper, S., Wells, H., Williams, K., Wood, N., Allen, T., et al. (2017). The Met Office unified model global atmosphere 6.0/6.1 and JULES global land 6.0/6.1 configurations. *Geoscientific Model Development*, 10(4):1487–1520.

Wang, D., Jensen, M. P., D'Ivorio, J. A., Jozef, G., Giagrande, S. E., Johnson, K. L., Luo, Z. J., Starzec, M., and Mullendore, G. L. (2020). An observational comparison of level of neutral buoyancy and level of maximum detrainment in tropical deep convective clouds. *Journal of Geophysical Research: Atmospheres*, 125(16):e2020JD032637.

Wang, R., Chen, J., and Wang, X. (2017). Comparison of IMERG level-3 and TMPA 3B42v7 in estimating typhoon-related heavy rain. *Water*, 9(4):276.

Wang, Z. and Elsberry, R. L. (2010). Modulation of the African easterly jet by a

mesoscale convective system. *Atmospheric Science Letters*, 11(3):169–174.

Ward, M. N. (1998). Diagnosis and short-lead time prediction of summer rainfall in tropical North Africa at interannual and multidecadal timescales. *Journal of Climate*, 11(12):3167–3191.

Warner, C., Simpson, J., Van Helvoirt, G., Martin, D., Suchman, D., and Austin, G. (1980). Deep convection on day 261 of gate. *Monthly Weather Review*, 108(2):169–194.

Weckwerth, T. M. and Parsons, D. B. (2006). A review of convection initiation and motivation for IHOP_2002. *Monthly Weather Review*, 134(1):5–22.

Wei-Jen Chang, S. (1982). The orographic effects induced by an island mountain range on propagating tropical cyclones. *Monthly Weather Review*, 110(9):1255–1270.

Weisman, M. L., Davis, C., Wang, W., Manning, K. W., and Klemp, J. B. (2008). Experiences with 0–36-h explicit convective forecasts with the WRF-ARW model. *Weather and Forecasting*, 23(3):407–437.

Weisman, M. L. and Klemp, J. B. (1982). The dependence of numerically simulated convective storms on vertical wind shear and buoyancy. *Monthly Weather Review*, 110(6):504–520.

Weisman, M. L. and Klemp, J. B. (1986). Characteristics of isolated convective storms. In *Mesoscale Meteorology and Forecasting*, pages 331–358. Springer.

Weisman, M. L. and Rotunno, R. (2004). "A theory for strong long-lived squall lines" revisited. *Journal of the Atmospheric Sciences*, 61(4):361–382.

White, B., Buchanan, A., Birch, C., Stier, P., and Pearson, K. (2018). Quantifying the effects of horizontal grid length and parameterized convection on the degree of convective organization using a metric of the potential for convective interaction. *Journal of the Atmospheric Sciences*, 75(2):425–450.

Willetts, P., Marsham, J., Birch, C., Parker, D., Webster, S., and Petch, J. (2017). Moist convection and its upscale effects in simulations of the indian summer monsoon with explicit and parametrised convection. In *EGU General Assembly Conference Abstracts*, pages 14407, https://ui.adsabs.harvard.edu/abs/2017EGUGA..1914407W/abstract.

Wood, N., Staniforth, A., White, A., Allen, T., Diamantakis, M., Gross, M., Melvin, T., Smith, C., Vosper, S., Zerroukat, M., et al. (2014). An inherently mass-conserving semi-implicit semi-lagrangian discretization of the deep-atmosphere global non-hydrostatic equations. *Quarterly Journal of the Royal Meteorological Society*, 140(682):1505–1520.

Woodhams, B. J., Birch, C. E., Marsham, J. H., Bain, C. L., Roberts, N. M., and Boyd, D. F. (2018). What is the added value of a convection-permitting model for forecasting extreme rainfall over tropical East Africa? *Monthly Weather Review*, 146(9):2757–2780.

Woodhams, B. J., Birch, C. E., Marsham, J. H., Lane, T. P., Bain, C. L., and Webster, S. (2019). Identifying key controls on storm formation over the Lake Victoria basin. *Monthly Weather Review*, 147(9):3365–3390.

Wu, M.-L. C., Reale, O., Schubert, S. D., Suarez, M. J., and Thorncroft, C. D. (2012). African easterly jet: Barotropic instability, waves, and cyclogenesis. *Journal of Climate*, 25(5):1489–1510.

Xu, R., Tian, F., Yang, L., Hu, H., Lu, H., and Hou, A. (2017). Ground validation of GPM IMERG and TRMM 3B42v7 rainfall products over southern tibetan plateau based on a high-density rain gauge network. *Journal of Geophysical Research: Atmospheres*, 122(2):910–924.

Yang, Q., Houze Jr, R. A., Leung, L. R., and Feng, Z. (2017). Environments of long-lived mesoscale convective systems over the central United States in convection permitting climate simulations. *Journal of Geophysical Research: Atmospheres*, 122(24):13–288.

Zhang, C., Nolan, D. S., Thorncroft, C. D., and Nguyen, H. (2008). Shallow meridional circulations in the tropical atmosphere. *Journal of Climate*, 21(14):3453–3470.

Zhang, G., Cook, K. H., and Vizy, E. K. (2016). The diurnal cycle of warm season rainfall over west africa. part ii: Convection-permitting simulations. *Journal of Climate*, 29(23):8439–8454.

Zhang, R. and Delworth, T. L. (2006). Impact of Atlantic multidecadal oscillations on India/Sahel rainfall and Atlantic hurricanes. *Geophysical Research Letters*, 33(17).

Zhao, M. (2014). An investigation of the connections among convection, clouds, and

climate sensitivity in a global climate model. *Journal of Climate*, 27(5):1845–1862.

Zulkafli, Z., Buytaert, W., Onof, C., Manz, B., Tarnavsky, E., Lavado, W., and Guyot, J.-L. (2014). A comparative performance analysis of TRMM 3B42 (TMPA) versions 6 and 7 for hydrological applications over Andean–Amazon river basins. *Journal of Hydrometeorology*, 15(2):581–592.